

DEPARTMENT OF PHARMACOLOGY
Medical Sciences Division



Contribution of the rostral thalamus to tauopathy

Doctor of Philosophy (D. Phil.) Thesis
Michaelmas Term, 2024

Barbara Sarkany

Lady Margaret Hall

Supervisors

Dr Tim Viney
Prof Vladyslav Vyazovskiy
Prof Frances Edwards

Department of Pharmacology
University of Oxford
Oxford, UK

“Those who contemplate the beauty of the earth find reserves of strength that will endure as long as life lasts.”

Rachel Carson

Abstract

The misfolding and accumulation of pathological tau protein (pTau) is a hallmark of several neurological diseases including Alzheimer's disease. The propagation of pTau and the vulnerability of distinct brain regions are still not well-understood. Mapping the subcortical progression of pTau accumulation focusing on the thalamus and identifying the subcellular location of the pathological proteins might reveal how pTau spreads in the human brain.

I assessed human *post-mortem* brain samples including thalamic regions which revealed that the density of pTau increased with the stage of the pathology (n=25 cases), with the anterodorsal thalamic nucleus (ADn) already affected in the 'pre-cortical phase' of Alzheimer's disease. This nucleus plays a major role in spatial navigation and orientation, which are disrupted early in Alzheimer's disease.

I observed that in the ADn the calretinin-expressing (CR) neurons were susceptible to pTau. Several studies support that pTau spread via synapses but the literature largely lacks the representation of pTau in human synaptic structures at the electron microscopic level. I found pTau in pre- and postsynaptic structures which supports the hypothesis of trans-synaptic spread. The majority of pTau+ boutons in the ADn contained vesicular glutamate transporter 2, which indicates a subcortical rather than cortical origin.

To get a more detailed picture of tau pathology I assessed its propagation in a tauopathy mouse model, THY-Tau22, which express a human mutant form (G272V and P301S) of tau. I observed that neuronal pTau spread to oligodendrocytes.

My observations support the hypothesis of trans-synaptic spreading of pTau and the involvement of glial cells in the propagation of the protein.

Acknowledgements

This thesis is the result of my research in neuroscience, specifically investigating the role of the thalamus in Alzheimer's disease, as part of my D.Phil. in Pharmacology at the University of Oxford. I would like to express my deepest gratitude to my supervisors, Dr Tim Viney, Prof Vladyslav Vyazovskiy, and Prof Frances Edwards.

In particular, I want to thank Dr Tim Viney for his unwavering support throughout my research journey, as well as for his inspiring scientific discussions and kindness. I am also immensely grateful to Prof Peter Somogyi for being a mentor and providing tremendous guidance. I thank to Prof Vladyslav Vyazovskiy and Prof Frances Edwards for the opportunity to participate in their stimulating lab meetings.

Since joining the Department of Pharmacology, I have been fortunate to meet wonderful scientists who provided me with a supportive and flourishing scientific environment. I have learned so much from their expertise and professionalism. Many thanks to Dr Linda Katona, Dr Istvan Lukacs, Dr Tugrul Ozdemir, Emily Hunter, Dr Rukhshanda Habib, Dr Sawa Horie, Dr Qianru Zhao, Dr Charalampos Sigalas, Dr Katja Hartwich, Michael Howarth, and Verena Gautsch for fostering a great research environment and offering support and advice during the early stages of my scientific journey. I am also grateful to our current lab members, Dr Sara Hijab and Shan Jiang, for their inspiring scientific discussions and friendly support. I wish to thank the support of several members of the Institute of Experimental Medicine in Hungary including Prof Laszlo Acsady, Dr Csaba David and Katalin Lengyel. I also extend my gratitude to Mrs Klara Somogyi and Mrs Mary Gilgunn-Jones for their warm, friendly support. Additionally, I would like to thank Lady Margaret Hall for all the support provided and for offering the right environment for a healthy work-life balance.

Most importantly, I am profoundly thankful to my entire family for their constant belief in me and their unwavering support. I am especially grateful to my son, who has brought immense joy into my life.

Statement of Authorship

I, Barbara Sarkany, DPhil student at the University of Oxford, Department of Pharmacology, hereby declare that parts of the data presented in this thesis, submitted for the degree of Doctor of Philosophy at the university of Oxford, are the work of other people.

I assessed different brain regions including thalamus, mammillary nucleus, dorsal raphe, locus coeruleus in human *post-mortem* brain sections from 26 cases. I imaged and processed thalamic sections from 25 cases. The cortical, dorsal raphe, locus coeruleus sections were processed and imaged by Dr Csaba David (Figure 3.6, 3.7) a postdoctoral researcher in Prof Laszlo Acsady's group, Institute of Experimental Medicine, Hungary. Shamis Osman, Istvan Bodi, and Claire Troakes from the London Neurodegenerative Diseases Brain Bank tested AT8 in the brainstem of 3 cases. Cortical sections were first assessed by Dr Tim Viney (Figure 3.3 j). I carried out the final assessment of the sections.

I examined 11 cases using electron microscopy, 4 cases were suitable for quantifications. Three samples (3 blocks from 3 cases, (78/336 synapses)) were assessed by Prof Peter Somogyi (Figure 4.3, 4.6).

Figure 5.1 and 5.2 was made by Dr Tim Viney and the Figure 5.2 A was imaged by Dr Katja Hartwich. Normalized intensity measurements of AT8 immunoreactivity in THY-Tau22 mice was carried out by Dr Tim Viney.

Dr Tim Viney also carried out 13 of 15 the injections of viral vectors into the rostral thalamus of wild type mice (Table 5.1).

The results of this thesis are published in two papers: (Sárkány et al 2024, Viney et al 2022), as indicated in relevant sections.

1 Table of Contents

1. General introduction 12

1.1 Anatomy and connectivity of the thalamus 13

1.2 The thalamus in brain disorders 17

1.3 Tau protein and tauopathies 18

1.4 Posttranslational modification of tau 21

1.5 Alzheimer's disease 21

1.6 Aims of this thesis 27

2 Materials and methods 28

2.1 Materials and methods of human brain tissue project 28

2.1.1 Human samples 28

2.1.2 Tissue processing 28

2.1.3 Fluorescent immunohistochemistry 30

2.1.4 Brightfield immunohistochemistry 30

2.1.5 Initial electron microscopic assessment of brain sections 31

2.1.6 Single- and double-labeling pre-embedding immunohistochemistry for combined light and electron microscopy 31

2.1.7 Data collection 33

2.1.8 Data analysis 34

2.1.8 Imaging 35

2.2 Materials and methods of animal model projects 36

2.2.1 Experimental model and subject details 36

2.2.2 Tissue processing 37

2.2.3 Fluorescent immunohistochemistry 37

2.2.4 Single- and double-labeling pre-embedding immunohistochemistry and electron microscopy 40

2.2.5 Imaging 43

3 Result: Distribution of pathological Tau in the human rostral thalamus and colocalization with calcium binding proteins 44

3.1 Introduction 44

3.2 Methods 47

3.2.1 Samples 47

3.2.2 Immunohistochemistry 50

3.2.3 Imaging 51

3.2.4 Data analysis 51

3.3 Results 54

3.3.1 Delineation of thalamic nuclei with calretinin and other markers 54
3.3.2 The anterodorsal thalamic nucleus shows early and consistent vulnerability to Tau pathology 56
3.3.3 Involvement of mammillary bodies, locus coeruleus, and dorsal raphe at different Braak stages 66
3.3.4 Vulnerable neuronal cell populations in the anterodorsal thalamic nucleus 69
3.4 Discussion 73
3.4.1 Diagnosis of Alzheimer's disease 73
3.4.2 Distribution of pTau 73
3.4.3 Consistent pattern of the pathology and its potential implication 74
3.4.4 Origin and subcellular distribution of pTau 76
3.4.5 Limitations of the study 76
4 Result: Mapping the subcellular distribution of Tau filaments in *post-mortem* human thalamus at different disease stages and assessing amyloid-β plaque burden 77
4.1 Introduction 77
4.2 Methods 80
4.2.1 Initial electron microscopic assessment of brain sections 80
4.2.2 Single- and double-labelling pre-embedding immunohistochemistry for combined light and electron microscopy 80
4.2.3 Electron microscopy 81
4.2.4 Imaging 81
4.3 Results 83
4.3.1 Subcellular distribution of pTau in the human ADn 83
4.3.2 Different subcellular compartments of CR-expressing cells accumulate pTau 85
4.3.3 Identification of small corticothalamic and large subcortical synaptic boutons 87
4.3.4 Large subcortical vesicular transporter 2-expressing presynaptic terminals preferentially contain pTau 87
4.3.5 The distribution of presynaptic and postsynaptic pTau suggests transsynaptic spread 89
4.3.6 Lack of extracellular amyloid-beta plaques in the ADn 96
4.4 Discussion 98
4.4.1 Subcellular localisation of pTau 98
4.4.2 Subcortical glutamatergic input linked to pTau accumulation 98
4.4.3 Transsynaptic spread of pTau 99
4.4.4 Double-walled vesicles 100
4.4.5 Plaques do not emerge in ADn 101

4.5 Limitations of the study 102
5 Result: Propagation of pTau, and glial and vascular contribution to neurodegenerative diseases 103
5.1 Introduction 103
5.2 Methods 106
5.2.1 Animals 106
5.2.2 Mouse tissue processing 107
5.2.3 Virus injections 108
5.2.4 Fluorescent immunohistochemistry 108
5.2.5 Single- and double-labelling pre-embedding immunohistochemistry and electron microscopy 109
5.2.6 Imaging 110
5.3 Result 110
5.3.1 Propagation of pTau in THY-Tau22 mice 110
5.3.2 Spread of pathological tau to oligodendrocytes from neurons in THY-Tau22 mice 116
5.3.3 Modelling of rostral thalamic tau pathology in wild type mice 121
5.3.4 Disrupted vascular structure in the human ADn 124
5.4 Discussion 127
5.4.1 Modelling of neurological diseases 127
5.4.2 Oligodendrocytes might facilitate the spread of pTau 128
5.4.3 Vascular pathology in Alzheimer's disease and in other neurodegenerative diseases 129
5.5 Limitations of the study 130
6 General discussion 132
6.1 Main findings 132
6.2 Significance and origin of tau pathology 132
6.3 Propagation of pathological proteins 137
6.4 Propagation of pTau in transgenic mice 141
6.5 Vascular pathology of ADn 144
6.6 Limitations of the study 148
6.7 Conclusion and outlook 149
7 References 151

List of Figures

Figure 1.1 Structure of the thalamus 16
Figure 1.2 Anatomy of the thalamus and connectivity of the anterior thalamic nuclei 16
Figure 1.3 Braak staging 23
Figure 3.1 Identification of tau pathology in the rostral thalamus using pixel classifier 53
Figure 3.2 Thalamic regions delineated with calretinin immunoreactivity 55
Figure 3.3 Progression of Tau pathology in the rostral thalamus and the cerebral cortex 59
Figure 3.4 Serial sections of rostral thalamus for Braak stage III 61
Figure 3.5 Serial sections of rostral thalamus for Braak stage VI 62
Figure 3.6 Tau pathology in the locus coeruleus and dorsal raphe nucleus in early-stage cases 67
Figure 3.7 Accumulation of pTau in the mammillary body 68
Figure 3.8 Calretinin expressing and PCP4 expressing neurons show complementary pattern in the human rostral thalamus 71
Figure 3.9 PTau-containing neurons in the anterodorsal thalamic nucleus express calretinin 72
Figure 4.1 Electron micrographs of synaptic elements and tau filament bearing soma, dendrite and myelinated axons in the human anterodorsal thalamic nucleus 84
Figure 4.2 A range of subcellular compartments from CR-expressing neurons contain tau filaments in the human anterodorsal thalamic nucleus 86
Figure 4.3 Large vGLUT2-expressing neurons preferentially accumulate pTau in the ADn 88
Figure 4.4 Light and electron microscopic localization of pTau to vGLUT2+ presynaptic terminals and postsynaptic dendrites in the ADn 91
Figure 4.5 Localization of pTau to vGLUT2-expressing presynaptic terminals 93
Figure 4.6 Accumulation of pTau pre-, and postsynaptically 95
Figure 4.7 . Amyloid plaques accumulated in nuclei adjacent to the ADn 97
Figure 5.1 Age-related increase of pTau in THY-Tau22 mice 113
Figure 5.2 Selective distribution of pTau in THY-Tau22 mice 114
Figure 5.3 Accumulation of pTau in oligodendrocytes 117
Figure 5.4 . Cortical pTau+ neurons and oligodendrocytes 119
Figure 5.5 PTau expressed in the rostral thalamus after AAV-GFP-Tau (P301L) injection 123
Figure 5.6 Electron micrographs of disrupted blood vessels in the ADn of cases with tau pathology 125
Figure 6.1 Hypothesis of pTau propagation in Alzheimer's disease 146

List of Tables

Table 1.1 Isoform composition of tauopathies....20
Table 2.1 List of primary antibodies....39
Table 2.2 List of secondary antibodies....39
Table 2.3 List of chemicals and resources....42
Table 3.1 List of Post-mortem human brain tissue cases....48
Table 3.2 List of Post-mortem human brain tissue cases, additional information....49
Table 3.3 Intensity scores for pTau in subcortical brain regions....63
Table 3.4 Intensity scoring for pTau in the rostral thalamus and cerebral cortex....64
Table 3.5 Quantification of pTau coverage and immunopositive cell counts....65
Table 5.1 List of mice injected with virus....107

List of abbreviations

A
AAV adeno-associated virus
ADn anterodorsal thalamic nucleus
ADNC Alzheimer's disease neuropathologic change
AgD argyrophilic grain disease
AM anteromedial thalamic nucleus
AMI acute myocardial infarction
AP antero-posterior
ARTAG aging-related tau astrogliopathy
Art.scler arteriosclerosis
AV anteroventral thalamic nucleus

B
BA Brodmann area
BBB blood-brain barrier
BSA Bovine Serum Albumin

C
CA1d distal CA1 region
CAA cerebral amyloid angiopathy
CB calbindin
CBD corticobasal degeneration
CHF congestive heart failure
Chr. chronic
COPD chronic obstructive pulmonary disease
CR calretinin-expressing
CT computed tomography

D
DAB diaminobenzidine
DRn dorsal raphe nucleus

E
EC entorhinal cortex
ECS enhancement conditioning solution

F
FFIF Flash-frozen immersion fixed
FFPE Formalin-fixed paraffin-embedded
FT freeze–thaw
FTDP-17 frontotemporal dementia with parkinsonism linked to chromosome 17
fMRI functional magnetic resonance imaging

G
GA glutaraldehyde

H
HBL Human Brain Research Laboratory
HD head direction
HRP horseradish peroxidase
HT hypertension
HTE hypertensive encephalopathy
huTau human tau protein

I
IHD chronic ischemic heart disease
Iml internal medullary lamina of the thalamus

K
KCL King's College London

L
LATE limbic-predominant age-related **TDP-43** encephalopathy neuropathologic change
LBD Lewy body disease
LC locus coeruleus
LMB lateral mammillary body/nucleus

M
MB mammillary body
MD mediodorsal thalamus
ML medio-lateral
MMB medial mammillary body
MRI magnetic resonance imaging
mtt mammillothalamic tract
MTOR mammalian target of rapamycin

N
NA not available
NFTs neurofibrillary tangles
NGS normal goat serum
NHS normal horse serum
NIDDM non-insulin dependent diabetes mellitus

O
OBB Oxford Brain Bank

P

ParaS parasubiculum
PART primary age-related tauopathy
PB phosphate buffer (without saline)
PB-Az 0.1 M PB with 0.05% sodium azide (without saline)
PCP4 Purkinje Cell Protein 4
PET positron emission tomography
PFFF perfusion-fixed free-floating
PiD Pick's disease
PMD post-mortem delay
PreS presubiculum
ProS prosubiculum
PSP progressive supranuclear palsy
Ptchd1 patched domain containing
pTau pathological tau protein
PVT paraventricular thalamic nucleus

R

RE Reuniens nucleus
ROI region of interest
RS retrosplenial cortex
RSg granular retrosplenial cortex
RT room temperature

S

SUBd dorsal subiculum
SVD small vessel disease

T

TA tufted astrocytes
TBS 0.9% NaCl buffered with 50 mM Tris
TBS-Tx 0.9% NaCl buffered with 50 mM Tris, pH 7.4, with 0.3% Triton X-100
TRN thalamic reticular nucleus

V

vGLUT1 vesicular glutamate transporter 1
vGLUT2 vesicular glutamate transporter 2

3R three repeat (tau protein)
4R four repeat (tau protein)

1. General introduction

As the brain is the most complicated organ it is extremely challenging to understand and cure different neurological disorders. Most of these diseases can be characterized by misfolded proteins. Tau protein is a microtubule associated protein, that becomes misfolded in different neurodegenerative diseases including Alzheimer's disease, the most common form of dementia (Goedert et al 2010). I will refer to misfolded tau as pathological tau (pTau) in my thesis. A major risk factor of Alzheimer's disease is ageing; as life expectancy is increasing more and more people become affected (Hou et al 2019, Rao et al 2022).

Most of the studies focus on cortical structures including the hippocampus which has a well-defined structure and involved is in memory formation (Rao et al 2022). Despite being affected early on in disease progression, subcortical structures are typically overlooked in Alzheimer's disease research (Breijyeh & Karaman 2020). The thalamus is an anatomically complex brain region that consists of different nuclei; each nucleus has different functions, connectivity, and cell types. This complexity provides a unique opportunity to understand the propagation and selective vulnerability of tauopathies. It has been shown that the anterior thalamic nuclei are involved in spatial navigation and memory formation (Aggleton & Brown 1999, Aggleton et al 2022, Forno et al 2021). As a consequence, the tau pathology in the anterior nuclear group has been linked to the early signs of Alzheimer's disease, especially episodic memory impairments and spatial navigation deficits (Aggleton et al 2016).

The propagation of pTau in the brain is still not well understood. Many questions have yet to be answered including whether pTau spreads intracellularly or extracellularly, in an anterograde or retrograde manner, and which brain regions are affected the earliest. A popular hypothesis is that pTau propagates via synapses in a prion-like manner (Goedert et al 2010); this has been supported using tau-PET in humans (Vogel et al 2020). However, due to technical challenges; the literature lacks studies showing tau filaments in subcellular structures in the

human brain at electron microscopic level which could provide critical information regarding pTau spread. The mapping of pTau propagation can lead to early diagnosis and drug development. Moreover, identification of vulnerable cell types can lead to the discovery of novel drug targets.

I investigated the spread of pTau in the human brain focusing on the rostral thalamus both at the gross anatomical and subcellular levels. Moreover, I assessed the propagation of pTau in different animal models. The mapping of pTau propagation can lead to early diagnosis and drug development. Moreover, identification of vulnerable cell types can lead to the discovery of novel drug targets.

1.1 Anatomy and connectivity of the thalamus

The thalamus is a nuclear complex located in the diencephalon. Several decades ago it was viewed as a passive relay that transmits sensory and motor signals to the cortex. However, this view has been updated with the recognition that it has other critical functions such as regulating alertness, sleep and arousal, shaping consciousness and memory formation (Gent et al 2018, Herrero et al 2002, Mátyás et al 2018, Mitchell et al 2014, Torrico & Munakomi 2024). The cortex promotes the development of thalamic axons: it permits the growth of axons when they invade it; later the cortex sends a 'stop' signal causing their termination in layer 4 (Molnár & Blakemore 1995).

An established view of the functional organisation of the thalamus is that it receives two types of inputs: drivers and modulators (Sherman & Guillery 1998). The drivers are considered as the main sensory inputs such visual inputs from the retina to the lateral geniculate; the modulators modify the driver inputs such as the glutamatergic input from layer VI of neocortex (Sherman 2007, Varela 2014). The different thalamic nuclei can be divided into first order thalamic nuclei, which receive direct input from sensory organs, and higher

order thalamic nuclei, which mainly receive their input from the cortex, particularly from layer 5. In the case of sight, the lateral geniculate is a first order thalamic nucleus as it receives direct input from the retina; the higher order relay is the pulvinar that receives input from the layer V of cortex (Martin Usrey et al 2021).

The thalamus can be subdivided into 3 major groups: 'limbic' nuclei, sensorimotor nuclei, and nuclei bridging these two domains. The limbic nuclei consist of the anterior thalamic nuclei, the midline nuclei, the medial division of the mediodorsal nucleus and the central medial nucleus of the intralaminar complex (Vertes et al 2015). The ADn along with the anteroventral (AV) and anteromedial (AM) thalamic nuclei, comprises the anterior nuclear group (Figure 1.1) (Vertes et al 2015), which forms one functional unit with the hippocampal formation and the mammillary bodies – key components of the so-called Papez circuit (Aggleton et al 2022, Forno et al 2021, Papez 1995, Veazey et al 1982). However, some studies claim that the circuit is outdated and the anterior thalamic nuclei serve as a multifunctional hub (Aggleton et al 2022). (Aggleton et al 2022). It was claimed that the circuit is the basis of regulating emotions but later this view changed and its importance in memory formation was recognised (Weininger et al 2019). The circuit comprises the following connections: (1) the mammillothalamic tract (mtt) that links the medial and lateral mammillary nuclei to the anterior nuclei of the thalamus; (2) thalamocortical projection from the anterior nuclei to the cingulate gyrus; and (3) a projection from the cingulate cortex, via the cingulum, to the entorhinal cortex and also to the subiculum and hippocampus. The subiculum, via the fornix, returns information to the mammillary body (MB) (Aggleton et al 2016). A significant difference between the anterior thalamic nuclei is that the ADn receives glutamatergic input from the lateral mammillary body/nucleus (LMB), whereas the AV and AM receive input from the medial mammillary body (MMB). Each anterior thalamic nucleus is connected to the neocortex (Guison et al 1995, Hayakawa & Zyo 1989). The AV and the ADn have a reciprocal connection

with the presubiculum (PreS); the ADn has a unilateral connection with the granular retrosplenial cortex (RSg) whereas the AV has a bidirectional connection. The AV also receives input from the entorhinal cortex (EC). The AM projects to the EC and perirhinal cortex (PC) (Perry & Mitchell 2019).

The cortical terminals in thalamus are vesicular glutamate transporter 1 (vGLUT1) expressing whereas the thalamic terminals in the cortex and the mammillothalamic terminals in the thalamus are vesicular glutamate transporter 2 (vGLUT2) expressing (Rovó et al 2012) (Figure 1.2).

The anterior thalamic nuclei are involved in spatial navigation; the ADn and the AM contains head-direction cells, place cells and border cells which function as an internal compass (Jankowski et al 2015, Taube 1995, Tsanov et al 2011); AV comprises place cells and neurons modulated by theta oscillations (Lomi et al 2023); place cells are neurons that fire when the subject is at a specific location (O'Keefe 1976). Lesions of the anterior nuclear group disrupt spatial memory in rodents (Frost et al 2021, Mitchell & Dalrymple-Alford 2006, Perry et al 2018), and its degeneration in alcoholics causes memory deficits (Harding et al 2000).

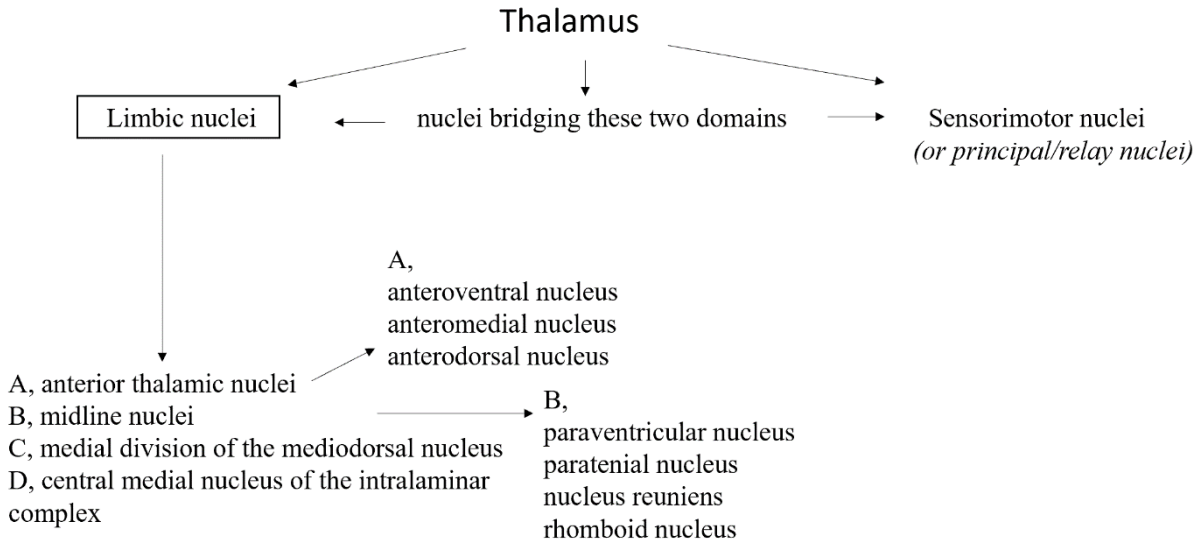


Figure 1.1 Structure of the thalamus

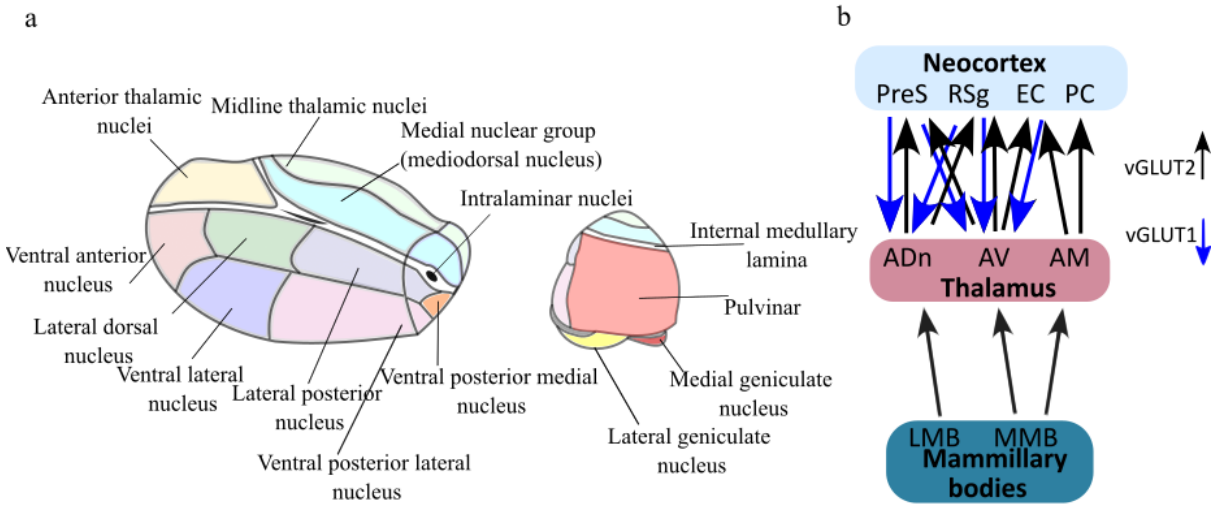


Figure 1.2 Anatomy of the thalamus and connectivity of the anterior thalamic nuclei
(a) Schematics show the anatomy of the thalamus and (b) part of the neurocircuit of the anterior thalamic nuclei. ADn, anterodorsal thalamic nucleus, AV; anteroventral thalamic nucleus; AM, anteromedial thalamic nucleus; PreS, presubiculum; RSg, granular retrosplenial cortex; EC, entorhinal cortex; PC, perirhinal cortex; LMB, lateral mammillary body, MMB medial mammillary body. Black arrow, vGLUT2+ axon terminals; blue arrow, vGLUT1+ axon terminals.

1.2 The thalamus in brain disorders

The thalamus is overlooked in different brain disorders as most studies assess the involvement of cortical structures; shifting the focus on the thalamus might facilitate early diagnosis and the development of effective therapies.

Thalamic pain syndrome is caused by stroke; the prevalence is high after stroke; it emerges in up to 8% of the patients (Dydyk & Munakomi 2024). The treatment of the disease remains difficult and often does not alleviate the pain and hypersensitivity (Ri 2022). Interestingly, it has been shown that the thalamus is affected in schizophrenia as well, and that dopaminergic transmission is dysregulated (Plavén-Sigray et al 2022). Furthermore, there is substantial cell loss in the anterior thalamic nuclei, mediodorsal thalamic nucleus, and pulvinar (Byne et al 2009, Young et al 2000). However, studies are inconsistent, and some have not shown changes in the thalamus (Dorph-Petersen & Lewis 2017).

Moreover, it has been shown that the severe atrophy of medial mammillary body in Korsakoff's syndrome plays role in the genesis of episodic memory impairment due to the disrupted input into the anterior thalamic nuclei (Kopelman 2015).

The anterior thalamic nuclei are also promising targets of deep brain stimulation in pharmacoresistant focal epilepsy syndromes. Interestingly, in a temporal lobe seizure model, lesioning of the mtt which connects the MB and the anterior thalamic nuclei prevents seizures (Mirski & Ferrendelli 1987). The anterior thalamic nuclei comprise a potential stimulation target on the basis of their widespread connectivity with the temporal lobe (as part of the Papez circuit) (Andrade et al 2006), and bilateral deep brain stimulation of the anterior thalamic nuclei reduces seizures in human subjects (Fisher et al 2010).

It has been shown that the ADn is severely and selectively vulnerable to pTau accumulation and neurodegeneration (Braak & Braak 1991b, Sárkány et al 2024, Xuereb et al 1990). This along with the fact that one of the earliest signs of Alzheimer's disease is memory

deficit, suggests that the anterior thalamic nuclei might be involved in the progression of Alzheimer's disease and may contribute to these memory deficits. Moreover, it has been shown that the thalamus accumulates amyloid plaques in Alzheimer's disease (Braak & Braak 1991b).

1.3 Tau protein and tauopathies

Tau protein is a microtubule associated protein that helps the assembly and stabilization of microtubules (Cleveland et al 1977). Tau is a highly soluble disordered protein in different diseases it acquires rigid folds and forms insoluble filaments (Skrabana et al 2006). Alois Alzheimer described the first tangle-like structures in the brains of Alzheimer's cases using light microscopy (Alzheimer et al 1995). Neuropil threads are fine, distorted nerve cell processes that are immunoreactive for pTau (AT8 epitope), tangles are intracellular aggregates of pTau (Brion 1985, Calderon-Garcidueñas & Duyckaerts 2017). Kidd showed using electron microscopy that these tangles consist of paired helical filaments (Kidd 1963).

The formation of neurofibrillary tangles (NFTs) is a complex biochemical process. There are several hypothesis about their formation, the leading hypothesis is that the first step is the phosphorylation of the tau proteins at distinct epitopes, which leads to dimerization and oligomerization of misfolded tau proteins. Subsequently, the oligomers form paired helical or straight filaments, and they produce the NFTs. The paired helical filaments are strongly linked to Alzheimer's disease, but in other tauopathies such as progressive supranuclear palsy (PSP), corticobasal degeneration (CBD) and Pick's disease (PiD) the straight filaments are dominantly observed (Murray et al 2007, Šimić et al 2016). Several early studies have suggested that the NFTs exert a toxic effect on neurons, although it was described that NFT-bearing neurons may survive for decades (Morsch et al 1999).

Tau proteins are thought to be localised in axons, and after becoming misfolded they are transported into other part of the cells (Christensen et al 2019, Iwata et al 2019).

Tauopathies are a class of neurodegenerative diseases characterized by neuronal or glial pTau inclusions causing behavioural, movement, language, and memory deficits. Although a stereotypical classification system has been widely adopted (Braak stageing, described below), most patients show multimorbidity and overlapping characteristics of different tauopathies (Zhang et al 2022). It is important to note that pTau can emerge in aged subjects without any documented cognitive impairments; this phenomenon is called primary age-related tauopathy (PART) (Crary et al 2014).

In the brain, six isoforms of tau are expressed by the alternative splicing of the MAPT mRNA; they differ by the absence or presence of 1 or 2 N-terminal inserts and either three (3R) or four (4R) 31- or 32-amino acid repeats in the microtubule-binding domain. The length of tau isoforms ranges from 352 to 441 amino acids. These isoforms accumulate in a subset of neurons and glia in different tauopathies, and they can have different spatiotemporal distributions (Table 1.1), (Goedert et al 2017). However, it is not known how different isoforms enter cells. In Alzheimer's, disease filamentous inclusions contain all isoforms, PiD filaments contain 3R tau, PSP filaments contain 4R tau. The mutation in the MAPT gene can lead to neurodegenerative diseases such as frontotemporal dementia with parkinsonism linked to chromosome 17 (FTDP-17) (Hutton et al 1998).

In primary tauopathies such as PiD, PSP, and CBD, pTau is the major hallmark whereas in secondary tauopathies there is another prominent aggregate, such as amyloid-β in Alzheimer's disease (Zhang et al 2022). Each disease is characterised with unique pTau conformation based on electron cryo-microscopy; however, this method is not able to image the disordered part of the protein (Fitzpatrick et al 2017).

3R+4R Tauopathies
Alzheimer's disease
Amyotrophic lateral sclerosis
Anti-IgLON5-related Tauopathy
Chronic traumatic encephalopathy
Diffuse neurofibrillary tangles with calcification
Down's syndrome
Familial British dementia
Familial Danish dementia
Gerstmann-Sträussler-Scheinker disease
Niemann-Pick disease, type C
Non-Guamanian motor neuron disease with neurofibrillary tangles
Postencephalitic parkinsonism
SLC9A6-related parkinsonism
Tangle-only dementia
Familial frontotemporal dementia and parkinsonism (some MAPT mutations)
3R Tauopathies
Pick's disease
Familial frontotemporal dementia and parkinsonism (some MAPT mutations)
4R Tauopathies
Argyrophilic grain disease
Corticobasal degeneration
Guadeloupean parkinsonism
Globular glial Tauopathy
Huntington's disease
Progressive supranuclear palsy
Tau astrogliopathy
Familial frontotemporal dementia and parkinsonism (some MAPT mutations)

Table 1.1 Isoform composition of tauopathies

Isoform composition of tauopathies, grouped by the 3R and 4R sequences, adapted from (Goedert et al 2017).

1.4 Posttranslational modification of tau

Post-translational modifications (PTMs) are biochemical modifications that emerge after translation. Intrinsically disordered proteins, which includes the tau protein, are more vulnerable to PTM as they do not have a well-defined structure, and the modifications can significantly change their dynamics and flexibility (Dyson 2011). It has been recognised that PTMs affect protein function and contribute to neurodegeneration. Tau can undergo several forms of posttranslational modifications, including phosphorylation, glycosylation, nitration, methylation, acetylation, sumoylation, cleavage or truncation and polyamination. Phosphorylation is the most common tau post-translational modification; and the tau protein can be phosphorylated at multiple sites. It has been shown that phosphorylation of tau at distinct sites reduces its ability to interact with microtubules and promotes the formation of aggregates (Iqbal et al 1986). Interestingly, phosphorylation can be protective as it has been shown in hibernating animals (Arendt et al 2003).

1.5 Alzheimer's disease

More than 55 million people live with dementia worldwide. Alzheimer disease, which is the most common form of dementia, is a progressive neurodegenerative disease and may contribute to 60–70% of cases (Shin 2022). The main hallmarks of the disease are the accumulation of two misfolded proteins: amyloid-β and tau. Extracellular amyloid-β is derived from the amyloid-β precursor protein, which is cleaved by β-secretase and γ-secretase (Zhang et al 2010). It has multiple roles including such as anti-microbial effect and being protective against oxidative stress (Kagan et al 2012, Zou et al 2002). Braak and Braak classified the distribution of pTau into six stereotypical stages relating to the gradual transition to Alzheimer's disease. In stage I-II the transentorhinal cortex is affected, in stage III-IV pTau spreads to some distinct areas of the hippocampus, and in stage V-VI the neocortex is

extensively affected (Figure 1.3) (Braak et al 2006). This staging is a useful guide to assess the pathology, but subcortical regions are not incorporated.

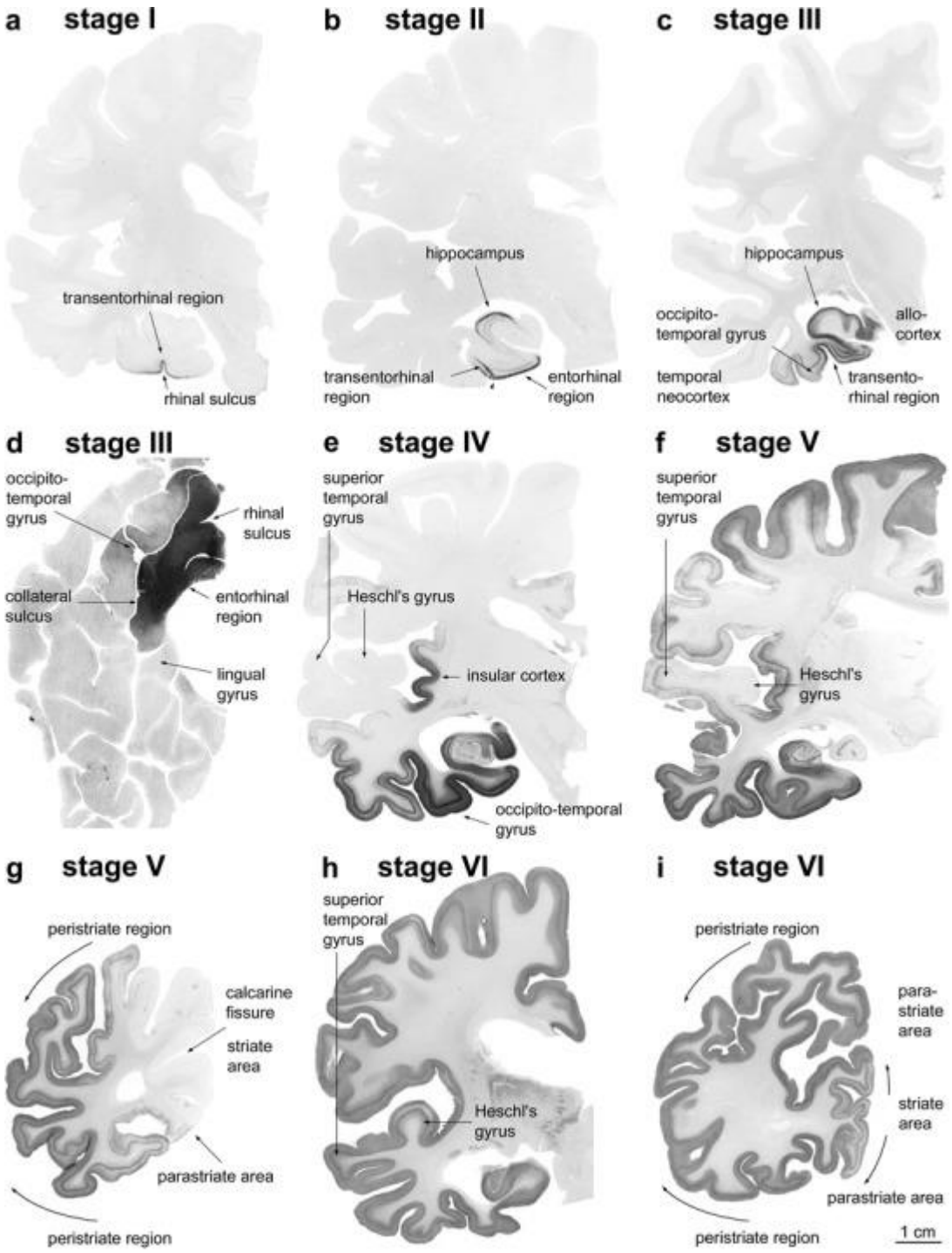


Figure 1.3 Braak staging

Stages I–VI of cortical tau pathology in 100 μm sections immunostained for hyperphosphorylated tau (AT8). Figure is from (Braak et al 2006, Braak & Braak 1991b).

Most cases are sporadic; the prevalence of familial Alzheimer's disease is less than 1-5%. The mutation of three genes is associated with early-onset Alzheimer's disease: amyloid precursor protein, presenilin 1, and presenilin 2, several gene mutations linked to late-onset Alzheimer's disease include apolipoprotein ε4, sortilin-related receptor 1, TREM2, PICALM (Harold et al 2009, Kleinberger et al 2014, Stoddart et al 2022, Tanzi 2012).

The primary risk factor of the disease is ageing. Over the age of 65 years, 10% of the population develops Alzheimer's disease (Hou et al 2019). Other risks factors are infections, injuries, diabetes and vascular disease (Hou et al 2019, McGrath et al 2022, Mielke et al 2022, Nguyen et al 2020, Smeland et al 2023). Vascular factors impact the development and progression of the disease by increasing the rate of formation of protein aggregates or decreasing the rate of elimination (O'Brien & Markus 2014). The blood-brain barrier (BBB) is part of the neurovascular unit together with pericytes, vascular smooth cells and glial cells. It is a selective semi-permeable membrane between the blood and the interstitium of the brain, allowing cerebral blood vessels to regulate molecule and ion transport between the blood and the brain (Zenaro et al 2017). Neuroimaging studies demonstrate its breakdown in Alzheimer's disease. Moreover, the dysfunction of the BBB induces microbleeds and impaired glucose transport (Ittner et al 2010).

The early signs of the disease includes impairments in spatial navigation, episodic memory, depression and aggression (Kumar et al 2024). Episodic memory refers to the ability to form, store, and recall memories of specific past events along with contextual details and is the first memory system that declines with age (Tromp et al 2015). Spatial navigation is particularly sensitive in Alzheimer's disease and might be the earliest marker of the disease (Allison et al 2016).

As the anterior thalamic nuclei are involved in spatial navigation, they might be responsible for the early signs of the disease including disorientation (Frost et al 2021, Mitchell & Dalrymple-Alford 2006, Perry et al 2018).

There is still no effective drug against Alzheimer's disease, however, it has been shown that high doses of vitamin B6, B12 and folic acid are able to slow down the progression of mild cognitive impairment, especially in people with a high omega-3 fatty acid status. These vitamins are able to reduce the level of the amino acid homocysteine that is thought to be causally responsible for brain atrophy (Smith et al 2018, Smith et al 2010).

Is has been widely accepted that not all types of cells are vulnerable in tauopathies including Alzheimer's disease (Braak & Braak 1988). However, subpopulations both neurons and glial cells are susceptible (Hansen et al 2018, Nishimura et al 1995, Verkhratsky et al 2010). It has been shown that cortical layer III and V pyramidal cells are significantly affected in Alzheimer's disease, which are a class of glutamatergic neurons (Braak & Braak 1991c). Moreover, the assessment of layer III pyramidal cells revealed that a cellular subpopulation that expresses the calcium binding calbindin are particularly sensitive in Alzheimer's disease (Hof & Morrison 1991). Furthermore, it has been shown that deep-layer Wolframin immunopositive hippocampal pyramidal neurons preferentially accumulate pTau, followed by neurodegeneration in aged THY-Tau22 mice which express the mutant form of the human tau protein (Viney et al 2022). These mice express human tau with two mutations (G272V and P301S) under the control of the thy1.2 promoter, ensuring strong neuronal expression in the forebrain. The mutations were selected because they are linked to frontotemporal dementia with parkinsonism (FTDP-17) and enhance tau aggregation (Schindowski et al 2006, Sperfeld et al 1999, Spillantini et al 1998). The mutations were selected because they are linked to frontotemporal dementia with parkinsonism (FTDP-17) and enhance tau aggregation (Sperfeld et al 1999, Spillantini et al 1998). Parvalbumin-expressing neurons of the neocortical layers

II-IV and V-VI are relatively resistant in Alzheimer's disease (Morrison et al 1998). As far as I consider, there is no study that assessed which neuronal cell types bear tau tangles in the thalamus, only that certain cells are severely affected (Braak et al 2006, Braak & Braak 1988).

Though the ratio of neuronal and glial tau aggregates varies across diseases, in most tauopathies, glial cells are affected (Kahlson & Colodner 2015). In Alzheimer's disease predominantly neurons are affected although glial cells are also involved, pTau in oligodendrocytes forms coiled bodies (Nishimura et al 1995). In other tauopathies oligodendrocytes are major components such as the PSP and CBD (Kahlson & Colodner 2015). At least 6 different types of astrocytic tau pathologies can be distinguished. Astrocytic plaques, tufted astrocytes, ramified astrocytes, and globular astroglial inclusions are seen predominantly in primary tauopathies, while thorn-shaped astrocytes and granular/fuzzy astrocytes are observed in aging-related tau astrogliopathy (ARTAG) (Kovacs 2020).

Several questions remain open regarding cell-type-specific vulnerability including which molecular components makes the cells vulnerable and how pTau spreads between different cell types.

1.6 Aims of this thesis

In the introduction I discussed the anatomy and function of the thalamus and tauopathies. Several questions are raised in the introduction. Firstly, does the thalamic tau pathology precedes the cortical one? Secondly, which cell types are vulnerable? Finally, which subcellular structures accumulate pTau and do they reveal subcellular routes of pTau spread?

To answer these questions, in *Chapter 3* I followed the propagation of pTau in the rostral thalamus along the different Braak stages in *post-mortem* human brain tissues. Moreover, I used different molecular markers to identify vulnerable cell types. In *Chapter 4*, I investigated how pTau may spread between neurons and what is the origin of pTau in the ADn. I used electron microscopy to study the subcellular distribution of pTau. *In Chapter 5*, I explored the propagation of pTau using two animal models: THY-Tau22 mice and wild type mice injected with adeno-associated virus (AAV) encoding a mutant form (P301L) of the human tau protein and GFP.

2 Materials and methods

2.1 Materials and methods of human brain tissue project

2.1.1 Human samples

Human brain samples were obtained from the Department of Pathology, Szt. Borbála Hospital, Tatabánya, Hungary via the Human Brain Research Laboratory (HBL, Institute of Experimental Medicine, Hungary), the MRC London Neurodegenerative Diseases Brain Bank (KCL, King's College London, UK), the Queen Square Brain Bank for Neurological Disorders (QSBB, UCL, London, UK), and the Oxford Brain Bank (OBB). The reported Braak Stage (Braak & Braak 1991c) for each case was based on a standardized examination of the severity and extent of pTau in the cerebral cortex. Braak stage 0 is defined by a lack of tau pathology and no detectable cognitive impairment. At stage I, pTau is observed in the entorhinal cortex (EC), followed by the hippocampus at stage II. By stage III, pTau is located in other areas of the medial temporal lobe and is associated with amyloid-ß plaques and mild cognitive impairment. Alzheimer's disease is associated with the later stages (III-VI), with pTau having spread beyond the medial temporal lobe. Psychiatric conditions for the HBL cases (Table 3.1) were previously assessed at the Department of Psychiatry, Szt. Borbála Hospital, Tatabánya, Hungary. See detailed tables of cases in Chapter 3.

2.1.2 Tissue processing

Perfusion-fixed tissue blocks from the HBL were received as previously described (Gilvesy et al 2022) and are from the same collection of cases reported by Gilvesy et al. (Gilvesy et al 2022) but with different numbering. Briefly, brains were removed 2-4 h post-mortem and vertebral arteries and internal carotid arteries were cannulated. Perfusion was carried out using physiological saline containing 0.33% heparin (1.5 L for 30 min), followed

by Zamboni fixative containing 4% w/v paraformaldehyde and ~0.2% w/v picric acid in 0.1 M phosphate buffer (PB, $Na_2HPO_4 \cdot 2H_2O$ = 0.08M, $NaH_2PO_4 \cdot H_2O$ = 0.02M, distilled water, pH=7.4), (4 L for 2 h). Tissue blocks were removed and post-fixed overnight in the same solution then washed and stored in 0.1 M PB with 0.05 % sodium azide (PB-Az). Experiments were performed in compliance with the 1964 Declaration of Helsinki, approved by the Regional Committee of Science and Research Ethics of Scientific Council of Health (ETT TUKEB 31443/2011/EKU and ETT TUKEB 15032/2019/EKU). Blocks were serially sectioned into 50-µm-thick coronal sections using a Leica VTS-1000 Vibroslicer (Leica Microsystems, Wetzlar, Germany). Free-floating sections were incubated in 20% sucrose for cryoprotection then subjected to freeze-thaw over liquid nitrogen. Next, sections were incubated in 1% hydrogen peroxide to reduce endogenous peroxidase activity. Sections were washed several times in 0.1 M PB then stored in PB-Az at 4°C.

Formalin-fixed paraffin-embedded (FFPE) samples were obtained from KCL (n=6 blocks) under Tissue Bank ethics approval (18/WA/0206). A microtome (Reichert-Jung, 2035) was used to prepare 5-10 µm thick sections (up to ~300 sections per block) and transferred onto slides (Superfrost Plus) in 37°C water. A series of 10 µm tissue sections were also obtained from QSBB (n=3 blocks) under Tissue Bank ethics approval (Human Tissue Authority Licence No 12198). In preparation for immunohistochemical tests, sections were first deparaffinized in xylene (100%) and rehydrated in a descending ethanol series (100%, 95%, 70%, 50%). Flash-frozen immersion fixed (FFIF) (n=2 blocks) samples were obtained from the OBB.

Masking of epitopes caused by fixation was reversed using antigen retrieval by incubating sections in 10 mM Sodium Citrate Buffer at pH 6 at 90°C in a water bath for 30 min before the blocking step in immunohistochemistry.

2.1.3 Fluorescent immunohistochemistry

Perfusion-fixed sections were blocked for 45 min in 4% Bovine Serum Albumin (BSA; Sigma) and FFPE section were blocked in 10% Normal horse serum (Vector Lab), followed by a 3-day incubation in primary antibody solution (Table 2.1) in 0.1 PB at 4°C. Sections were washed 3 times in 0.1 M PB then incubated in secondary antibody solution in 0.1 M PB for 1 hour at room temperature (RT) or overnight at 4°C. Finally, sections were mounted in Vectashield. Every experiment included controls for the method by leaving out the primary antibodies from the full protocol.

2.1.4 Brightfield immunohistochemistry

For light microscopic visualization, sections were blocked in 4% (vol/vol) Normal Goat Serum (NGS) or 4% BSA in 0.1 M PB. This was followed by incubation with primary antibodies (Table 2.1) and observed similar distributions for pTau to that of AT8. After washing in 0.1 M PB, sections were reacted with biotinylated secondary antibodies (Table 2.2) diluted in 0.1 M PB and incubated overnight at 4°C. Subsequently, sections were incubated with 1:100 Avidin+Biotin-HRP (horseradish peroxidase) complex (Vector labs) in 0.1M PB at 4°C. The vGLUT2 immunoreaction was enhanced with tyramide signal amplification (1:50; Akoya Biosciences). Next, sections were processed using 0.5 mg/mL diaminobenzidine (DAB; Sigma-Aldrich) as chromogen, 2% w/v nickel ammonium sulphate, and 0.4% w/v ammonium chloride in 0.1 M PB. Subsequently, hydrogen peroxide was added to a final concentration of 0.002% w/v to initiate DAB polymerization. After 12–20 min (depending on immunolabeling intensity), reactions were stopped by washing 3 × 10 min in 0.1 M PB. Free-floating sections were fixed onto glass sides using chrome alum gelatin. Next, sections were incubated in xylene for 5 min and mounted in DPX (Merck).

2.1.5 Initial electron microscopic assessment of brain sections

To assess the subcellular structure of thalamic sections without any immunoreactions, sections were post-fixed in glutaraldehyde (GA) fixative (2.5% GA, ~0.2% picric acid, 4% paraformaldehyde in 0.1 M PB) for 1-2 hours. Subsequently, sections were treated with 1% OsO_4 in 0.1 M PB washed in 0.1 M PB and in distilled water. Next, sections were incubated in 50% and 70% ethanol, then with 1% uranyl acetate dissolved in 70% ethanol. Dehydration of sections was continued in an ascending alcohol series 70%, 90%, 95%, 100%) followed by acetonitrile. Finally, sections were embedded in epoxy resin (Durpucan AMC, Fluka, Sigma-Aldrich).

After overnight incubation at RT, they were transferred onto glass slides. To polymerize epoxy resin, sections were incubated at 55°C for 2 days. Selected regions of the thalamus were cut out and re-embedded in epoxy blocks. Series of 50-70 nm-thick sections were cut with an ultramicrotome (Leica Ultracut UTC) and collected onto pioloform-coated single slot copper grids. Some sections were counterstained with lead citrate to increase contrast.

2.1.6 Single- and double-labeling pre-embedding immunohistochemistry for combined light and electron microscopy

Floating sections from Cases 4, 12, 17 were washed 3X in 0.9% NaCl buffered with 50 mM Tris buffered saline (pH 7.4; TBS) and then blocked in 4% (vol/vol) normal goat serum (NGS) in TBS for 45 min. Next, sections were incubated with primary antibodies in TBS for 3 days at 4°C. The following conditions were used:

1. Single labelling primary antibody (AT8) with immunogold labelling visualized by silver intensification
2. Single labelling antibody (vGLUT2/CR) with peroxidase reaction
3. Double labelling primary antibodies, followed by a silver-intensified immunogold reaction (AT8) and a peroxidase reaction (vGLUT2/CR)

4. Negative control: no primary antibody, immunogold and biotinylated secondary antibodies followed by silver-intensification and DAB treatment

Sections were subsequently rinsed 3x in TBS and blocked for 30 min at RT in 0.1 % Cold Water Fish Skin Gelatin (CWFS) solution containing 0.8% (vol/vol) NGS diluted in TBS to reduce the non-specific binding of secondary antibodies. Sections were incubated overnight at 4°C in CWFS solution containing biotinylated secondary antibody and/or immunogold-conjugated secondary antibodies (1:200 donkey anti-mouse ultra-small immunogold (Aurion, 100.322). Sections were washed 3x in TBS and 1x in 0.1M PB followed by incubation in 2% GA diluted in 0.1 M PB to fix the secondary antibody conjugated to immunogold particles.

After repeated washes in 0.1 M PB and TBS, sections were incubated overnight at 4°C in Avidin+Biotin-HRP complex diluted in TBS. Tissues were treated with enhancement conditioning solution (ECS; Aurion) diluted 1:10 in distilled water for 3x 5 min. To visualize immunogold particles, sections were incubated in silver enhancement solution (SE-LM, Aurion) for 20 min at 20°C in the dark and then washed in ECS. Following 2x 2 min washes in distilled water and 2x 10 min washes in 0.1 M PB, peroxidase was visualized using DAB (0.5 mg/mL) as chromogen developed with 0.01% H_2O_2. Subsequently, sections were washed in distilled water and treated with 0.5% OsO_4 in 0.1 M PB for 20 min on ice in the dark. To enhance contrast, sections were incubated in 1% uranyl acetate diluted in distilled water or diluted in 70% ethanol after incubation in 50% ethanol for 25 min on ice. Next, the dehydration of sections was carried out in an ascending alcohol series (50%, 70%, 90%, 95%, 100%) followed by acetonitrile, then sections were embedded in epoxy resin. After overnight incubation at RT, they were transferred onto glass slides. To polymerize epoxy resin, sections were incubated at 55°C for 2 days. Selected regions of the thalamus were cut out and re-embedded in epoxy blocks. Series of 50-70 nm-thick sections were cut with an ultramicrotome

(Leica Ultracut UTC) and collected onto pioloform-coated single slot copper grids. Some sections were counterstained with lead citrate to increase contrast.

2.1.7 Data collection

Light microscopy: Samples were obtained from 18 cases (Table 3.1) at different anterior-posterior levels. Three thalamic and hippocampal sections/case and two RSC sections/case were assessed.

Fluorescence immunohistochemistry: Tissues were collected from 5 cases that had at least 10 pTau+ cells in the ADn (5 cases were excluded as they had less than 10 pTau+ cells). Three sections/case were assessed, and average values are shown for CR/AT8 colocalization.

Electron microscopy: Samples were selected from 4 cases that had sufficient quality for analysis. Data were collected from one thalamus section/case, from which 3 areas were assessed. Analysis was performed by two independent individuals (Barbara Sarkany, Prof Peter Somogyi) per case; one person was blind to the Braak stages. Only synaptic structures were quantified. Electron opaque ('dark') boutons were excluded from the analysis due to the likely loss of antigenicity. Dark bouton frequency was as follows: Case 4, 28.57% (n=20/70); Case 17, 29.13% (n=30/103). Tissue quality prevented an unbiased synapse density quantification, because of the large spaces amongst cellular profiles; therefore, random sampling of synapses was carried out. The frequency was influenced by the size of the boutons and dendrites. Structures were followed through 4-5 serial sections (~4.7 sections/structure). The primary magnification was 2000-3000x, then the structures were imaged and identified at 3000-6000x magnification. Background labelling for AT8 was very low. Immunopositivity of a cellular profile for AT8 was defined by the presence of at least 1 silver-gold particle (~12.1 particles/structure on average). Bouton area was measured across 3 serial electron micrographs

and the average was calculated. Boutons without distinct membranes were not included in the analysis.

2.1.8 Data analysis

To delineate thalamic nuclei in digitized AT8-immunolabeled sections, adjacent calretinin (CR)-immunoreacted sections were aligned with the TrakEM2 plugin in Fiji. Outlines of each thalamic nucleus were defined in the CR-immunolabeled section and imported as regions of interest (ROI) into the corresponding digitized AT8-immunolabeled section, with manual alignment required for some ROIs.

The ADn was defined by the high density of CR+ cells between the MD and AV. The AV was defined by a lack of CR+ cells, located in the dorsal part of the thalamus. The nucleus reuniens could not be accurately delineated with CR; therefore, we defined the reuniens nuclear complex (RE) as the area around the third ventricle. The AM was defined by the rostral-caudal level of sections, being located at similar level to the MB. Separation of the AM and AV at this level cannot be delineated. The paraventricular thalamic nucleus (PVT) was defined as the dorso-ventral band of CR+ cells adjacent to the midline. The MD was defined as a large nucleus lacking CR+ neurons lateral of the PVT. The TRN was identified by its net-like structure containing CR+ cells. Imaged sections were analysed in QuPath and Python.

For quantitative analysis, pTau coverage per thalamic nucleus was detected in QuPath using an artificial neural network (ANN_MLP) pixel classifier (Figure 3.1). Only perfusion-fixed sections were assessed, as FFPE sections lacked sufficient quality. Neuronal cell bodies were counted in QuPath by manually selecting every cell to generate counts. Every case with thalamic sections was assessed.

For pTau intensity scoring, the distribution of pTau in each area was defined by the following scores: 0, lacking detectable pTau; 0.5, containing trace inclusions; 1, sparse; 2,

moderate; 3, dense. Median values for early, middle, and late-stage cases are reported. Both perfusion-fixed and FFPE sections were assessed. For cortical sections, scoring was carried out blind to the case/Braak stage.

2.1.8 Imaging

Slide scanner

Glass slides were digitized using a Pannoramic MIDI II scanner (3DHISTECH; Budapest, Hungary) with a Plan-Apochromat objective lens (20x magnification, NA 0.8, lateral resolution 0.346 x 0.325 μm/pixel) and pco.edge 4.2 4MP camera. For transmitted color brightfield images, 3 focus levels were applied. Representative images were captured in CaseViewer.

Confocal microscopy

For confocal microscopy, an LSM 710 was used with Plan-Apochromat 40x/1.4, 63x/1.4, and 100x/1.46 objectives (ZEN 2008 5.0 or ZEN Black 14.0 software). Laser lines (solid-state 405 nm, argon 488 nm, HeNe 543 nm and HeNe 633nm) were configured with the appropriate beamsplitters. The pinhole was set to ~1 Airy Unit for each channel. Brightfield images were acquired with a Zeiss AX10 microscope using an AxioCam HRc camera (63x/1.4 objective). For representative confocal images, maximum intensity projections were used for z-projections.

Electron microscopy

Specimens were studied on a Jeol 1010 transmission electron microscope equipped with a digital GATAN Orius camera (Department of Physiology, Anatomy and Genetics, Oxford University) and on a Hitachi 7100 electron microscope with a Veleta CCD camera (Olympus Soft Imaging Solutions, Germany), (Institute of Experimental Medicine; Budapest, Hungary). Signals were observed within the same locations and also in different structures,

indicating that the experiment did not produce false-positive double-labeling results. Magnification within the range of 2000X–10000X.

2.2 Materials and methods of animal model projects

2.2.1 Experimental model and subject details

The THY-Tau22 transgenic mouse line was created by the group of Prof Luc Buée (University of Lille, Inserm, CHU-Lille, France), with Thy1.2 driving expression of human *MAPT* with G272V and P301S mutations (Schindowski et al 2006). The vector was then microinjected into a C57BL6/CBA background and backcrossed to C57BL6 for more than five generations. All transgenic mice used in the study (~50% were female) were heterozygous; non-transgenic littermates were used as wild-type controls for all experiments. Transgenic animals were screened for the Tau transgene by PCR analysis of DNA prepared from tail biopsies. The forward (5′-ATGGCTGAGCCCCGCCAGGAG-3′) and the reverse (5′-TGGAGGTTCACCAGAGCTGGG-3′) primers were used to amplify a 250-bp fragment of Tau DNA (Schindowski et al 2006). All animal procedures were approved by the local Animal Welfare and Ethical Review Body under approved personal and project licenses in accordance with the Animals (Scientific Procedures) Act, 1986 (UK) and associated regulations. We bred mice on a C57Bl6j background, as in the original publication.

Animals were maintained in individually ventilated cages with their littermates on a 12/12 h light-dark cycle (lights on at 07:00) and all behavioral tests were carried out during the daytime. Implanted mice were also grouped housed wherever possible. Room temperature was maintained at 21°C and humidity was between 50-60 %. All mice were fed on a standard RM3 diet (pellets, product 801700, Special Diets Services).

2.2.2 Tissue processing

Mice were deeply anesthetized with sodium pentobarbital (50 mg/kg, i.p.) and transcardially perfused with saline followed by 4% paraformaldehyde, 15% v/v saturated picric acid, and 0.05% glutaraldehyde in 0.1 M phosphate buffer (PB), pH 7.4. Some brains were post-fixed overnight in fixative lacking the glutaraldehyde. After washing in 0.1 M PB, 70 µm coronal sections were cut using a Leica Microsystems VT 1000S Vibroslicer and stored in 0.1 M PB with 0.05% sodium azide at 4°C. Sections were permeabilized in Tris-buffered saline (0.9% NaCl buffered with 50 mM Tris, pH 7.4; TBS) with 0.3% Triton X-100 (TBS-Tx) or through rapid 2x freeze–thaw (FT) over liquid nitrogen (cryoprotected in 20% sucrose in 0.1 M PB).

2.2.3 Fluorescent immunohistochemistry

Sections were blocked for 1 h in 20 % (vol/vol) normal horse serum (NHS) in TBS/TBS-Tx followed by 3 d incubation at 4°C in primary antibody solution (Table 2.1) containing 1 % (vol/vol) NHS in TBS/TBS-Tx. Sections were washed 3 times in TBS/TBS-Tx then incubated in secondary antibody solution (Table 2.2) containing 1 % (vol/vol) NHS in TBS/TBS-Tx for 4 h RT or overnight at 4°C. After 3 washes, sections were mounted in Vectashield.

Fluorescence measurements: To measure the intensity of AT8 immunoreactivity (Fig. 5.1), 10x magnification epifluorescence tiles were made of the hippocampal formation. Three 300 μm^2 regions of interest (ROIs) were selected, covering the prosubiculum (ProS) and two regions of distal CA1d (CA1d). The mean pixel intensity was normalized relative to a background ROI. At least 2 mice per age group were measured (very young animals, <4.5 months; young animals, 8-16 months old; ageing mice, 8-16 months old; aged mice, >16

months old). Quantification was blind to genotype and age. The assessment was carried out by Dr Tim Viney.

Antibody	Epitope	Concentration and dilution	Specificity information	Source	Identifier
Mouse anti-AT8	Phosphorylation at S202 and T205 residues of human Tau	200 µg/mL, 1:2500 for DAB 1:5000 for IF	Immunoblot. AT8 did not recognise wildtype or mutated recombinant tau proteins prior to brain extract phosphorylation (Goedert et al., 1995)	Thermo Fisher Scientific	Cat# MN1020
Rabbit anti-Calretinin		Antiserum, 1:1000 for DAB 1:2000 for IF	Western blot supplied by Swant. No signal in knockout animals	Swant	Cat# 7699/3H
Mouse anti-vGLUT2	Recombinant rat vGLUT2 amino acids 510-582	Purified, 1:500 for DAB	Similar to immunoreactivity characterized in mouse hippocampus by Herzog et al. 2006 J. Neurochem.	Sigma Aldrich	Cat# MAB5504
Guinea pig anti-vGLUT2	Recombinant protein from rat vGLUT2	Antiserum, 1:8000 for DAB with Tyramide	Evaluated by Western Blot on Mouse brain lysates (Sigma Aldrich)	Synaptic Systems	Cat# 135 404
Mouse anti-CP13	Detects Tau phosphorylated at S202.	Cell culture supernatant, 1:1000 for DAB	Tau knock out mice	Dr Peter Davies	
Mouse anti-PHF-1	Around S396 and S404 phosphorylated sites of human tau	Cell culture supernatant, 1:1000 for DAB	Tau knock out mice	Dr Peter Davies	
Rabbit anti-Purkinje cell protein 4 (PCP4)	A peptide at C-terminus (C-15) of PCP4	1:1000 for IF	Evaluated transfected and non-transfected cells	Santa Cruz Biotechnology	Cat# sc-74816
Rabbit anti-Tau	Phospho T231 of tau	1:1000 for IF		Abcam	Cat# ab151559

Rabbit anti-Olig2	Recognizes the ~32 kDa Olig-2 protein	1:1000 for DAB, 1:500 for IF		Millipore	Cat# AB9610
Rabbit anti-T22	Oligomeric tau	1:1000 for IF	Western Blot detected tau oligomers in Alzheimer's disease, but not control, human brain tissue lysate	Millipore	Cat# ABN454
Complement C1q-like protein 2 (C1QL2)	Amino acids of C1QL2: CRMICDPYTAAPGGEPPGAKAQPPGPSTAALEVMQDLSANPPPPFIQGPKGD	1:1000 for IF			
Mammalian target of rapamycin (mTOR)	Residues surrounding Ser2481 of human mTOR	1:1000 for IF		Cell Signaling	Cat# 2983
Patched domain containing 1 (Ptchd1)	Synthetic peptide between 611-639 amino acids from the Central region of human Ptchd1	1:1000 for IF		Invitrogen	Cat# PA5-48191

Table 2.1 List of primary antibodies

Host	**Primary antibody species**	**Alexa 488**	**Cy3**	**Cy5**	**IgG (H&L) Ultra Small**	**Biotinylated Goat anti-rabbit**
Donkey	mouse	1:1000	1:400	1:250		
Goat	mouse				1:200	
Donkey	rabbit	1:1000	1:400	1:250		
Goat	rabbit					1:200
Donkey	guinea pig	1:1000	1:400	1:250		
Goat	guinea pig					1:200

Table 2.2 List of secondary antibodies

2.2.4 Single- and double-labeling pre-embedding immunohistochemistry and electron microscopy

Floating sections from two cases (21.5 months and 22.5 months female) were washed 3x in TBS and blocked in 5% (vol/vol) normal goat serum (NGS) in TBS for 45 min. Next, sections were incubated with AT8 and/or Olig2 primary antibodies in TBS for 6 d at 4°C. The following immunoreactions were performed: (1) One primary antibody with immunogold labelling followed by silver intensification; (2) one primary antibody with peroxidase reaction; (3) two primary antibodies, visualized by a silver-intensified immunogold reaction, followed by an immunoperoxidase reaction; (4) negative control, no primary antibody, immunogold and biotinylated secondary antibodies followed by silver-intensification. After incubation with primary antibodies, sections were rinsed three times in TBS and blocked for 30 min at RT in 0.1 % Cold Water Fish Skin Gelatin (CWFS) solution containing 0.8% NGS (vol/vol) and 0.05% sodium azide in TBS to reduce non-specific background reactions. Next, sections were incubated overnight at 4°C in 1:300 biotinylated goat anti-rabbit IgG (Vector Labs, BA-1000) and 1:200 donkey anti-mouse ultrasmall immunogold (Aurion, 100.322) in CWFS solution. Sections were washed several times in TBS and once in 0.1 M PB followed by incubation with 2% GA in PB to fix the antibodies conjugated to immunogold particles. After repeated washes in TBS, sections were incubated overnight at 4°C in avidin-biotinylated horseradish peroxidase complex (Vectastain ABC Elite kit, Vector Laboratories) in TBS. To visualize immunogold particles, they were intensified with silver: first the sections were treated with enhancement conditioning solution (ECS; Aurion) diluted 10x with distilled water for 3x5 min. To enlarge the gold particles further, sections were then incubated in silver enhancement solution (SE-LM, Aurion) for 20 min at 20°C and washed in ECS. Subsequently, peroxidase was visualized using 3,3-diaminobenzidine (DAB; 0.5 mg/mL, Sigma-Aldrich) as chromogen developed with 0.01% H_2O_2. The same method and reagents were used for single and double labeling. After washing sections in PB, they were treated with 0.5% OsO_4 (a fixative and heavy metal

contrasting agent) in 0.1 M PB for 20 min on ice to control reaction time. Next, dehydration of sections was carried out in ascending ethanol series (50%, 70%, 90%, 95%, 100% (vol/vol)) and in acetonitrile. To enhance contrast for electron microscopy, sections were incubated in 1 % uranyl acetate diluted in 70% ethanol for 25 min between the 70% and 90% ethanol steps. Subsequently, sections were placed in epoxy resin (Durpucan AMC, Fluka, Sigma-Aldrich), incubated overnight at RT and transferred onto slides. For polymerization, sections were incubated at 60°C for 2 d. Selected regions of proximal dorsal subiculum (SUBd) and/or distal CA1d were re-embedded into Durcupan blocks. A series of ~50 nm-thick sections were cut with an ultramicrotome (Leica Ultracut UTC) and collected on pioloform-coated copper grids.

Chemicals and reagents		
Normal goat serum	Vector Laboratories	Cat# S-1000
Normal horse serum	Vector Laboratories	Cat# S-2000
Cold Water Fish Skin Gelatin	Aurion	Cat# 900.033
Enhancement conditioning solution (ECS)	Aurion	Cat# 500.055
Silver enhancement solution SE-LM	Aurion	Cat# 500.022
Diaminobenzidine (DAB)	Sigma-Aldrich	Cat# D5637-1G
Chromium(III) potassium sulfate dodecahydrate	Sigma-Aldrich	Cat# 243361
Gelatin from bovine skin	Sigma-Aldrich	Cat# G9391
Acetonitrile	VWR Chemicals	Cat# 83657.32
DPX Mountant	Merck	Cat# 6522
Ultra-purified recombinant AAV8 virus, pilot-scale packaging pAAV-CBh>EGFP:T2A:Tau(P301L):WPRE	Vector Builder	Catalog # AAV8SP(VB211015-1033pqq)-C
Critical commercial assays		
Vectastain ABC Elite kit	Vector Laboratories	Cat# PK6100; RRID: AB_2336819
Vectashield Antifade Mounting Medium	Vector Laboratories	Cat# H-1000; RRID: AB_2336789
TSA Biotin Reagent Pack	Akoya Biosciences	Cat# SAT700001EA
Software and algorithms		
Fiji	ImageJ	https://imagej.net/software/fiji
Zen 2008, Zen Black, Zen Blue,	Zeiss	www.zeiss.co.uk
Python		https://www.python.org/
CaseViewer	3DHISTECH	https://www.3dhistech.com/solutions/caseviewer
QuPath	(Bankhead et al 2017)	https://qupath.github.io/
Experimental models		
C57BL6j mice	Charles River Laboratories	https://www.criver.com/
THY-Tau22 mice	(Schindowski et al 2006)	https://www.informatics.jax.org/allele/MGI:3717232

Table 2.3 List of chemicals and resources

2.2.5 Imaging

Fluorescent microscopy

Sections were visualized and imaged with widefield epifluorescence using a Leitz DMRB microscope (Leica Microsystems) equipped with PL Fluotar objectives (magnification/numerical aperture: 5x/0.15, 10x/0.3, 20x/0.5, 40x/0.7; OpenLab software) or an AXIO Observer Z1 microscope (LSM 710; Zeiss) equipped with Plan-Apochromat 10x/0.3, 20x/0.8 and 40x/1.4 objectives (Axiovision or ZEN Blue 2.6 software).

Confocal microscopy

For confocal microscopy, the LSM 710 was used with Plan-Apochromat 40x/1.4, 63x/1.4, and 100x/1.46 objectives (ZEN 2008 5.0 or ZEN Black 14.0 software). Laser lines (solid-state 405 nm, argon 488 nm, HeNe 543 nm and HeNe 633 nm) were configured with the appropriate beamsplitters. The pinhole was set to ~1 Airy Unit for each channel.

Electron microscopy

Ultrathin sections were counterstained with lead citrate and studied on a Jeol 1010 transmission electron microscope equipped with a digital GATAN Orius camera (Department of Physiology, Anatomy and Genetics, Oxford University).

3 Results: Distribution of pathological Tau in the human rostral thalamus and colocalization with calcium binding proteins

3.1 Introduction

A major function of Tau is to stabilize neuronal microtubules. The accumulation and apparent spread of pTau are associated with a broad spectrum of neurodegenerative diseases including Alzheimer's disease, progressive supranuclear palsy and corticobasal degeneration (Arima 2006, Braak & Del Tredici 2016). Unlike amyloid-beta plaques, the accumulation of pTau correlates with cognitive decline (Bejanin et al 2017). However, it remains uncertain how pTau spreads in the human brain. Since animal models might not recapitulate the characteristics of pTau propagation, it is important to define the cellular and subcellular compartments in the human brain that are involved in the progression of pTau.

Despite the main focus on cortical regions such as hippocampus and EC in Alzheimer's research, specific subcortical regions such as the rostral thalamus, locus coeruleus (LC), dorsal raphe nucleus (DRn) and MB are also selectively vulnerable to pTau (Andrés-Benito et al 2017, Ehrenberg et al 2017, Gilvesy et al 2022, Stratmann et al 2016, Theofilas et al 2018). It is still not well-understood which subcortical regions are affected the earliest and whether they are affected earlier than the cortex.

I assessed different cortical and subcortical areas with the main focus on the thalamus. The thalamus is an anatomically complex brain region that consists of several different thalamic nuclei, each with different cell types, connectivity and function. This complexity provides a unique opportunity to understand the propagation of pTau. First, Braak and Braak (Braak & Braak 1991b) observed pTau in the rostral part of the thalamus; the pathology showed a striking difference between different nuclei. However, the temporal and spatial progression

of the pathology is limited in understanding, it is not known which nuclei are affected the earliest.

Distinct regions of the thalamus including the anterior thalamic nuclei are involved in spatial navigation which is early affected in Alzheimer's disease (Aggleton et al 2016) Identification of affected cell types in different neurodegenerative diseases is critical for the understanding of biological factors that cause susceptibility and for therapy development, as it the case for dopaminergic neuronal loss in Parkinson's disease (Kalia & Lang 2015). Examination of layer III pyramidal cells of the human prefrontal cortex showed that a neuronal subpopulation that express the calcium binding calbindin protein are particularly sensitive in AD (Hof & Morrison 1991). Wolframin-expressing neurons are susceptible to pTau in human EC, and in mice pTau has been suggested to propagate from Wolframin+ EC cells to CA1, which is linked to memory impairments (Delpech et al 2021).

My aim was to map the temporal and spatial progression of pTau in the rostral thalamus in relation to the well-established cortical pathological staging. Moreover, I aimed to identify neuronal cell populations that are susceptible to pTau accumulation.

The thalamus has an abundance of cells expressing calcium binding proteins. Calcium binding proteins have heterogenous expression in the mammalian brain, therefore, they can be used to identify different cell subpopulations. Their main function is to buffer and modulate the cytosolic calcium level. There are three calcium binding proteins that show a specific distribution in the thalamus: calbindin (CB), calretinin (CR) and parvalbumin (PV). Calretinin and calbindin have overlapping distributions across the different thalamic nuclei whereas the expression of PV is complementary (Münkle et al 2000). Jones (Jones 1998) proposed the matrix-core theory: smaller CB+ neurons project mainly to superficial cortical layers, especially to layer 1, in a diffuse pattern and form a "matrix" of thalamocortical input, whereas the PV+ neurons project mainly to the middle cortical layers, primary to layer 4, in a

topographically organised fashion forming a “core” (Jones 1998, Sherman & Guillery 1998). One of the limitations of this theory that many thalamic cells express more than one calcium-binding protein. Moreover, there is a significant morphological variation in connections made by thalamocortical projections that cannot be classified neither core or matrix (Sherman & Usrey 2024).

Additionally, it has been previously reported that in the brain of adult rhesus monkeys, Purkinje Cell Protein 4 (PCP4) shows a selective expression in the thalamus (Murray et al 2007).

Importantly, vesicular glutamate transporters 1 and 2 (vGLUT1, vGLUT2) also delineate the different thalamic nuclei. Vesicular glutamate transporters pack the neurotransmitter glutamate into synaptic vesicles that will be released into the synaptic cleft following sufficient depolarization of the terminal. The two transporters can differentiate a large portion of innervation: vGLUT1 indicates cortical origin, whereas vGLUT2 shows subcortical origin (Herzog et al 2001, Rovó et al 2012).

In my study the thalamic nuclei were delineated with CR. I assessed anterior thalamic sections at different anterior-posterior levels.

3.2 Methods

3.2.1 Samples

I assessed human *post-mortem* brain samples from 26 cases with different Braak stages: early (Braak stages 0-II; n=15), middle (Braak stages III-IV, n=6), and late (Braak stages V-VI, n=5) cases (Table 3.1, Table 3.2, Table 3.3, Table 3.4) (Sárkány et al 2024). In this Chapter I tested and/or analysed thalamic sections from 25 cases, cortical sections from 8 cases, LC sections from 13 cases, MBs from 6 cases and DRn from 1 case. Three types of brain tissues were used: Perfusion-fixed free-floating (PFFF), Flash-frozen immersion fixed (FFIF) sections, formalin-fixed paraffin-embedded (FFPE) (Table 3.2).

For quantitative assessment the AT8 antibody was used that recognises the serine 202 and threonine 205 residues of Tau (Goedert et al 1995). A similar pTau distribution was observed using PHF1 and CP13 antibodies. The PHF1 recognises recognises phosphorylated serine 396 and serine 404 residues of Tau and CP13 recognises phosphorylated serine 202 residue of Tau. The T22 antibody, which recognizes oligomeric tau, was tested but produced an unspecific signal.

Case	Group	Braak Tau Stage	Clinical Diagnosis (Neuro/Psych)	Age	Sex	Thal (Aβ) phase	CERAD	NIA-AA ABC Score for AD	AD Probability NIA-AA 2012
1	Early	0	WNL	86	m	0	0	A0B0C0	Not AD
3	Early	0	Schizophrenia	72	m	0	0	A0B0C0	Not AD
4	Early	0	Schizophrenia	57	f	0	0	A0B0C0	Not AD
5	Early	0	Schizophrenia	71	f	4	NA	A3B0C0	Low
22	Early	0	WNL	61	f	0	0	A0B0C0	Not AD
24	Early	0	WNL	61	f	0	0	A0B0C0	Not AD
20	Early	I	WNL	59	f	3	1	A2B1C1	Low
6	Early	I	WNL	65	m	2	0	A1B1C0	Low
7	Early	I	WNL	71	m	1	1	A1B1C1	Low
8	Early	I	WNL	74	m	NA	0	AxB1C0	Not AD
9	Early	I	WNL	81	m	1	0	A1B1C0	Low
2	Early	II	WNL	72	f	2	1	A1B1C1	Not AD
23	Early	II	WNL	87	f	1	0	A1B1C0	Low
25	Early	II	WNL	75	f	0	0	A0B1C0	Not AD
26	Early	II	WNL	85	f	1	0	A1B1C0	Low
10	Middle	III	WNL	86	m	NA	NA	AxB1Cx	Not AD
11	Middle	III	NA	80	f	2	1	A1B2C1	Low
12	Middle	III	NA	82	f	2	3	A1B2C3	Intermediate
13	Middle	III	Schizophrenia	84	m	1	0	A1B2C0	Low
21	Middle	III	WNL	77	f	4	1	A3B2C1	Intermediate
14	Middle	IV	NA	89	f	0	0	A0B2C0	Low
15	Late	V	Circumscribed brain atrophy	78	m	5	3	A3B3C3	Definite
16	Late	V	AD	71	m	NA	3	AxB3C3	High
17	Late	VI	NA	81	f	4	3	A3B3C3	Definite
18	Late	VI	AD	72	m	NA	3	AxB3C3	Intermediate≤
19*	Late	VI	NA	76	f	NA	3	AxB3C3	Intermediate≤

Table 3.1 . List of Post-mortem human brain tissue cases

Abbreviations: WNL, within normal limits; NA, not available; AD, Alzheimer's disease; CERAD, Consortium to Establish a Registry for Alzheimer's Disease; NIA-AA, National Institute on Aging and Alzheimer's Association; PMD, *post-mortem* delay time; CERAD neuritic plaque score: none (0), sparse (1), moderate (2), frequent (3). *Only cortical sections were available.

Case	Primary pathological diagnosis	Further pathological diagnosis	APOE	PMD (h)	Cause of death	Major comorbidities	Sections	Source
1	WNL		E3/E3	6	AMI		FFPE	KCL
3	WNL	Mild SVD	NA	2.5	Cardiac arrest	IHD, COPD	PFFF	HBL
4	WNL		NA	3	Respiratory arrest	CHF, COPD	PFFF	HBL
5	WNL		NA	4	Heart failure	IHD, HT, art.scler., obesity	PFFF	HBL
22	WNL		NA	3	AMI	Art.scler., obesity, HT, NIDDM	PFFF	HBL
24	WNL	HTE	NA	5.05	Cardiogenic shock	IHD	PFFF	HBL
20	WNL		NA	26.3	AMI	Art.scler.	FFIF	OBB
6	PART	Mild SVD	NA	53	Bronchopneumonia	Art.scler.	FFPE	QSBB
7	WNL	Mild CAA	E3/E3	24	Disseminated cancer		FFPE	KCL
8	WNL		E3/E3	42	Pancreatic cancer		FFPE	KCL
9	PART	Mild SVD	NA	2.5	Bronchopneumonia	Art.scler., IHD	PFFF	HBL
2	PART	Mild CAA	NA	36	Disseminated cancer		FFPE	QSBB
23	WNL		NA	3	NA		PFFF	HBL
25	WNL	Mild SVD	NA	4.5	AMI	Art.scler., COPD, obesity	PFFF	HBL
26	PART	Mild SVD, CAA	NA	3	CHF	Acute peritonitis, COPD	PFFF	HBL
10	PART		E3/E3	52	CHF		FFPE	KCL
11	ADNC	Moderate SVD	NA	3	Ileus	IHD, HT	PFFF	HBL
12	ADNC		NA	2	AMI	IHD, HT	PFFF	HBL
13	ADNC	Moderate SVD, TA	NA	3	Respiratory arrest	COPD	PFFF	HBL
21	ADNC		E3/E4	69	NA	Chr. arthritis, HT	FFIP	OBB
14	ADNC	AgD (grains, TA)	NA	2.5	NA		PFFF	HBL
15	ADNC	Mild SVD; Limbic LBD	NA	5	Rectal cancer		FFPE	QSBB
16	ADNC	Mild CAA	E3/E4	5	Haemorrhagic shock		FFPE	KCL
17	ADNC	Moderate SVD; LATE;	NA	2	NA		PFFF	HBL
18	ADNC	Severe CAA	E3/E3	5	NA		FFPE	KCL
19*	ADNC		NA	2.2	Heart failure	Art.scler., IHD, HT	PFFF	HBL

Table 3.2 List of Post-mortem human brain tissue cases, additional information

Abbreviations: NA, not available; PART, primary age-related tauopathy; ADNC, Alzheimer`s disease neuropathologic change; SVD, small vessel disease; HTE, hypertensive encephalopathy; CAA, cerebral amyloid angiopathy; TA, tufted astrocytes; AgD, argyrophlic grain disease; LBD, Lewy body disease; LATE, limbic-predominant age-related TDP-43 encephalopathy neuropathologic change; AMI, acute myocardial infarction; CHF, congestive heart failure; IHD, chronic ischaemic heart disease; COPD, chronic obstructive pulmonary disease; HT, hypertension; NIDDM, non-insulin dependent diabetes mellitus; Art.scler, arteriosclerosis; Chr., chronic; FFPE, formalin-fixed paraffin-embedded (10-µm-thick sections); PFFF, perfusion-fixed free-floating (50-µm-thick free-floating sections); FFIF,

flash-frozen immersion-fixed (50-µm-thick free-floating sections); KCL, London Neurodegenerative Diseases Brain Bank; HBL Human Brain Research Laboratory; OBB, Oxford Brain Bank; QSBB, Queens Square Brain Bank. *Only cortical sections were available.

3.2.2 Immunohistochemistry

To visualize the targeted antigens either brightfield or fluorescent immunohistochemistry was used.

Fluorescent immunohistochemistry: PFFF sections were blocked for 45 min in 4% bovine serum albumin and FFIF and FFPE sections were blocked in 10% or 20% normal horse serum, followed by a 3-day incubation in primary antibody antibodies (Table 2.1) solution. Sections were washed three times in 0.1 M PB and then incubated in secondary antibody solution for 1 h or overnight. Autofluoresence signal from lipofuscin was not quenched. Finally, sections were mounted in Vectashield.

Brightfield immunohistochemistry: Sections were blocked in 4% (vol/vol) normal goat serum (NGS) or 4% BSA in 0.1 M PB. This was followed by incubation with primary antibodies (1–3 days) (Table 2.1). Subsequently, for experiments that included anti-vGLUT2 tests, sections were incubated with 1:100 avidin + biotin-HRP (horseradish peroxidase) complex. The vGLUT2 immunoreaction was enhanced with tyramide signal amplification. Next, sections were processed using 0.5 mg/mL diaminobenzidine (DAB; Sigma-Aldrich) as chromogen, 2% nickel ammonium sulfate, and 0.4% ammonium chloride in 0.1 M PB. Subsequently, hydrogen peroxide was added to a final concentration of 0.002% w/v to initiate DAB polymerization and the subsequent forming an insoluble brown precipitate. After 12–20 min, reactions were stopped by washing in 0.1 M PB. Free-floating sections were fixed onto glass sides using chrome alum gelatin. Next, sections were incubated in xylene for 5 min and mounted in DPX. Every experiment on thalamic sections was carried out by me. Additional immunoreactions to detect pTau in the LC, MB, and DRn were carried out by Faddi Krisztina

and Dr Csaba David. Cortical sections were processed and digitised by the group of Prof Laszlo Acsady, Institute of Experimental Medicine, Budapest, Hungary. Shamis Osman, Istvan Bodi, and Claire Troakes from the London Neurodegenerative Diseases Brain Bank tested AT8 in the brainstem of 3 cases.

3.2.3 Imaging

Slide scanner

Glass slides were digitized using a Pannoramic MIDI II scanner or with Hamamatsu NanoZoomer 2.0HT slide scanner. For confocal microscopy, an LSM 710 was used with Plan-Apochromat 40×/1.4, 63×/1.4, and 100×/1.46 objectives (ZEN 2008 5.0 or ZEN Black 14.0 software).

Confocal microscopy

For representative confocal images, maximum intensity projections were used for z-projections.

3.2.4 Data analysis

The initial scoring of the cortical sections was carried out by Dr Tim Viney blind to the Braak stage. Blinding was used to avoid bias caused by Braak staging which was carried out by a neuropathologist.

Pixel classification: To delineate thalamic nuclei in digitized AT8-immunolabeled sections, adjacent CR-immunoreacted sections were aligned with the TrakEM2 plugin in Fiji. For quantitative analysis, pTau coverage per thalamic nucleus was detected in QuPath using an artificial neural network (ANN_MLP) pixel classifier (Figure 3.1). Only perfusion-fixed sections were assessed, as FFPE sections lacked sufficient quality. Neuronal cell bodies were counted in QuPath by manually selecting every cell to generate counts. For pTau intensity

scoring, the distribution of ptau in each area was defined by the following scores: 0, lacking detectable pTau; 0.5 (i), containing trace inclusions; 1 (+), sparse/mild; 2 (++), moderate; 3 (+++), dense (Table 3.2, Table 3.3, Table 3.5). Both PFFF and FFPE sections were assessed.

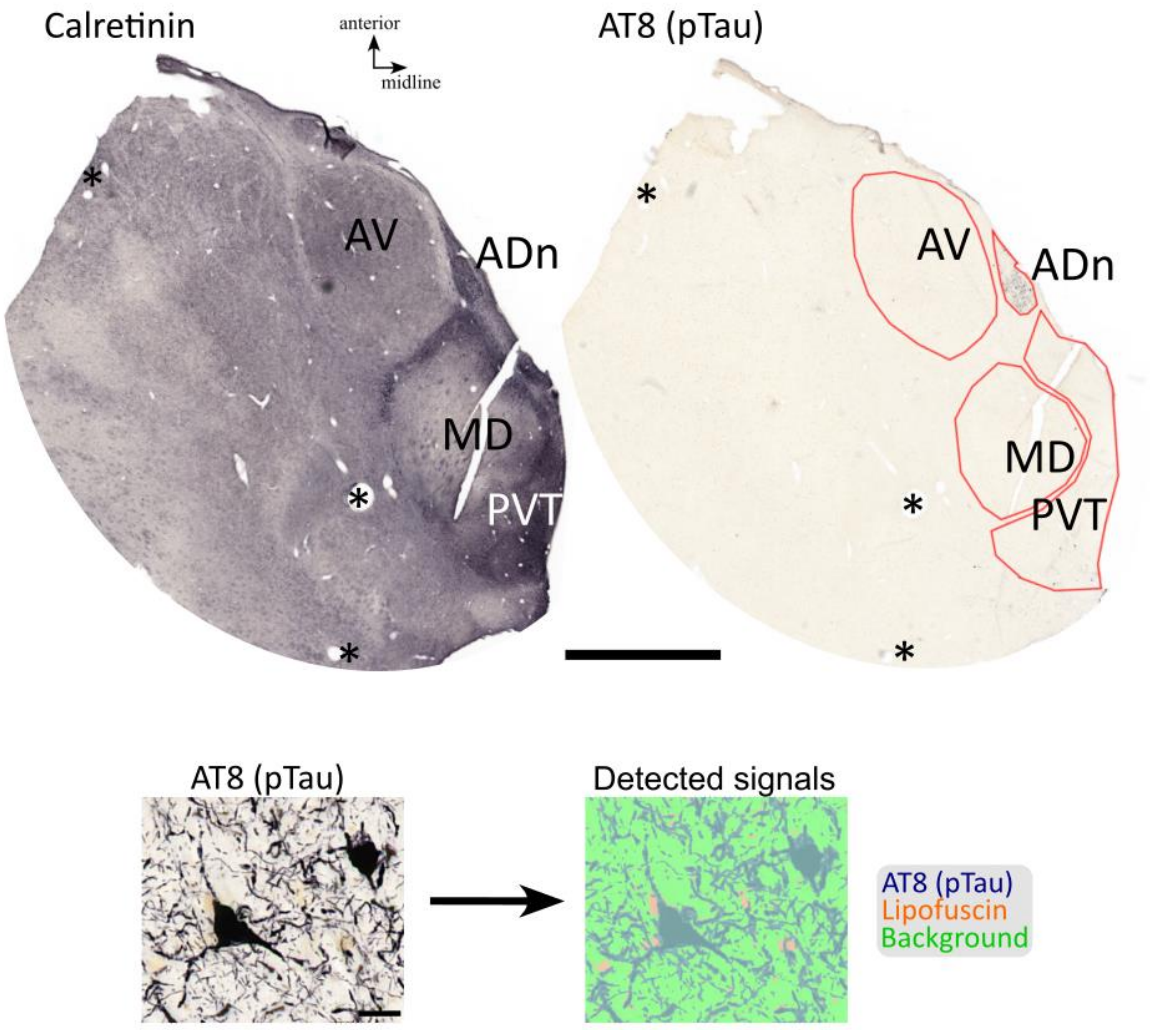


Figure 3.1 Identification of tau pathology in the rostral thalamus using pixel classifier
Thalamic nuclei were delineated by CR immunoreactivity (left), followed by AT8 signal detection (right) using a pixel classifier (see Methods). Braak stage III, Case 12. Abbreviations: ADn, anterodorsal nucleus; AV, anteroventral nucleus; MD, mediodorsal thalamic nucleus; iml, internal medullary lamina of thalamus; PVT, paraventricular thalamic nucleus. Scale bars: 2 mm, 30 μm (inset). Scale bars: 4 mm, 20 μm (enlarged ADn region).

3.3 Results

3.3.1 Delineation of thalamic nuclei with calretinin and other markers

Different molecular markers can be used to identify different thalamic nuclei. Calretinin immunopositive neurons in the thalamic sections were visualized with HRP-based DAB reaction end-product (Figure 3.2, Figure 3.4, Figure 3.9). In line with previous studies I found a high density of CR expression in cell bodies in the ADn, LD, internal medullary lamina of the thalamus (iml), along the midline in the PVT and in the RE. The MD mediodorsal thalamus (MD) and AV contained only a few CR immunopositive somata (Figure 3.2, Figure 3.4, Figure 3.9). This confirms that CR can be used to delineate the different rostral thalamic nuclei.

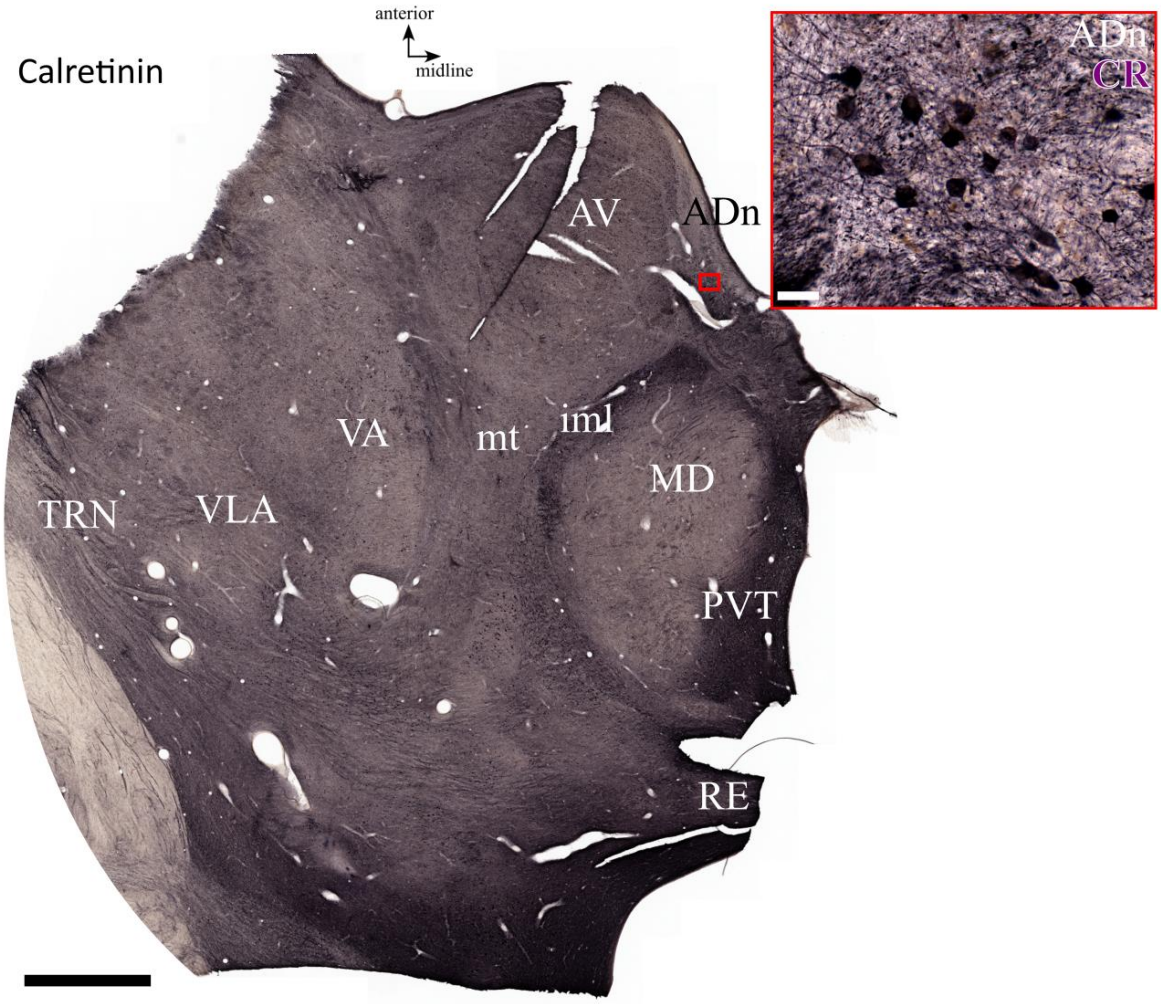


Figure 3.2 Thalamic regions delineated with calretinin immunoreactivity
Brightfield image of CR (CR immunoreactivity; HRP-based diaminobenzidine (DAB) end-product) in 50-µm-thick sections of rostral thalamus. Braak Stage VI, Case 17. Abbreviations: ADn, anterodorsal nucleus; AV, anteroventral nucleus; MD, mediodorsal thalamic nucleus; iml, internal medullary lamina of thalamus; PVT, paraventricular thalamic nucleus; RE, reuniens nuclear complex; TRN, reticular thalamic nucleus; VA, ventral anterior thalamic nucleus; VLA, ventral lateral ant. thalamic nucleus. Scale bars: 2 mm, 30 µm (inset).

3.3.2 The anterodorsal thalamic nucleus shows early and consistent vulnerability to Tau pathology

In order to determine how pTau may propagate in thalamus, I assessed early (Braak stages 0–II; *n* = 15), middle (Braak stages III–IV, *n* = 6), and late (Braak stages V–VI, *n* = 5) cases, comparing the rostral thalamus (*n* = 25 cases) to the cortex (hippocampal formation and cingulate areas) and to other subcortical areas (Figure 3.3 a-f, Figure 3.4, Figure 3.5, Figure 3.6, Figure 3.7, Table 3.1, Table 3.2, Table 3.4, Table 3.3, Table 3.5).

I examined rostral thalamic sections at different anterior-posterior levels between the level of the mammillary body and the level of red nucleus. I quantified pTau (AT8+) coverage and cells that were immunoreactive for pTau with AT8 antibody. I confirmed the data with a pTau-intensity scoring system in a larger number of samples comprising the perfusion-fixed sections and 10-µm-thick FFPE sections (Figure 3.3 i, j; Table 3.3).

To delineate the different nuclei in the sections showing pTau distribution images of whole sections were aligned with previously scanned sections showing nuclei delineated with CR. The density of pTau was detected with a pixel classifier based on neural network (Figure 3.1).

I found pTau+ neurons and processes (axons and dendrites) restricted to the ADn **in controls** (‘pre-Braak’ stage 0; n=4/6 cases; coverage=0.56%, pTau+ cells=1.29 mm^{-2}, intensity score=1; Figure 3.3 a, g-i, Figure 3.9 a; Table 3.3). This might suggest that Tau pathology is an age-related change.

In contrast to the ADn, when I examined all **early stages cases** (Braak stages 0-II, n=15 cases), I found that the other rostral thalamic nuclei, even those adjacent to the ADn, lacked pTau (Figure 3.3 a, Figure 4.4, Table 3.3, Table 3.4, Table 3.5). Among the postsynaptic targets of the ADn (Shibata 1993a, Shibata 1993b), both the EC and retrosplenial cortex (RS; Brodmann area (BA) 30, 29 and 26), but not the presubiculum (PreS), exhibited sparse pTau.

In the RS pTau also localised in terminals (EC score=1, n=3 cases, RS score=0.5, n=2 cases; Figure 3.3 b and j; Table 3.4).

At middle stages (Braak stages III-IV, n=6 cases), I found that the ADn contained moderate levels of pTau (coverage=8.54%, pTau+ cells=11.65 mm^{-2}, intensity score=2.65; Figure 3.3 c, g, h and i, 2; Table 3.3, Table 3.4, Table 3.5) whereas other nuclei showed sparse pTau (AV: coverage=0.15%, pTau+ cells=14.49 mm^{-2}, score=0.5; PVT: coverage=0.96%, pTau+ cells=1.91 mm^{-2}, score=1.38; Figure 3.3 c, g, h and i; Table Table 3.4, Table 3.5). In the cortical areas, pTau accumulated at moderate-to-intense levels, with the RS, EC and prosubiculum (ProS) showing intense pTau immunoreactivity; the PreS displayed sparse immunolabeling at this stage (RS score=3; EC score=3; ProS score=3; PreS score=1; Figure 3.3 d and j; Table 3.4). In the RS, pTau was concentrated in the granular RS (BA 29 and 26).

At late stages (Braak stages V-VI), which included cases with Alzheimer's disease (Table 3.1, Table 3.2) (Braak & Braak 1991c), intense pTau was observed in the ADn, with a high density of pTau+ cells (n=4/4 cases; coverage = 36.31%, pTau+ cells=118.89 mm^{-2}, intensity score=3; Figure 3.3 e, g, h and i, Figure 3.5; Table 3.4, Table 3.5). The LD showed a high pTau density in the late stages, matching that of the ADn (Figure 3.3 i and Figure 3.5; Table 3.4). The PVT had a similar pTau coverage to middle-stage ADn (n=5/5 examined cases; 11.62%, score=1.38; Figure 3.3 c, e, g and i, Figure 3.5; Table 3.3, Table 3.4, Table 3.5) and had the highest pTau+ cell count after the ADn (29.13 cells mm^{-2}). I observed that the RE was similarly affected (score=2). In contrast, the AV had lower coverage and pTau+ cell counts (coverage=6.28%, pTau+ cells=14.49 mm^{-2}, intensity score=1) followed by the MD, which remained relatively sparse compared to the other nuclei (coverage=1.62%, pTau+ cells=2.84 mm^{-2}, score=1.25; Figure 3.3 e, g, h and i; Table 3.3, Table 3.4, Table 3.5). The GABAergic thalamic reticular nucleus (TRN) lacked pTau immunopositive (pTau+) somata; only axons and axon terminals were pTau+ (coverage= 2.98%, pTau+ cells=0 mm^{-2}, score=2 Figure 3.3 e,

g, h and i, Figure 3.5, Table 3.4, Table 3.5), in line with previously published data (Tourtellotte et al 1990). In the cortex, pTau severely affected each examined area (Figure 3.3 f and j; Table 3.4), consistent with previous findings. (Braak & Braak 1991a).

In conclusion, the ADn is very early and severely affected, and the pathology in the thalamus progresses along Braak stages.

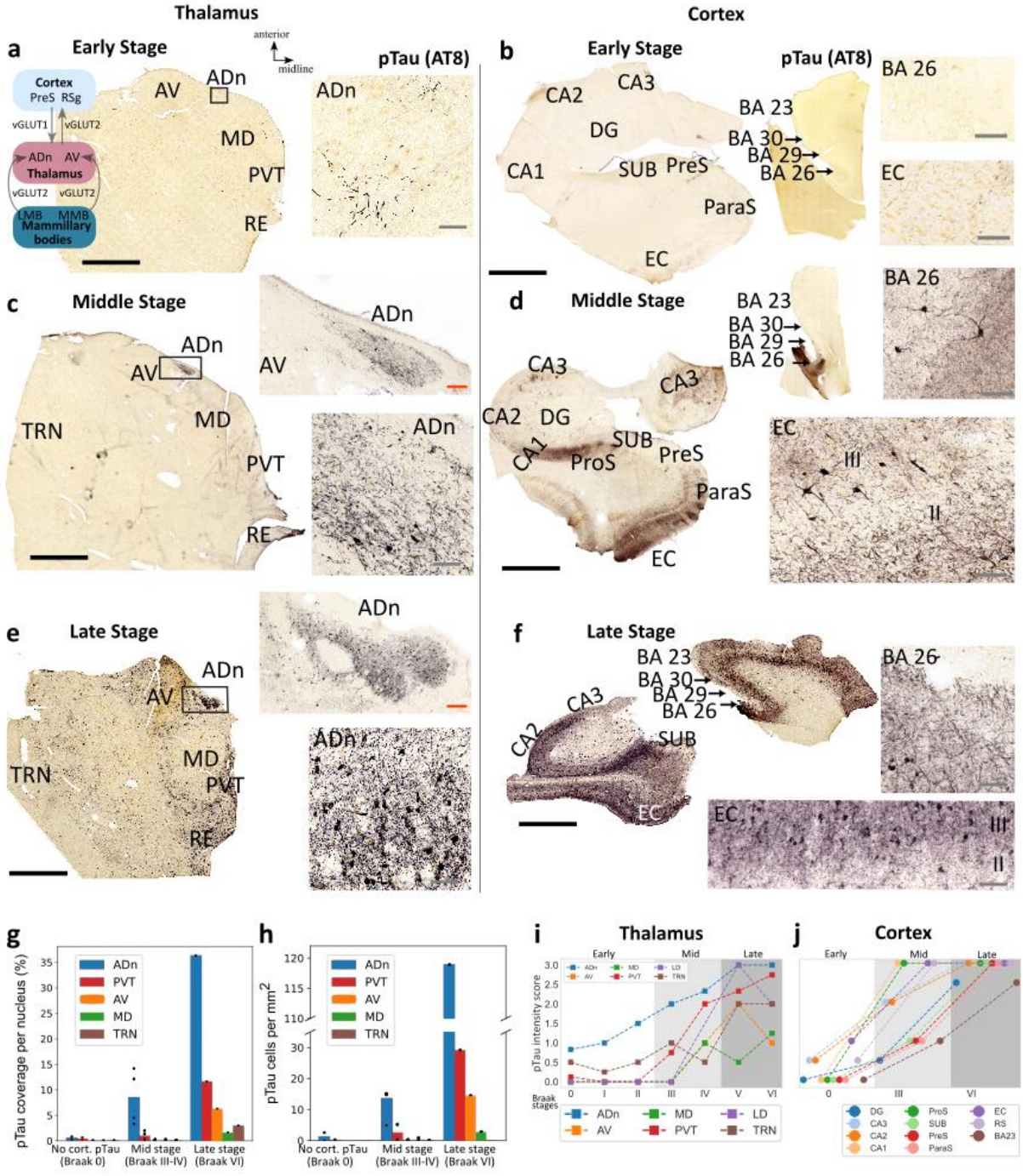


Figure 3.3 Progression of Tau pathology in the rostral thalamus and the cerebral cortex
(a-f) Brightfield images of pTau (AT8 immunoreactivity; HRP-based diaminobenzidine (DAB) end-product) in 50-µm-thick sections of rostral thalamus, hippocampal formation, parahippocampal gyrus, and cingulate gyrus. (a) Braak Stage 0, Case 5. Note pTau+ dendrites in the ADn (right). Inset, schematic of neural circuit. (b) Braak Stage 0, Case 5 (hippocampal formation) and Case 3 (cingulate gyrus). (c) Braak stage III, Case 12. (d) Braak stage III, Case 11 (hippocampal formation) and Case 12 (cingulate gyrus). (e) Braak stage VI, Case 17. (f) Braak stage VI, Case 19 (hippocampal formation) and Case 17 (cingulate gyrus). (g-h) Quantification of pTau coverage (g) and pTau+ cells (h) for early (n=2), middle (n=3), and late (n=1) stage cases. (i,j) Scoring of pTau intensity across different thalamic nuclei (n=26 cases) and cortical areas (n=8 cases). Scores: undetectable pTau (0), trace inclusions (0.5), sparse (1), moderate (2), dense (3). Median values are shown (see Table 3.5 for individual datapoints).

Abbreviations: ADn, anterodorsal nucleus; AV, anteroventral nucleus; MD, mediodorsal thalamic nucleus; PVT, paraventricular thalamic nucleus; RE, reuniens nuclear complex; TRN, reticular thalamic nucleus; DG, dentate gyrus; ProS, prosubiculum; ProS, presubiculum; ParaS, parasubiculum; EC, entorhinal cortex; BA, Brodmann area; RS, retrosplenial area (BA30, dysgranular retrosplenial cortex; BA29 and BA26, granular retrosplenial cortex); LMB, lateral mammillary nucleus; MMB, medial mammillary nucleus. Scale bars: black, 4 mm; red, 250 µm; gray, 80 µm.

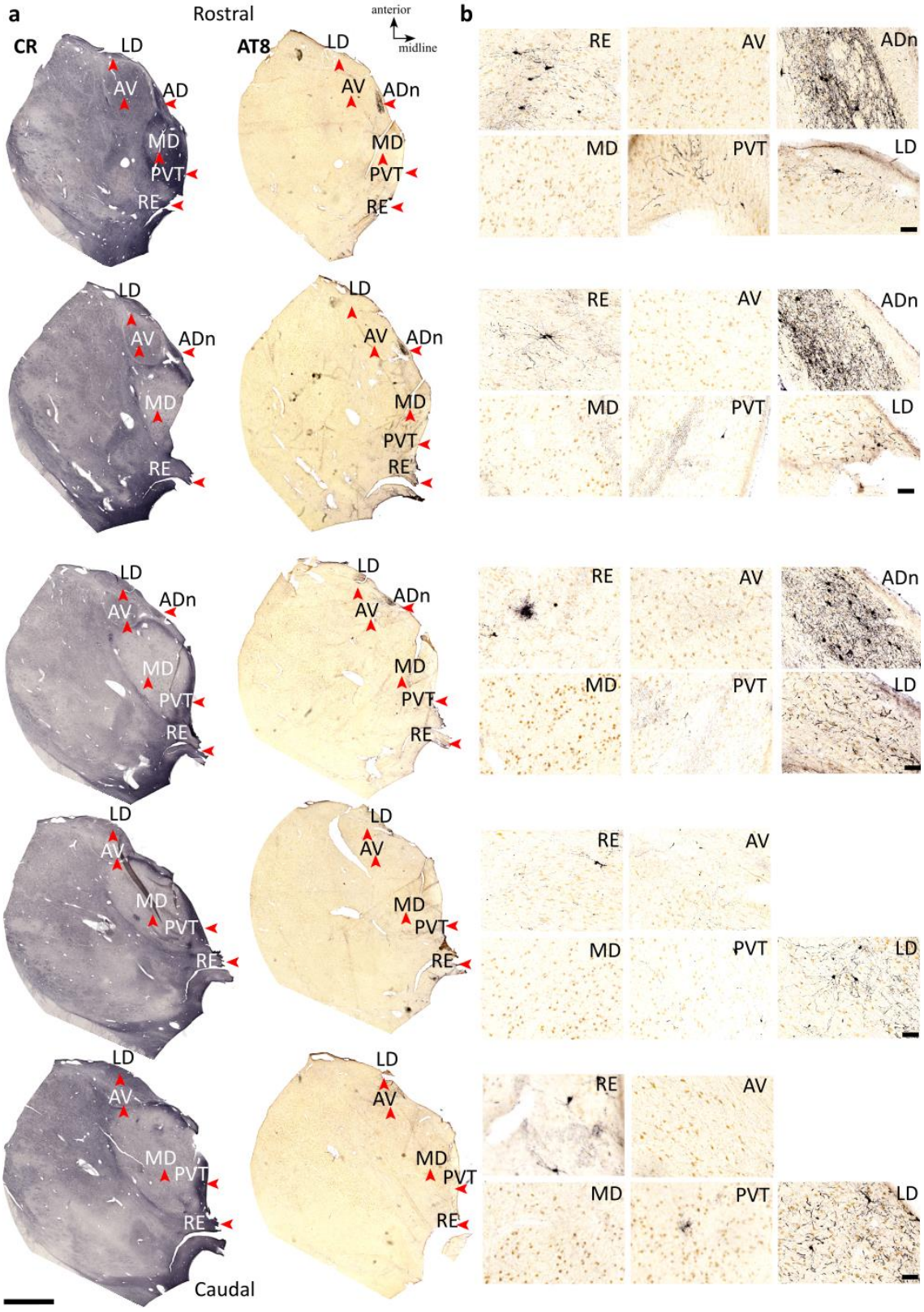


Figure 3.4 Serial sections of rostral thalamus for Braak stage III

(a,b) Serial sections showing the distribution of CR (left) and pTau (AT8, right) at different rostral-caudal levels by DAB-HRP immunoreaction (nickel intensified, grey/black). Note variable pTau immunoreactivity in the laterodorsal nucleus (LD) across the rostro-caudal axis. Sections are 100 µm apart (Case 12, Braak stage III). Scale bars: 4 mm (a), 100 µm (b).

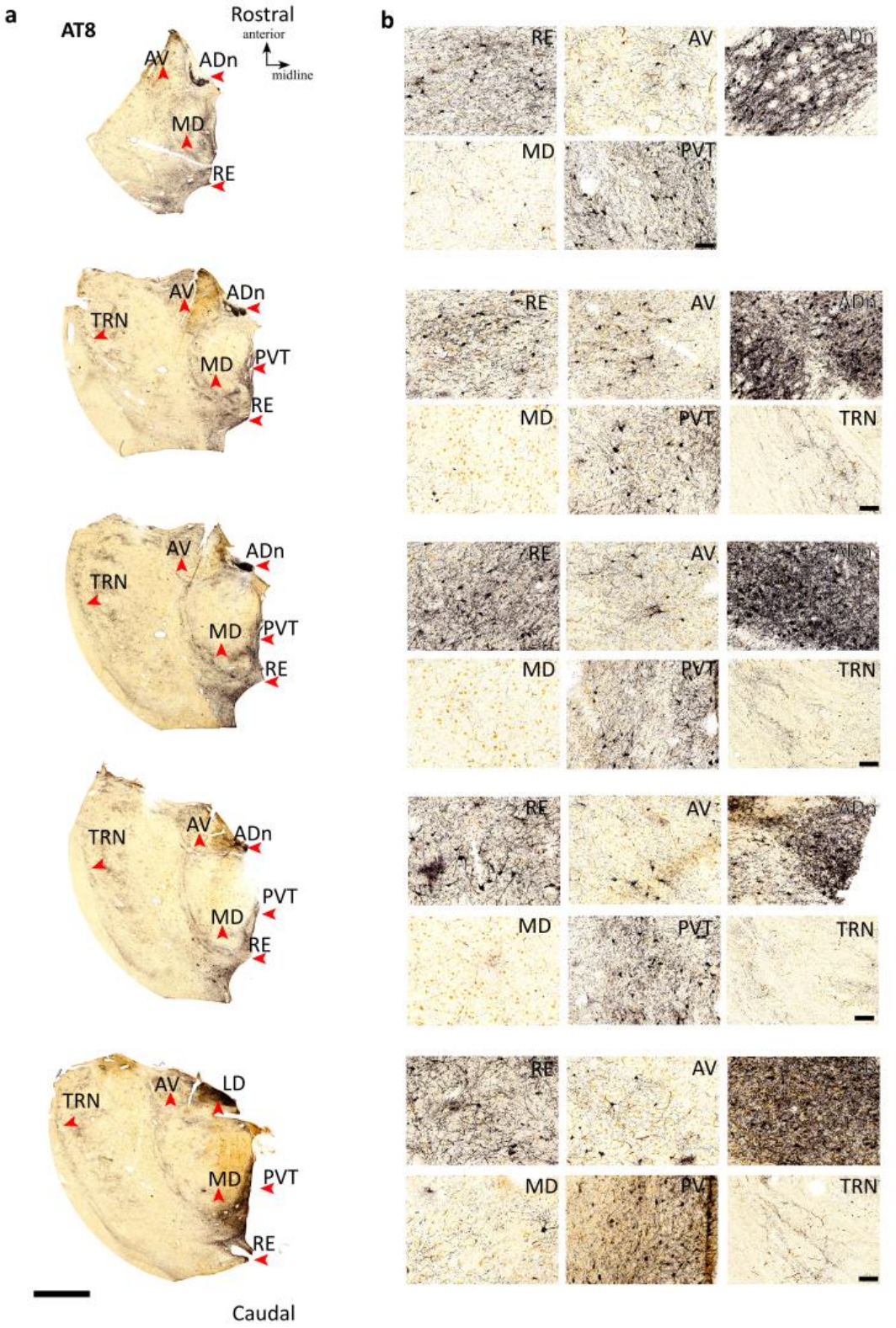


Figure 3.5 Serial sections of rostral thalamus for Braak stage VI
(a,b) Serial sections showing the distribution of pTau (AT8) at different rostral-caudal levels by DAB-HRP immunoreaction (nickel intensified, grey/black). Sections are 100 µm apart (Case 17, Braak stage VI). Scale bars: 4 mm (a), 100 µm (b).

Case	Group	Braak Stage	ADn	AV	MD	PVT	RE	LD	TRN	MMB	LMB	TM	LC	DRn	Evaluated sections
1	Early	0	++ (2/2)	- (2/2)	- (3/3)	- (2/3), + (1/3)	- (1/1)	- (2/2)	- (3/3)	NA	NA	NA	i (1/1)	NA	FFPE
3	Early	0	- (2/2)	- (2/2)	- (2/2)	- (2/2)	NA	NA	i (1/2), - (1/2)	NA	NA	NA	NA	NA	PFFF
4	Early	0	+ (3/3)	- (3/3)	- (3/3)	i (1/2), - (1/2)	i (3/3)	NA	i (3/3)	NA	NA	NA	NA	NA	PFFF
5	Early	0	+ (2/3), - (1/3)	- (3/3)	- (3/3)	i (3/3)	- (1/1)	NA	i (3/3)	NA	NA	NA	NA	NA	PFFF
22	Early	0	- (1/1)	- (1/1)	- (1/1)	- (1/1)	NA	NA	i (1/1)	NA	NA	NA	+ (8/8)	NA	PFFF
24	Early	0	+ (2/2)	- (1/1)	- (1/1)	- (1/1)	NA	NA	- (1/1)	- (6/6)	- (5/5)	- (6/6)	NA	NA	PFFF
20	Early	I	+ (2/2)	- (2/2)	NA	NA	NA	NA	NA	- (1/1)	- (1/1)	NA	NA	NA	FFIF
6	Early	I	NA	- (3/3)	NA	- (3/3)	- (2/2)	NA	NA	- (3/3)	- (3/3)	NA	i (1/1)	NA	FFPE
7	Early	I	+ (2/2)	- (3/3)	- (3/3)	+ (2/3), - (1/3)	- (2/2)	NA	- (3/3)	NA	NA	NA	- (1/1)	NA	FFPE
8	Early	I	NA	NA	- (3/3)	NA	NA	- (3/3)	NA	NA	NA	NA	i (1/1)	NA	FFPE
9	Early	I	i (1/1)	- (1/1)	- (1/1)	- (1/1)	NA	NA	NA	NA	NA	NA	+ (7/8) ++ (1/8)	NA	PFFF
2	Early	II	NA	- (3/3)	NA	- (3/3)	- (1/1)	- (3/3)	- (3/3)	- (2/2)	NA	- (3/3)	NA	NA	FFPE
23	Early	II	++ (5/5)	- (3/3)	- (3/3)	i (2/3), - (1/3)	i (3/3)	NA	i (3/3)	++ (2/2)	+ (1/1)	++ (2/2)	+ (7/7)	NA	PFFF
25	Early	II	++ (1/2), + (1/2)	- (2/2)	- (2/2)	NA	NA	NA	i (2/2)	NA	NA	NA	NA	NA	PFFF
26	Early	II	+ (2/3), ++ (1/3)	- (3/3)	- (1/1)	- (3/3)	i (1/1)	NA	i (1/1)	NA	NA	NA	i (3/4), + (1/4)	++ (4/4)	PFFF
10	Middle	III	+ (1/1)	- (1/1)	- (3/3)	- (2/3), + (1/3)	- (1/1)	- (3/3)	- (3/3)	NA	NA	NA	NA	NA	FFPE
11	Middle	III	++ (3/3)	- (2/3), + (1/3)	- (2/2)	i (2/2)	+ (1/1)	NA	+ (3/3)	NA	NA	NA	++ (6/6)	NA	PFFF
12	Middle	III	++ (3/3)	- (3/3)	- (3/3)	+ (3/3)	+ (2/2)	+ (3/3)	+ (3/3)	NA	NA	NA	++ (5/5)	NA	PFFF
13	Middle	III	++ (3/3)	+ (2/3), - (1/3)	+ (1/2), - (1/2)	++ (2/2)	+ (3/3)	NA	+ (3/3)	NA	NA	NA	NA	NA	PFFF
21	Middle	III	++ (2/2)	- (2/2)	NA	NA	+ (1/1)	NA	++ (3/3)	NA	NA	NA	NA	NA	FFIF
14	Middle	IV	++ (2/3), +++ (1/3)	+ (3/3)	- (1/1)	++ (3/3)	NA	NA	i (3/3)	+++ (6/6)	+++ (3/3)	+++ (3/3)	++ (4/4)	NA	PFFF
15	Late	V	+++ (3/3)	++ (3/3)	NA	++ (3/3)	NA	NA	++ (2/2)	++ (3/3)	NA	++ (3/3)	++ (1/1)	++ (1/1)	FFPE
16	Late	V	+++ (1/1)	NA	+ (3/3)	+++ (2/3), ++ (1/3)	++ (1/1)	+++ (2/2)	++ (3/3)	NA	NA	na	NA	NA	FFPE
17	Late	VI	+++ (3/3)	++ (3/3)	+ (3/3)	++ (3/3)	++ (3/3)	na	++ (3/3)	++ (7/7)	+++ (6/6)	+++ (5/5)	+++ (8/8)	NA	PFFF
18	Late	VI	NA	- (1/1)	++ (1/2), + (1/2)	+++ (1/2), ++ (1/2)	++ (1/1)	++ (1/1)	++ (2/2)	NA	NA	NA	NA	NA	FFPE
19	Late	VI	NA	NA	NA	NA	NA	NA	NA	NA	NA	NA	NA	NA	PFFF

Table 3.3 Intensity scores for pTau in subcortical brain regions

The distribution of pTau in each subcortical region was defined by the following scores per case: -, lacking detectable pTau; *i*, trace inclusions; +, sparse/mild; ++, moderate; +++, dense. Numbers in parentheses show the number of brain sections evaluated. Abbreviations: NA, brain region was not available; FFPE, formalin-fixed paraffin-embedded (10 µm thick); PFFF, perfusion-fixed free-floating (50 µm thick); FFIF, flash-frozen immersion-fixed (50 µm thick). *Immunofluorescence sections were used to evaluate thalamus.

Location Stage:	0	I	II	III	IV	V	VI
ADn	0(1), 1(2), 2(1)	1(2)	1(1), 1.5(1), 2(1)	1(1), 2(3)	2(1)	3(2)	3(1)
AV	0(4)	0(3)	0(4)	0 (3), 1(1)	1(1)	2(1)	2(1)
LD	NA	0(1)	0(1)	0(1), 1(1)	NA	3(1)	2(1), 3(1)
MD	0(4)	0(3)	0(3)	0 (3) 1(1)	0(1)	1(1)	1(2)
PVT	0(2), 0.5(2)	0(2)	0(2), 1(0.5)	0(1), 0.5(1), 1(1), 2(1)	2(1)	2(1), 3(1)	2(1), 3(1)
TRN*	0(2), 0.5(3)	0(2)	0(1), 0.5(3)	0(1), 1(4)	0(1)	2(2)	2(2)
RE	0(2), 0.5(1)	0(2)	0(1), 0.5(2)	0(1), 1(3)	1(1)	2(1)	2(2)
DG	0(3)	NA	NA	0(1), 0.5(1), 1(1)	NA	NA	2(1), 3(1)
CA3	0(1), 0.5(1), 1(1)	NA	NA	1(1), 2(1), 3(1)	NA	NA	3(2)
CA2	0(1), 0.5(1), 1(1)	NA	NA	1(1), 2(1), 3(1)	NA	NA	3(2)
CA1	0(2), 1(1)	NA	NA	2(1), 3(2)	NA	NA	3(2)
Prosubiculum	0(2), 2 (1)	NA	NA	2(2), 3(3)	NA	NA	3(2)
Subiculum	0(2), 1(1)	NA	NA	1(2), 2(1)	NA	NA	3(2)
Presubiculum	0(2), 0.5(1)	NA	NA	0(1), 1(2)	NA	NA	3(2)
Parasubiculum	0(2), 1(1)	NA	NA	1(2), 3(1)	NA	NA	3(2)
Entorhinal area	0(1), 1(1), 2(1)	NA	NA	3(3)	NA	NA	3(1)
RS (BA30, BA 29, BA 26)*	0(1), 1(1)	NA	NA	3(3)	NA	NA	3(2)
BA 23	0(2)	NA	NA	1(3)	NA	NA	3(1), 2(1)

Table 3.4 Intensity scoring for pTau in the rostral thalamus and cerebral cortex

The distribution of pTau in each area was defined by the following median scores: 0, lacking detectable pTau; 0.5, containing trace inclusions; 1, sparse; 2, moderate; 3, dense. Numbers in parentheses show the number of cases with that score out of the total in the given stage. *Axons containing pTau were sometimes present even when score 0 was given. For the RS, at early and middle stages, pTau was concentrated in BA 26 and 29, with one case (Case 12) exhibiting some pTau in BA 30. NA, not available.

Case	Braak stage	Thalamic nucleus	pTau coverage (%)	pTau cell frequency (cell/mm^2)
4	0	AV	0.07	0
		ADn	0.84	2.58
		MD	0.06	0
		PVT	0.66	0.32
		TRN	0.08	0
5	0	AV	0.09	0
		ADn	0.28	0
		MD	0.05	0
		PVT	0.11	0.04
		TRN	0.07	0
11	III	AV	0.08	0.11
		ADn	3.31	4.97
		MD	0.07	0.02
		PVT	0.13	0.05
		TRN	0.04	0
12	III	AV	0.17	0.03
		ADn	12.14	15.13
		MD	0.19	0
		PVT	0.4	0.47
		TRN	0.09	0
13	III	AV	0.31	0.32
		ADn	4.52	14.84
		MD	0.3	0.93
		PVT	1.99	5.2
		TRN	0.19	0.03
14	IV	AV	0.18	0.14
		ADn	14.2	19.59
		MD	-	-
		PVT	1.34	4.58
		TRN	0.07	0
17	VI	AV	6.28	14.49
		ADn	36.31	0
		MD	1.62	2.84
		PVT	11.62	29.13
		TRN	2.98	0

Table 3.5 Quantification of pTau coverage and immunopositive cell counts
Pixel-classifier quantification of pTau coverage and cell counts from perfusion-fixed tissue.

3.3.3 Involvement of mammillary bodies, locus coeruleus, and dorsal raphe at different Braak stages

To provide additional context for the very early subcortical tau pathology in the ADn, I also assessed the MB, LC and DRn which are susceptible to early pTau accumulation (Ehrenberg et al 2017, Gilvesy et al 2022). At early Braak stages, in contrast to the sparse-moderate levels of pTau in the ADn, pTau accumulation in the LC was weak and localised to neuronal processes (n=7/8 trace inclusions or sparse; n=1/8 lacking pTau; Figure 3.6 a, b, Table 3.3) (Braak et al 2011). In middle and late stages, there was moderate pTau in cell bodies, dendrites and axons (Figure 3.6 c, Table 3.3). Interestingly, I detected pTau+ in somata that contained neuromelanin which formed by the polymerisation of norepinephrine (Descarries & Saucier 1972). This indicates that the noradrenergic system is affected by tau pathology. Dysregulation of the norepinephrine in the LC has been associated with AD-related cognitive deficits and neuropsychiatric disorders including depression and anxiety (Matthews et al 2002, Zubenko & Moossy 1988). The DRn also showed moderate pTau in one tested Braak stage II case (Table 3.3b). The LMB, which projects to the ADn (Figure 3.3) (Veazey et al 1982), lacked pTau in n=3/4 early-stage cases (Figure 3.7 a, Table 3.3). In one Braak stage II case, the ADn showed moderate-dense pTau and the LMB showed mild-moderate pTau (Case 23, Table 3.3b). In middle and late stages, moderate-dense pTau was present in the LMB (Table 3.3 c, d, Table 3.3). The adjacent MMB which is presynaptic to the AV, and tuberomammillary nucleus had a similar pattern to the LMB (Table 3.3, Table 3.3). The data confirm previous findings (Andrés-Benito et al 2017, Braak & Braak 1991b, Ehrenberg et al 2017, Gilvesy et al 2022). Additionally, to the neuronal pathology, I observed pTau immunopositive astrocytes in the MB (Figure 3.7). To conclude, I have confirmed that other subcortical regions are involved early on in Alzheimer's disease in parallel with the thalamic pathology.

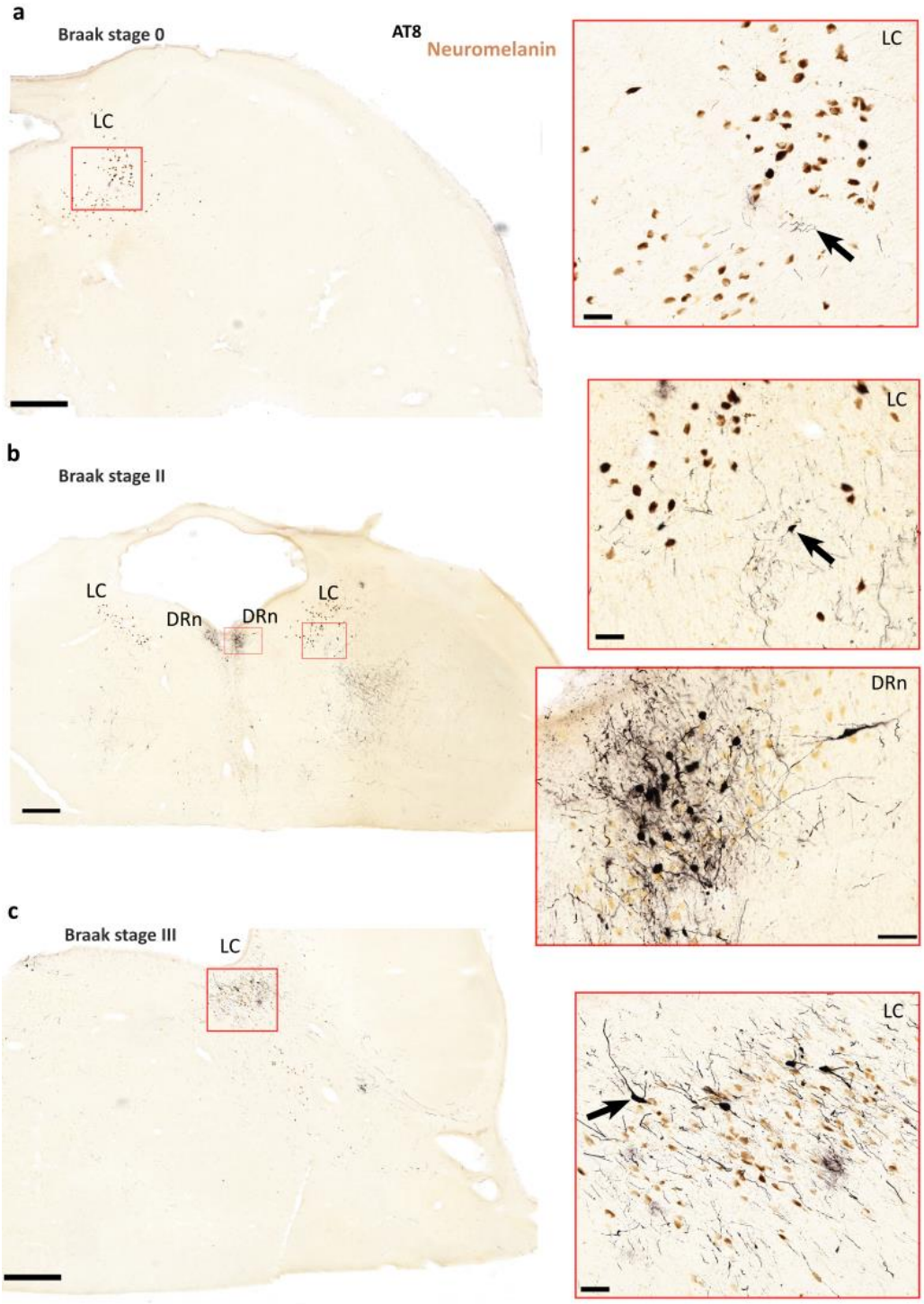


Figure 3.6 Tau pathology in the locus coeruleus and dorsal raphe nucleus in early-stage cases

(a-c) Brightfield images of pTau (AT8 immunoreactivity; HRP-based DAB end-product) in 50-µm-thick sections of the midbrain. (a) Sparse pTau restricted to axons or dendrites (e.g. arrow) in the locus coeruleus at Braak stage 0 (Case 22). Note lack of pTau within cell bodies that contain neuromelanin (brown). (b) Sparse pTau at Braak stage II (Case 26). Few small pTau+ cell bodies are detectable (e.g. arrow). In contrast, the DRn contains a higher density of pTau+ neurons. (c) Sparse pTau at Braak stage III (Case 12). Some cell bodies contain pTau (e.g. arrow). Scale bars: 1 mm (main); 100 µm (insets).

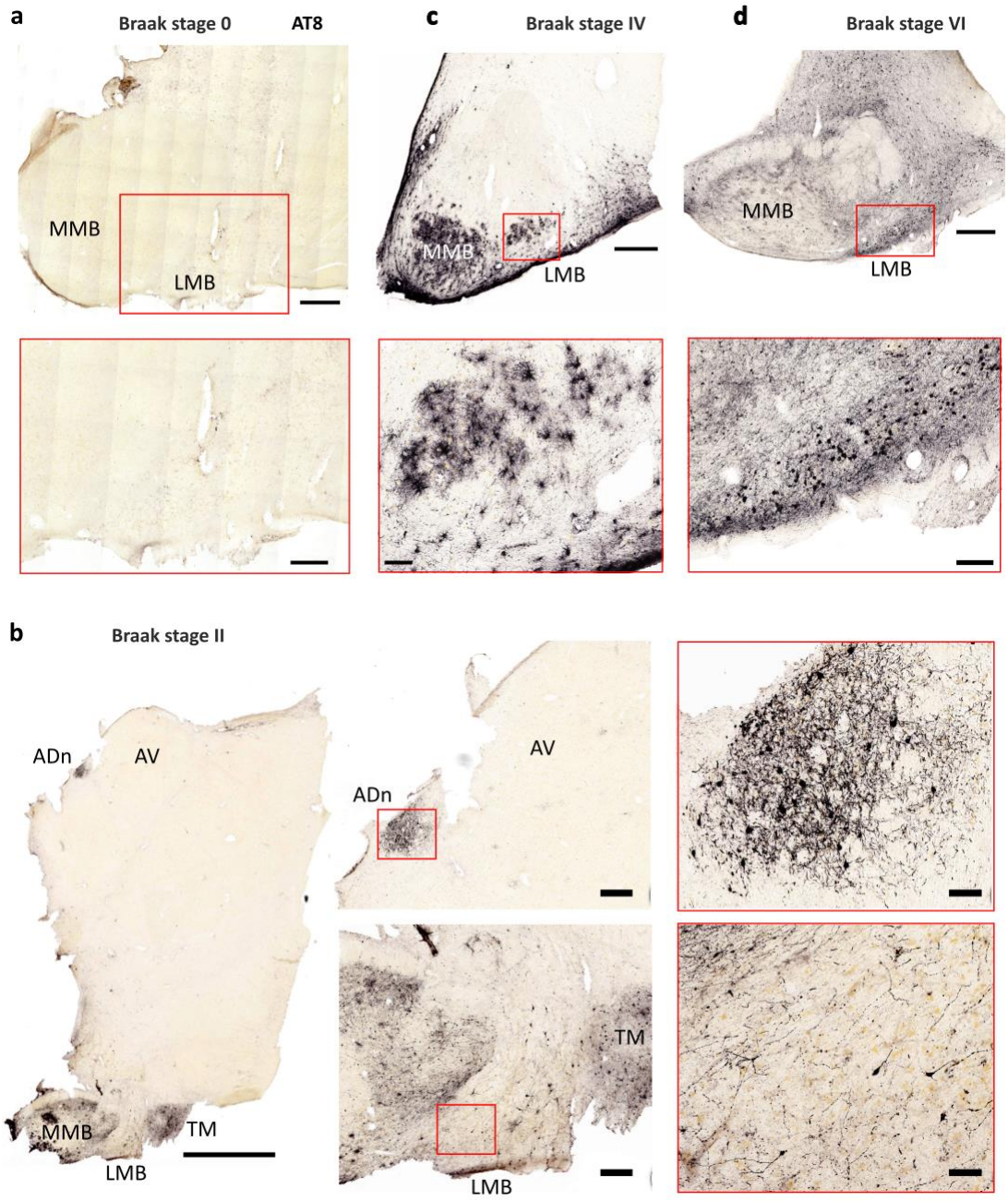


Figure 3.7 Accumulation of pTau in the mammillary body

(a-d) Brightfield images of pTau (AT8 immunoreactivity; HRP-based DAB end-product) in 50-µm-thick sections containing the mammillary body. (a) Lack of detectable pTau in the mammillary body at Braak stage 0 (Case 24). Inset, detail of region centered on the LMB. (b) A section containing both the rostral thalamus and mammillary body, Braak stage II (Case 23). The ADn contains a high density of pTau whereas the presynaptic LMB contains mild-moderate pTau. Right, detail of ADn and LMB. The MMB and TM contain moderate-dense pTau. (c) Tufted astrocytes containing pTau within the MMB and LMB in a Braak stage IV case (Case 14). Inset, enlarged view of LMB. (d) Dense pTau covering the entire mammillary body at Braak stage VI (Case 17). Inset, enlarged view of LMB. Scale bars: (a) 800 µm, 400 µm (inset); (b) 5 mm, 500 µm (middle insets) and 100 µm (right insets); (c) 800 µm, 100 µm (inset); (d) 1 mm, 250 µm (inset).

3.3.4 **Vulnerable neuronal cell populations in the anterodorsal thalamic nucleus**

To address which neuronal cell populations were affected by tau pathology, I tested different molecular markers (the number in brackets indicates the number of cases in which that immunohistochemical reaction was successful): PV, n=0/5 cases (n=2 PFFF, n=3 FFPE cases); CB, n=0/6 cases (n=3 PFFF, n=3 FFPE cases); CR, n=25/25 (n=15 PFFF, n=9 FFPE, n=3 FFIP cases) (Fortin et al 1998, Münkle et al 2000); and Purkinje Cell Protein 4 (PCP4), n=2/2 cases (n=2 PFFF cases) (Murray et al 2007) (Figure 3.8, Figure 3.9). I also tested complement C1q-like protein 2 (C1QL2) (n=0/1 case, (n=1 PFFF case), n=0/1 mouse), the mammalian target of rapamycin (mTOR) (n=0/1 case, (n=1 PFFF case), n=0/1 mouse), and patched domain containing 1 (Ptchd1) (n=0/1 case, (n=1 PFFF case), n=0/1 mouse), which are selectively expressed or enriched in the ADn (Roy et al 2021). From these markers only PCP4, CB, CR were detectable in human *post-mortem* brain sections using fluorescent immunohistochemistry. This can be explained by the impaired tissue quality due to *post-mortem* delay time and the limitation of the method and the specificity of antibodies. To the best of my knowledge, the distribution of PCP4 immunopositve neurons in the human thalamus have not been described. The expression of PCP4 was complementary to the distribution of CR. Similarly to monkey thalamus (Murray et al 2007) high density of PCP4 expressing neurons were found in the MD; moreover, the AV, the VA, the VLA and dorsal part of the LD contained high number of PCP4+ neurons. The ADn, the PVT and the RE only had a few PCP4+ neurons.

I performed double immunolabeling with AT8 (for pTau) and PCP4 or CB, or CR. I only observed one PCP4+ cell in the ADn that accumulated pTau (n=1/2 cases (n=2 PFFF cases)). Only the quality of AT8-CR double labelling allowed me to carry out a quantification (Figure 3.9 c, d).

I observed colocalization in neurons within the ADn, PVT, and RE (Figure 3.9 a, Figure 3.4, Figure 3.5) (Fortin et al 1998). In the TRN, CR-enriched neurons lacked pTau (Figure 3.9 f), consistent with the distinct lack of pTau+ TRN cell bodies (Figure 3.3 h). As the ADn contained pTau+ neurons even in control cases (Figure 3.3 a and h, Figure 3.9 a), I tested whether CR+ neurons were affected at early, middle and/or late stages. Even at Braak stage 0, CR was found in the majority of pTau+ neurons (64.3% CR+, n=1 case; Figure 3.9 a, b, and e). In the middle stage, a large proportion of pTau+ cells were CR+ (81.1%; n=3 cases; Figure 3.9 c and e), and in the late stage, 71.1% were CR+ (n=1 case; Figure 3.9 d and e). In conclusion, CR-expressing neurons were affected very early on, and at every stage, the majority of pTau immunopositive cells were CR+ in the ADn. In conclusion, pTau preferentially accumulates in CR-expressing neurons from Braak stage 0.

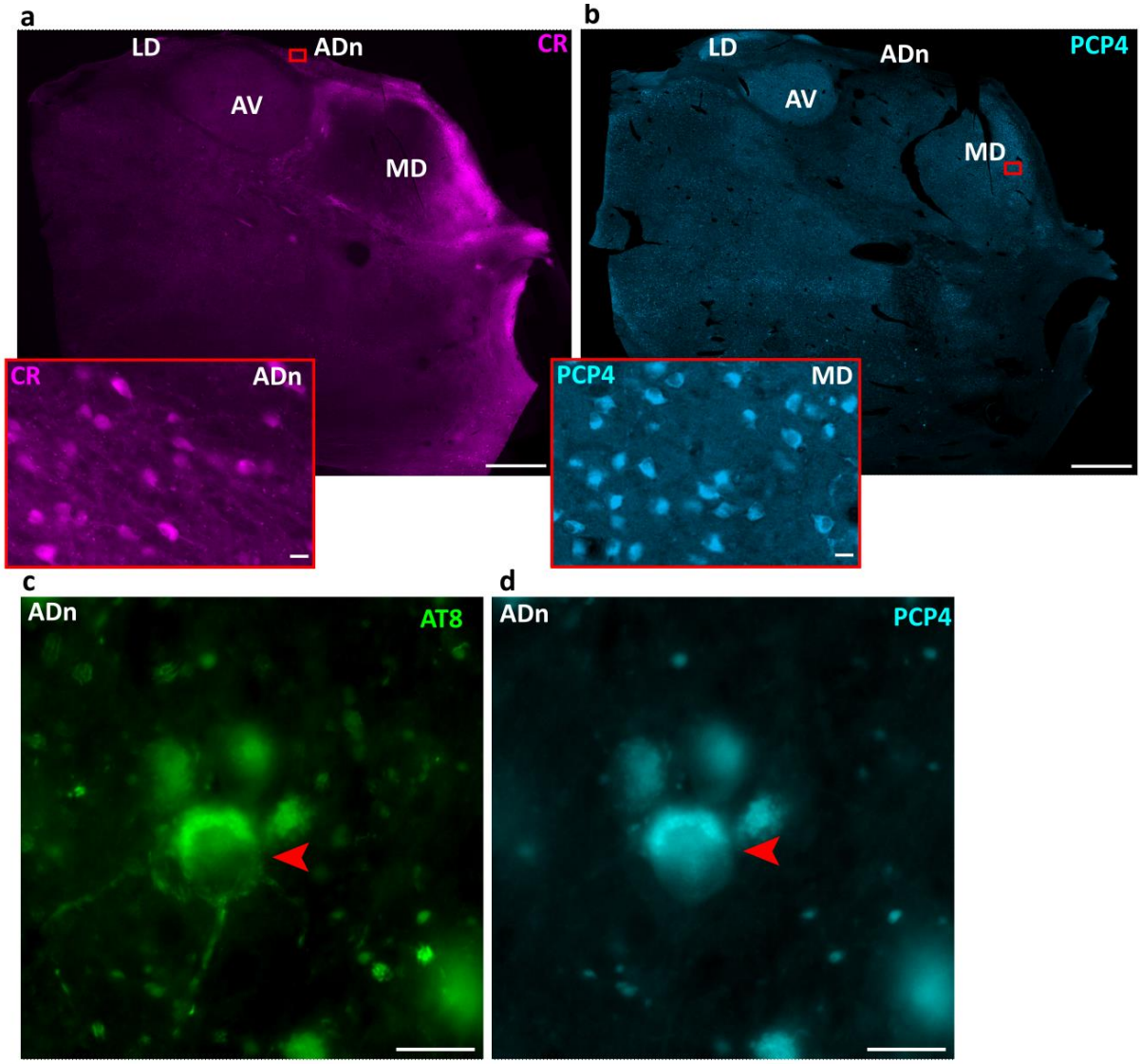


Figure 3.8 Calretinin expressing and PCP4 expressing neurons show complementary pattern in the human rostral thalamus

(a) Slide scanner images of the rostral thalamus immunoreacted for CR (Case 12, PFFF, 50-µm-thick section). Inset, detail of region centered on the ADn showing CR expressing neurons. (b) Slide scanner images of the rostral thalamus immunoreacted for PCP4 (Case 12, PFFF, 50-µm-thick section). Inset, detail of region centered on the ADn showing PCP4 expressing neurons. (c,d) Left, fluorescent image of a pTau+ cell (AT8+). Right the same cell showing immunopositivity for PCP4. Red arrowheads show the cell body. Scale bars: 2 mm (a,b); 20 µm (insets, a, b).

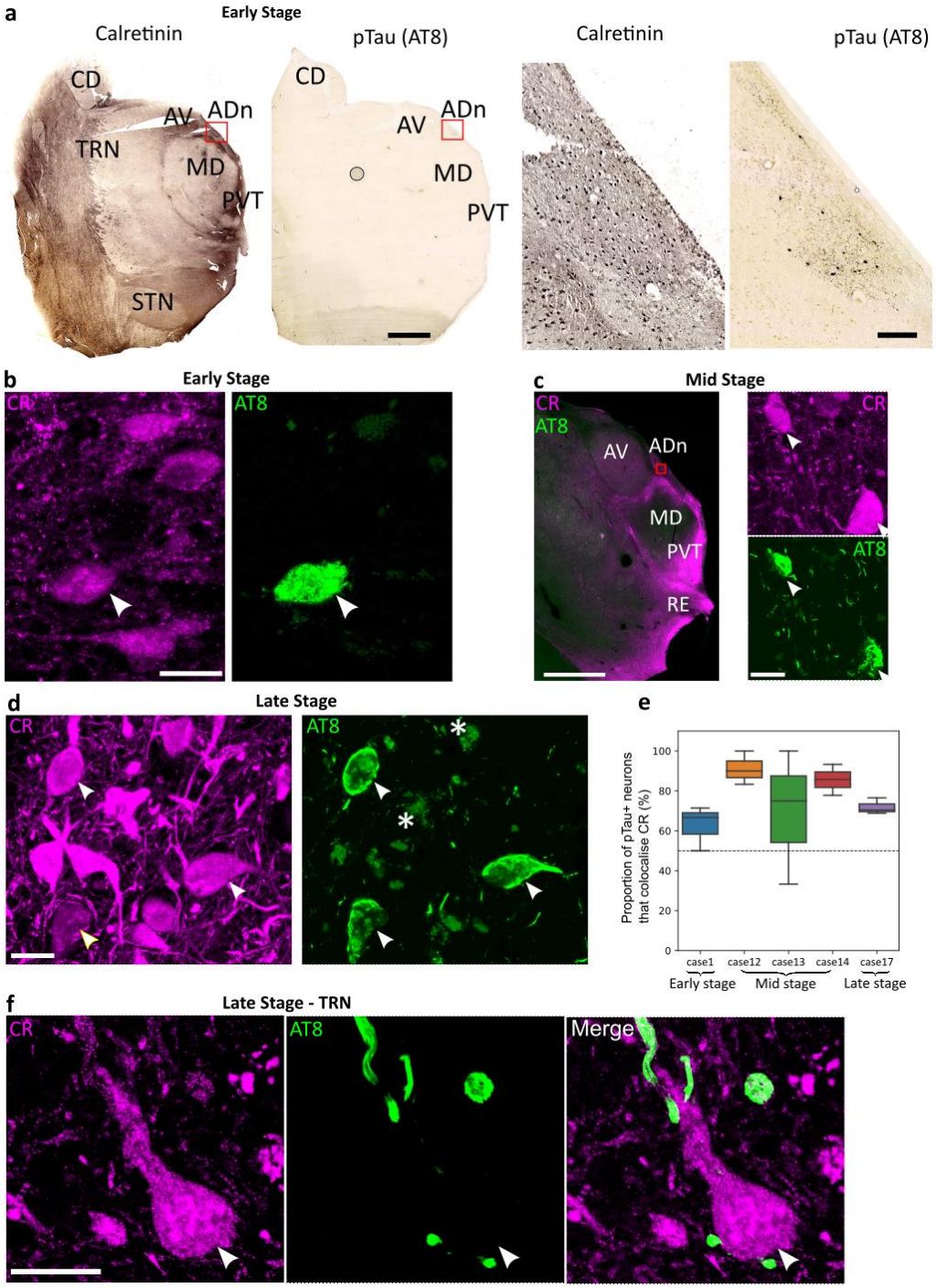


Figure 3.9 PTau-containing neurons in the anterodorsal thalamic nucleus express calretinin

(a) Brightfield images of the rostral thalamus at Braak Stage 0 (Case 1, FFPE, 10-µm-thick section). Left, adjacent sections immunoreacted for CR and AT8 (pTau) visualized with HRP-based DAB reaction end-product. Right, enlarged view of the ADn (red boxed region) revealing CR+ and pTau+ neurons. (b-d) Subpopulations of CR immunoreactive neurons (magenta) colocalize pTau (AT8, green; white arrowheads) in the ADn. (b) Early stage (Case 1, FFPE sample), confocal z-projection (5.7 µm thick). (c) Middle stage (Case 12, perfusion-fixed, 50-µm-thick section). Left, widefield fluorescence. Right, detail CR and AT8 colocalization in the ADn from an adjacent section (red boxed region), confocal z-projection (3.7 µm thick). (d) Late stage (Case 17, perfusion-fixed, 50-µm-thick section), confocal z-projection (3.9 µm thick). Faded green signal is lipofuscin (e.g. asterisks). (e) Box plots of the

percentage of AT8 immunoreactive cells in the ADn that were immunopositive for CR (early stage n=1, mid stage n=3, late stage n=1). (f) In the TRN, a CR+ neuron in close apposition to pTau+ boutons lack pTau (arrowhead, soma). Confocal z-projection, 2.2 µm thick (c). Scale bars: 4 mm (a left, c left); 250 µm (a right); 100 µm (c right); 20 µm (b, d, f). Abbreviations: CD, caudate nucleus; STN, subthalamic nucleus.

3.4 Discussion

3.4.1 Diagnosis of Alzheimer's disease

Determining which brain regions are affected first in Alzheimer's disease is crucial for early diagnosis and treatment. The current diagnostic approaches are not able to identify the disease early and precisely despite of the broad spectrum of tests. One of the main reasons is that co-pathology is frequent in patients. These tests can include cognitive tests (e.g. Mini-Mental State Examination), computed tomography scans (CT), magnetic resonance imaging (MRI), positron emission tomography (PET), genetic tests, and blood tests (Porsteinsson et al 2021, Roth et al 2023). Interestingly, for Parkinson's disease, a recently developed blood test able to predict the disease up to 7 years before symptoms onset. Furthermore, a promising blood test was developed in 2023 by Alzpath called the pTau217 assay to diagnose Alzheimer's disease. However, availability of pTau217 tests for research and clinical use has been limited (Ashton et al 2023, Kivisäkk et al 2024). The most accurate diagnosis for Alzheimer's disease can be only obtained by the *post-mortem* assessment of the brains. By focusing on the vulnerable areas of the thalamus imaging techniques such as MRI, fMRI can provide an earlier diagnosis.

3.4.2 Distribution of pTau

I observed that some of the rostral thalamic nuclei were affected by Tau pathology whereas others lacked pTau, the difference was striking, this is in accord with previous studies (Braak & Braak 1991b, Rüb et al 2016, Xuereb et al 1990).

I found that the ADn accumulated pTau even earlier than cortical regions including the EC and subiculum. In line with previous studies other subcortical regions including DRn, MB, LC also showed early sign of tau pathology (Ehrenberg et al 2017, Gilvesy et al 2022, Grinberg et al 2009, Thierry et al 2020). Nuclei adjacent to the ADn such as the AV and MD were relatively resistant to pTau, even in late stages, suggesting that in the thalamus, propagation of pTau is facilitated via specific synapses and circuits rather than geometrical proximity. The ADn, together with the AV and AM thalamic nuclei, comprise the anterior nuclear group, which forms one functional unit with the hippocampal formation and the mammillary bodies (the so-called Papez circuit) (Aggleton et al 2022, Forno et al 2021, Veazey et al 1982). (Aggleton & O'Mara 2022, Forno et al 2021, Veazey et al 1982). As a consequence, pathology of the anterior thalamic nuclei has been linked to the early cognitive biomarkers for Alzheimer's disease (episodic memory impairments and disorientation) (Aggleton et al 2016). Indeed, lesions of the anterior nuclear group impair spatial memory in rodents (Frost et al 2021, Mitchell & Dalrymple-Alford 2006, Perry et al 2018), and its degeneration in humans causes memory impairment (Harding et al 2000). Moreover, it has been shown that anterior thalamic nuclei are involved in the development of neuropsychiatric disorders such as schizophrenia and autism (Roy et al 2021).

In contrast to the well-defined connectivity of the Papez circuit, the diffuse widespread projections of the LC make it difficult to explain why the very early accumulation of misfolded forms of tau would propagate preferentially from the LC to the EC and not to all other areas the LC projects to (Braak & Del Tredici 2016).

3.4.3 Consistent pattern of the pathology and its potential implication

The early emerging pathology of ADn was consistent despite the diverse-, and multi-morbidity of the donors. Interestingly, of the four cases with schizophrenia, three of them had

pTau in the ADn. This can be explained by the age of the cases (61, 71, 84 years old) as the age is one the most important risk factors of Alzheimer's disease (Zhao et al 2020) although there are clinical and pathological analogies between Alzheimer's disease and schizophrenia including psychosis which is present in 50% of patients with Alzheimer's disease (White & Cummings 1996). This might indicate that ADn is involved in schizophrenia. Moreover, I found that the ADn was the most severely affected over the different Braak stages which is consistent with previous studies (Braak & Braak 1991b, Rüb et al 2016, Xuereb et al 1990). The ADn is involved is spatial navigation and contains head-direction cells (Taube 1995). The disorientation and impairment of spatial navigation is one of the earliest signs of Alzheimer's disease (Allison et al 2016). Thus, I hypothesize that the disrupted spatial orientation and navigation of Alzheimer's patients are arising from the accumulation of pTau in ADn. Tau pathology preferentially affected the calretinin-expressing subpopulation of glutamatergic neurons in the ADn, PVT and RE.

Neurons that are CR+ accumulated pTau even in Braak stage 0 and majority of the pTau+ neurons were immunopositive for CR in the ADn. This might alter the calcium homeostasis of the ADn (Ge et al 2022). An important question for future investigation is whether CR+ cells contain pTau because they are vulnerable to their accumulation or CR+ neurons are resistant, therefore, they might be able to survive for decades bearing pTau while in other neuronal cell populations the pTau accumulation leads to rapid cell death.

Interestingly, the TRN lacked pTau+ somata despite the high number of CR+ neurons. A possible explanation that the TRN consist of GABAergic neurons which are resistant to the accumulation of pTau.

3.4.4 Origin and subcellular distribution of pTau

If pTau had spread directly from the EC to the anterior nuclear group, we would have expected to detect pTau early on in the AV, but it was sparse even at the middle stage. An important difference between the anterior thalamic nuclei is that the ADn receives glutamatergic input from the LMB, whereas the AV and AM receive input from the MMB (Guison et al 1995, Hayakawa & Zyo 1989). To map the origin of pTau in the ADn it is critical to understand the subcellular distribution of pTau. One of the main questions is whether the cortical terminals or the subcortical terminals accumulate pTau earlier, this can be answered by identifying the boutons with different molecular markers such vGLUT1 and vGLUT2. Also, it is important to investigate whether pTau is able to spread between pre-, and postsynaptic sites.

3.4.5 Limitations of the study

The main limitation of most studies that assess human samples is the diversity among the donors including age, sex, education, comorbidities. The other limitation of human brain samples is that longer *post-mortem* delay times reduces the sample quality. To obtain well-fixed animal brain tissues perfusion fixation is a common practise but it rarely carried out in humans due to the technical challenges. We were able to obtain 15 cases processed with short *post-mortem* delay and with perfusion fixation, although the quality was variable. The quality of FFPE and FFIF sections were only adequate for the light microscopic study.

4 Results: Mapping the subcellular distribution of Tau filaments in *post-mortem* human thalamus at different disease stages and assessing amyloid-β plaque burden

4.1 Introduction

Two major hallmarks of Alzheimer's disease are amyloid-beta plaques and pathological tau proteins (Goedert et al 1988, Murphy & LeVine 2010).

Tau is a microtube associated protein that promotes microtubule assembly and stability. In some specific neurodegenerative diseases including Alzheimer's disease and cerebral palsy it becomes misfolded and loses its function. The amyloid-β plaques consist of amyloid-β peptides which are derived from amyloid-β precursor proteins which are cleaved by β-, and ɤ-secretase (Hur 2022). Both pTau and amyloid plaques accumulate in the different thalamic nuclei but their distribution is different (Braak & Braak 1991b).

The distribution of pTau correlates with cognitive decline and shows a specific pattern (Biel et al 2021, Goedert et al 1992, Li et al 1998). The propagation of pTau between different brains regions and between cells is not well-understood. To untangle the mechanism of spread it is crucial to understand which subcellular domains accumulate pTau. This is because they can indicate whether pTau is able to spread via synapses and whether it spreads in a retrograde and/or anterograde manner.

Tau proteins are thought to be localised in axons, and after becoming misfolded they are transported into other part of the cells (Christensen et al 2019, Iwata et al 2019). It has been challenging to detect and visualise pTau at the subcellular level in the human brain due to impaired tissue quality caused by *post-mortem* delay and due to the lack of adequate methods to preserve the brain. Although, early electron microscopic studies showed pTau in argyrophilic tubules of astrocytes and in oligodendroglia (Arima et al 1998, Nakano et al 1992).

Moreover, before the tau protein was identified (Cleveland et al 1977), neurofibrils resembling Tau filaments were shown by Terry and colleagues (Terry et al 1964, Terry 1963).

Surprisingly, the literature lacks detailed electron microscopic studies of the subcellular distribution of pTau even in animals despite the high tissue quality that can be achieved by brain perfusion without significant *post-mortem* delay. However, it is well-known that that the accumulation of misfolded tau within synaptic structures causes synaptic disfunction and synaptic loss (Hoover et al 2010, Kopeikina et al 2013).

There are several hypotheses about pTau propagation between cells. It has been shown that injection of brain extract from mutant P301S tau-expressing mice into wild-type tau-expressing mice induced the aggregation of tau into filaments and spreading from the site of injection to neighbouring brain regions (Clavaguera et al 2009). Moreover, it has been observed that the intracerebral injection of synthetic full-length wild type human tau mixed with dextran-sulphate causes tau propagation in mice (Masuda-Suzukake et al 2020). Many questions remained to be answered including whether pTau spreads across synapses, whether it spreads in retrograde and/or anterograde direction, and if it propagates as a monomer, oligomer or in fibrils? Are there synaptic structures that are more vulnerable than others, and if so, what biochemical conditions make these structures more vulnerable?

The ADn is a promising target to assess the subcellular distribution of pTau as this region accumulates pTau at very early stages of disease and adjacent areas; the AV and MD remarkably less vulnerable to pTau which might arise from their different connectivity and cell types. We were able to obtain brain tissues that were relatively well-preserved due to the relatively short (2-5 hour) *post-mortem* delay and perfusion fixation.

Each thalamic nucleus is innervated by different cortical and subcortical areas. Two vesicular glutamate transporters can differentiate a large portion of innervation: vGLUT1 indicates cortical origin, whereas vGLUT2 shows subcortical origin (Herzog et al 2001, Rovó

et al 2012). The ADn receives extensive input from the LMB (Guison et al 1995, Hayakawa & Zyo 1989) which comprise mainly large vGLUT2+ boutons, and cortical input primarily from the RSg and PreS (Mathiasen et al 2020). Furthermore, it has been shown that the ADn even receives direct input from the retina in rats (Itaya et al 1981, Mathiasen et al 2020).

Thalamic boutons have been classically divided into four groups: the large "RL" and small "RS" terminals contain round vesicles of uniform size. The F terminal contains a mixture of small round and flat vesicles. The P profile contains a relatively sparse population of vesicles showing a great variation in size (Partlow et al 1977).

For the purposes of clarity, in this thesis I refer to boutons by their size, shape and molecular identity, rather than these classical terms.

The main questions are which subcellular domains and particularly which specific kinds of boutons accumulate pTau in the ADn.

4.2 Methods

4.2.1 Initial electron microscopic assessment of brain sections

To assess the quality of thalamic sections without any immunoreactions, sections were post-fixed in glutaraldehyde fixative to preserve the cellular structures (2.5% GA, ~0.2% w/v picric acid, 4% paraformaldehyde in 0.1 M PB) for 1–2 h, dehydrated in descending series of ethanol and embedded in epoxy resin. The quality was determined by the density of the recognisable cellular structures with a particular focus on synapses.

4.2.2 Single- and double-labelling pre-embedding immunohistochemistry for combined light and electron microscopy

Free-floating sections (Table 3.2) were washed then blocked in 4% (vol/vol) NGS. Next, sections were incubated with primary antibodies (Table 2.1) in TBS for 3 days at 4 °C. Sections were incubated overnight at 4 °C in CWFS solution containing biotinylated secondary antibody and/or immunogold-conjugated secondary antibodies immunogold. After repeated washes, sections were incubated overnight at 4 °C in avidin + biotin-HRP complex diluted in TBS. Tissues were treated with enhancement conditioning solution (ECS). To visualize immunogold particles, sections were incubated in silver enhancement solution (SE-LM, Aurion) for 20 min at 20 °C in the dark and then washed in ECS. Peroxidase was visualized using DAB (0.5 mg/mL) as chromogen developed with 0.01% H2O2.

Subsequently, sections were treated with 0.5% OsO4 in 0.1 M PB for 20 min on ice in the dark. To enhance contrast, sections were incubated in 1% uranyl acetate diluted in distilled water or diluted in 70% ethanol after incubation in 50% ethanol. Next, the dehydration of sections was carried out in an ascending alcohol series, followed by acetonitrile; then sections were embedded in epoxy resin. After overnight incubation at RT, they were transferred onto glass slides. To polymerize epoxy resin, sections were incubated at 55 °C for 2 days.

4.2.3 Electron microscopy

Data were collected from one thalamus section/case, from which two areas were assessed. Samples were selected from 4/13 tested cases that had sufficient quality for analysis. Three samples (3 blocks from 3 cases) were assessed by Prof Peter Somogyi (78/336 synapses) who was blind to the Braak stages. Only synaptic structures were quantified. Electron opaque ('dark') boutons were excluded from the analysis due to the likely loss of antigenicity. Dark bouton frequency was as follows: Case 12, 0% (0/104), Case 25, 2.8% (n = 3/106), Case 4, 28.57% (n = 20/70); Case 17, 29.13% (n = 30/103). Tissue quality prevented an unbiased synapse density quantification, because of the large spaces among cellular profiles; therefore, random sampling of synapses was carried out. The frequency was influenced by the size of the boutons and dendrites. Structures were followed through 4–5 serial sections (~4.7 sections/structure). The primary magnification was 1500–3000×, then the structures were imaged and identified at 1500–6000× magnification. Background immunolabelling for AT8 was very low. Immunopositivity of a cellular profile for AT8 was defined by the presence of at least one silver–gold particle (~12.1 particles/structure on average). Bouton area was measured across three serial electron micrographs and the average was calculated. Boutons without distinct membranes were not included in the analysis.

4.2.4 Imaging

Light microscopy

Brightfield images were acquired with a Zeiss AX10 microscope using an AxioCam HRc camera (63×/1.4 objective).

Slide scanner

Glass slides were digitized using a Pannoramic MIDI II scanner (3DHISTECH; Budapest, Hungary) with a Plan- Apochromat objective lens (20× magnification, NA 0.8, lateral

resolution 0.346 × 0.325 μm/pixel) and pco.edge 4.2 4 MP camera. For transmitted colour brightfield images, three focus levels were applied. Representative images were captured in CaseViewer.

For electron microscopy, specimens were studied on three microscopes: a Jeol 1010 transmission electron microscope equipped with a digital GATAN Orius camera, at the Department of Physiology, Anatomy and Genetics, Oxford University; a JEOL 1400 transmission electron microscope equipped with a Rio digital camera, at the Sir William Dunn School of Pathology, Oxford University; and a Hitachi 7100 electron microscope with a Veleta CCD camera (Olympus Soft Imaging Solutions, Germany), at the Institute of Experimental Medicine, Budapest, Hungary.

4.3 Results

4.3.1 Subcellular distribution of pTau in the human ADn

To define synaptic structures at different stages of tau pathology, I assessed ultrathin (~50–60 nm) sections of the ADn. I obtained electron microscopic samples from 4 cases (Cases 4, 12, 25, 17) that were appropriately preserved for analysis (Figure 4.1 a–d; Braak stages 0, II, III, and VI).

To localise pTau to subcellular structures, a challenging but informative method is labelling tau filaments with gold-silver particles for electron microscopy. The advantage of this method is that tau filaments can be clearly visualised with the bound gold-silver particles compared to HRP-based DAB reaction which gives a diffuse signal and does not allow the precise identification of subcellular domains that accumulated the targeted antigens (Figure 4.1, Figure 4.3).

As it was expected after light and fluorescent microscopic assessments, cell bodies contained tau filaments (Figure 4.1 e). Previously, similar filaments were observed in the cortex of donors who had Alzheimer's disease (Arima 2006, Kidd 1963, Terry et al 1964, Terry 1963). These cells also accumulated lipofuscin (Figure 3.9 d, Figure 4.1 e) which is a complex mixture of oxidized cross-linked macromolecules such as protein, lipids, and sugars. As it is polymeric and highly cross-linked cannot be degraded (Moreno-García et al 2018).

Filaments immunolabelled for pTau were also localised to dendrites (Figure 4.1 f; Figure 4.7 d, g, h), and were aggregated into large bundles (>1 μm) (Figure 4.1 g). Tau filament bundles were immunolabelled predominantly on the cytoplasmic surface, most likely due to reagents not penetrating into the bundle (Figure 4.1 g). I also observed pTau in myelinated axons (Figure 4.1 h). In conclusion, tau filaments localised to a wide variety of subcellular compartments.

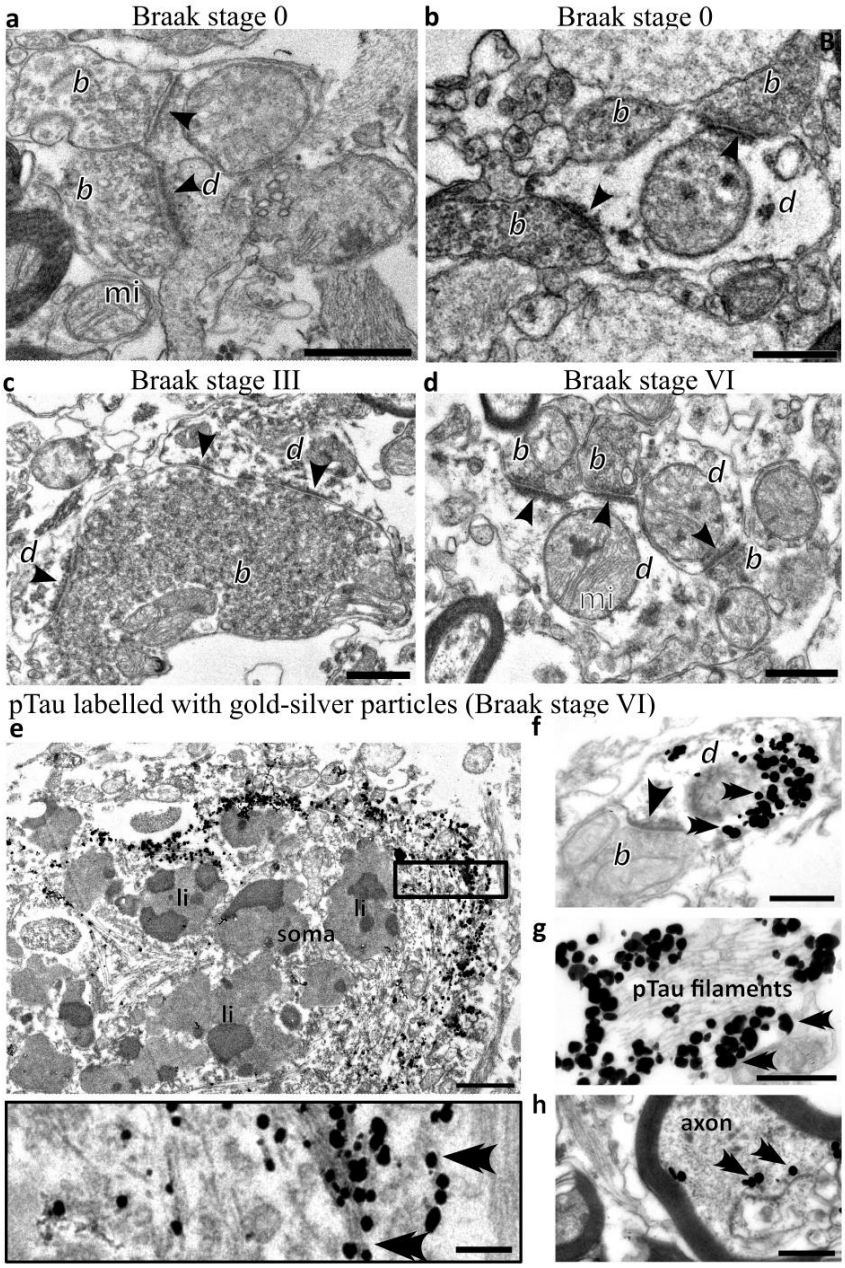


Figure 4.1 Electron micrographs of synaptic elements and tau filament bearing soma, dendrite and myelinated axons in the human anterodorsal thalamic nucleus

a–d Unlabelled synaptic boutons (*b*) and dendrites (*d*) forming synaptic junctions (arrowheads): a,b early stage (Braak stage 0, Cases 3 and 4); c middle stage (Braak stage III, Case 12); a large bouton containing a high density of synaptic vesicles forms multiple synapses with its postsynaptic partners; d late stage (Braak stage VI, Case 17), small terminals form junctions (arrowheads) with small calibre dendrites. e–h Immunolabelling for pTau (AT8, gold–silver particles, all from Case 17, stage VI): e localization of ptau in a cell body containing lipofuscin (li); inset, detail of the boxed region showing immunolabelled pTau filaments (double arrowheads mark gold–silver particles); f a thin, pTau+ dendrite receiving an asymmetric synapse (arrowhead) from a small bouton (b); g high power image of paired helical filaments associated with silver intensified immunogold particles demonstrating pTau immunoreactivity; h pTau immunolabelling in a myelinated axon. Mitochondrion, mi. Scale bars: 0.5 μm (a–h), 0.25 μm (e inset).

4.3.2 Different subcellular compartments of CR-expressing cells accumulate pTau

As described in Chapter 3 (Figure 3.9), CR-expressing neurons were found to be vulnerable to pTau accumulation from as early as Braak stage 0, with the majority of pTau immunopositive neurons showing CR immunoreactivity.

Next, my aim was to identify which subcellular compartments of CR-expressing neurons accumulate pTau (Case 17; Figure 4.3). From n=1 section I observed tau filaments in dendrites in post-synaptic structures that showed signs of degeneration e.g. damaged mitochondria, and both sites of dendrodendritic gap junctions (Figure 4.3 a,b,c). Moreover, pTau was localised to myelinated axons (Figure 4.3 d). The lack of pTau in boutons might have been caused by the limitation of the sampling. In conclusion, pTau is not restricted to the cell bodies and axons of CR-expressing neurons but can spread to dendrites.

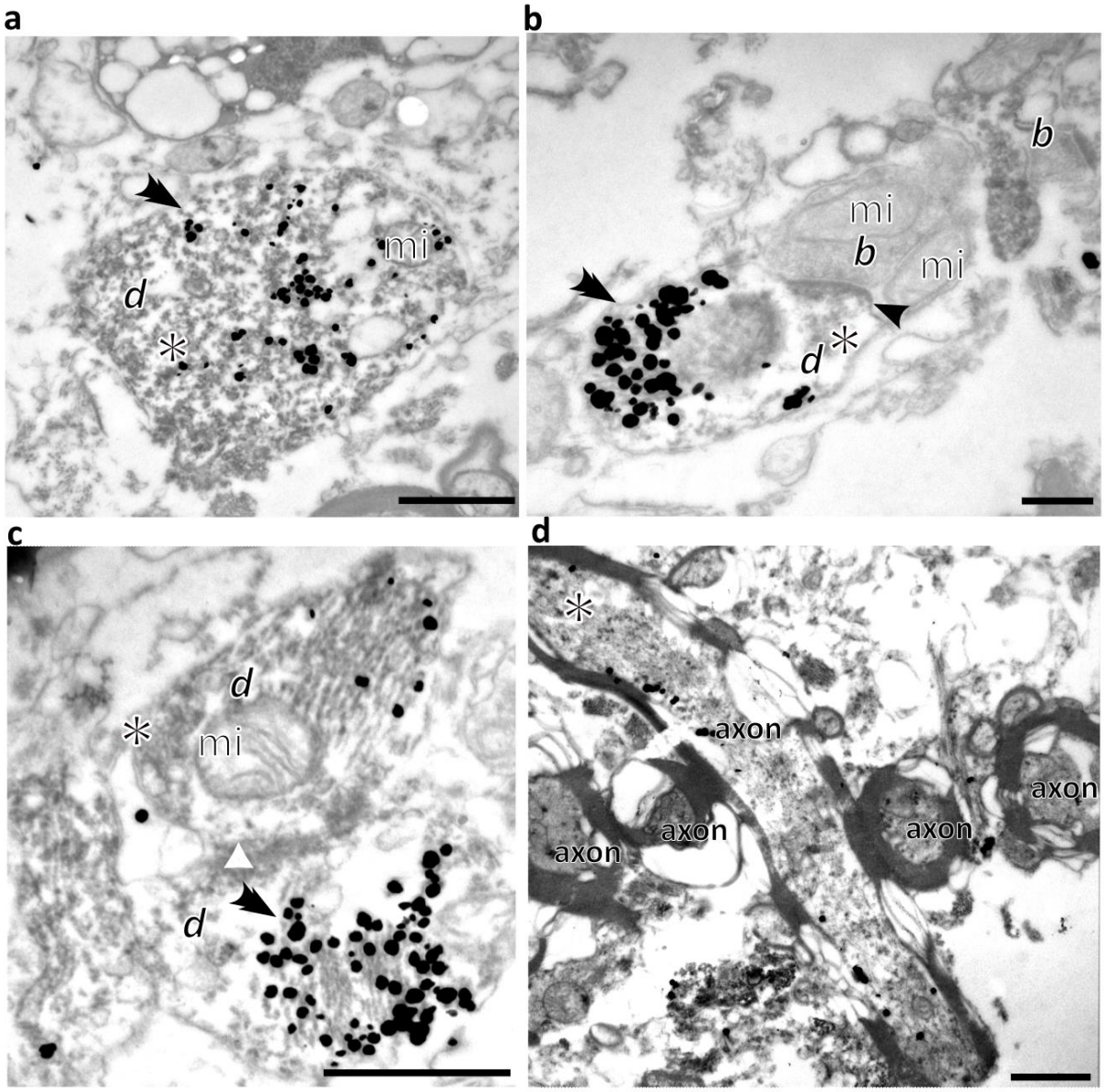


Figure 4.2 A range of subcellular compartments from CR-expressing neurons contain tau filaments in the human anterodorsal thalamic nucleus

(a-d) Electron micrographs (~50 nm thick) from Case 17, Braak stage VI. Double arrowheads highlight gold–silver particles recognising tau filaments (AT8); asterisks mark CR (HRP-based DAB end product). (a) Localisation of pTau to a CR-expressing dendrite**.** (b) Degenerating dendrite immunopositive for CR forming a synaptic junction (arrowhead) and containing tau filaments. (c) Dendrites immunopositive for CR forming a dendrodendritic gap junction (white arrowhead); both sites bear tau filaments. (d) Myelinated axon double immunopositive for CR and pTau. Scale bars: 1 μm.

4.3.3 Identification of small corticothalamic and large subcortical synaptic boutons

In the ADn I observed two main types of synaptic boutons with asymmetric synapses: large ~1–8 μm boutons (Figure 4.1 c; Figure 4.5 a–c), consistent with presynaptic axon terminals from the mammillary body (Somogyi et al 1978) and small <1 μm diameter boutons (Figure 4.1 d; Figure 4.5 a–c), resembling cortical presynaptic terminals (Sherman & Guillery 1998).

I asked which boutons are susceptible to accumulate pTau. Some presynaptic boutons from stage 0 (n = 20/70), stage II (n = 3/106), and stage VI (n = 31/103) had an electron opaque ('dark') appearance with degenerating cellular compartments such as mitochondria and vesicles (Figure 4.7 c). Some of these boutons contained large double-walled vesicles (80-100 nm) which might be autophagosomes (Figure 4.5 d) (Boland et al 2008, Nixon et al 2005).

Dark terminals can occur by *post-mortem* delay/inadequate fixation or this can be sign of neurodegeneration (Colonnier 1964, Szentágothai et al 1966).

4.3.4 Large subcortical vesicular transporter 2-expressing presynaptic terminals preferentially contain pTau

Large presynaptic terminals of subcortical origin contain vesicular glutamate transporter 2 (vGLUT2) (Rovó et al 2012). I observed a striking overlap between the distributions of vGLUT2 and AT8 immunoreactivities at the light microscopic level, especially in the ADn, RE, PVT, and internal medullary lamina (Figure 4.5 a). I hypothesized that this overlap indicates a strong association between vGLUT2 and pTau which is supported by the observation that thalamic nuclei that receive dense glutamatergic input might be predisposed to pTau accumulation (Xuereb et al 1990). My experiments provided additional information regarding the origin of the glutamatergic input that might facilitate pTau accumulation in distinct thalamic nuclei. Thalamic sections were immunoreacted for both vGLUT2 and AT8

which revealed that pTau was localised to vGLUT2+ boutons (Figure 4.5 b, e, f; Figure 4.7 b, d), confirming the hypothesis. Whereas some vGLUT2+ boutons showed no signs of abnormalities (Figure 4.5 c), others were degenerating (Figure 4.5 d; Figure 4.7 c). The degenerating vGLUT2+ boutons had clumped mitochondria (Figure 4.5 d). In several degenerating boutons which were immunoreactive for both vGLUT2 and pTau, tau filament bundles occupied a large proportion of the volume crowding out vesicles (Figure 4.5 b, e), which may disrupt neurotransmission. I also observed synaptic structures consisting of presynaptic vGLUT2+ boutons and postsynaptic dendrites that *both* contained pTau (Figure 4.5 f; Figure 4.7 d), suggestive of transsynaptic spread between the neurons of the mammillary bodies and ADn (Figure 6.1; Figure 3.7 b). The size distribution of pTau-positive terminals also confirmed that large rather than small presynaptic terminals preferentially accumulate pTau (Figure 4.5 a–c).

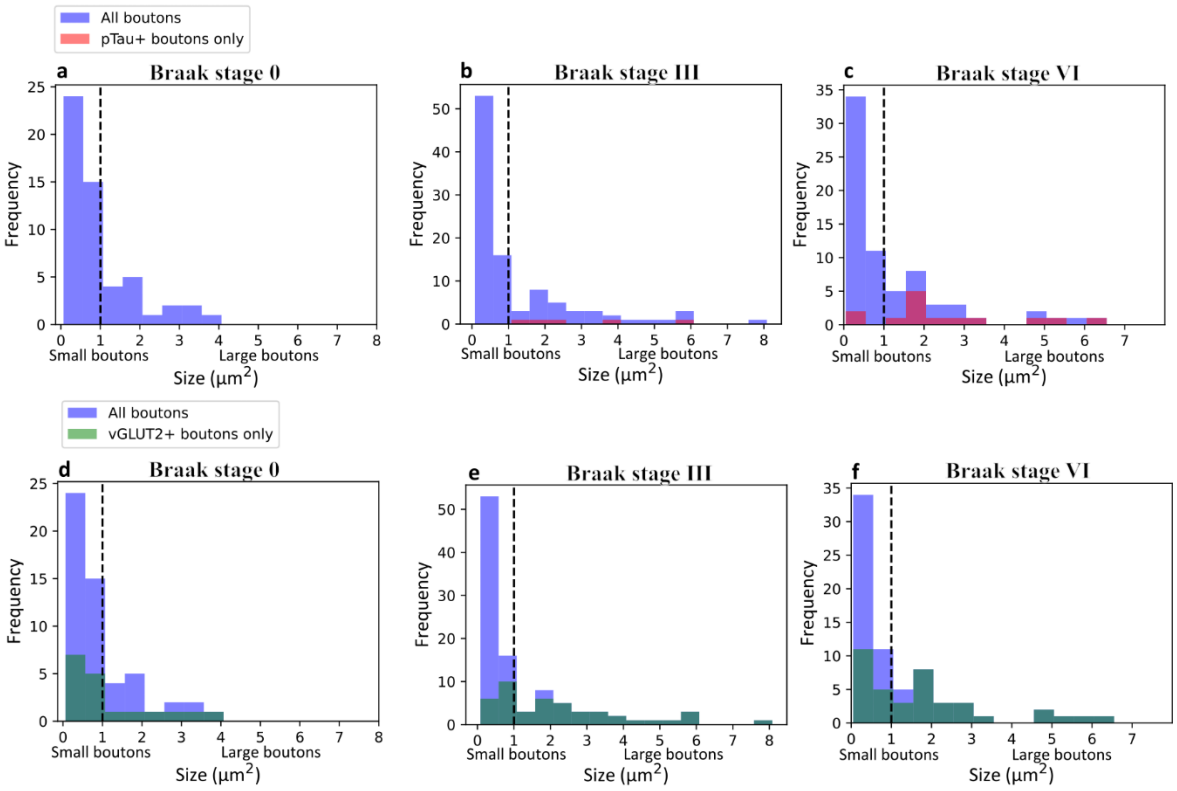


Figure 4.3 Large vGLUT2-expressing neurons preferentially accumulate pTau in the ADn
Distribution of the sizes of synaptic boutons in the ADn. Histograms for the sizes of synaptic boutons - (blue) along with the subset that contained pTau (a-c) vGLUT2 (d-f). Early stage: Case 4; middle stage: Case 12; late stage: Case 17.

4.3.5 The distribution of presynaptic and postsynaptic pTau suggests transsynaptic spread

Next, given the observation of pTau in both presynaptic terminals and postsynaptic dendrites (Figure 4.1 f, 4.5 b, d–f; Figure 4.4 b, d, g, h), I quantified how the synaptic distribution of pTau changed across different Braak stages, examining 652 presynaptic boutons and postsynaptic dendrites. At Braak stage 0, despite pTau being detectable at the light microscopic level (Figure 3.3 a, Figure 3.9 a), all sampled boutons and dendrites lacked pTau (*n* = 50/50 boutons, *n* = 62/62 dendrites; Case 4; Figure 4.5 g, h). Similarly, despite abundant pTau in the ADn at Braak stage II (Figure 3.3 i; Figure 4.4a; Table 3.3; Table 3.4), we did not detect pTau in boutons (*n* = 106/106) or dendrites (*n* = 109/109) at the electron microscopic level (Figure 4.6 a, b; Figure 4.7 e, f), probably due to the limited number of sampled structures and the limited sampling area (n=2 blocks/case). At Braak stage III, 5.8% of boutons (*n* = 6/104) and 21.6% of dendrites (*n* = 22/102) were immunopositive for pTau+ (Case 12; Figure 4.5 g, h; Figure 4.4 d). In this stage, the proportion of synapses in which *both* the presynaptic boutons and the associated postsynaptic dendrites contained pTau was 3.9% (*n* = 4/104; Figure 4.4 d; Figure 4.6 a, b). At Braak stage IV, I observed pTau within dendritic appendages in close apposition to vGLUT2+ boutons, which also contained pTau (Figure 4.4b).

At Braak stage VI, the proportion of affected boutons and dendrites significantly increased: 20.6% of boutons (*n* = 15/73) and 51.5% of dendrites (*n* = 52/101) were immunopositive for pTau (Case 17; Figure 4.5b, d–h). Moreover, 12.3% (*n* = 9/73) of synapses consisted of *both* pTau+ boutons and pTau+ dendrites (Figure 4.5f, g; Figure 44). This demonstrates that the proportions of both the presynaptic and postsynaptic structures containing pTau increase with Braak stage. Finally, I assessed the relationship between presynaptic vGLUT2 and vulnerability to pTau across Braak stages. At the early stage, I identified vGLUT2+ boutons (*n* = 18, Braak stage 0; *n* = 37, Braak stage II; Figure 4.6 c; 4.3

d), but did not observe pTau (Figure 4.6 c). In middle stage, from a total of 104 synaptic boutons, 5.8% (*n* = 6) were both vGLUT2 and pTau double immunopositive (Figure 4.4 d, 4.5, 4.6 a), whereas none of the vGLUT2 immunonegative boutons (*n* = 57) showed immunopositivity for pTau+. In other words, 100% of pTau+ boutons were vGLUT2+ (*n* = 6) and 12.8% of vGLUT2+ boutons (*n* = 47) were pTau+, supporting the hypothesis of selective vulnerability of subcortical vGLUT2+ axon terminals. Puncta adherentia are adhesive structures located outside of the active zone, and are associated with mammillothalamic terminals (Rovó et al 2012, Vaughn 1989).

I identified puncta adherentia between vGLUT2+ boutons and postsynaptic dendrites containing pTau (Figure 4.5 d). Furthermore, the small corticothalamic boutons lacked pTau (Figure 4.5 b, e), which suggests that pTau in the ADn is unlikely to spread anterogradely from the cortex. In the late stage, out of a total of 73 synaptic terminals, an even higher proportion showed vGLUT2 and pTau colocalization (16.4%; *n* = 12; Figure 4.6 c), in other words *~80%* of pTau+ boutons (*n* = 15) were immunopositive for vGLUT2. And of all vGLUT2+ boutons (*n* = 38), 31.5% were pTau+. The data on the colocalization of vGLUT2 and pTau is even likely to be an underestimate, given that large 'dark' boutons are likely to be degenerating mammillothalamic terminals (Figure 4.4 c, Figure 4.5 d). In summary, I found that large vGLUT2+ terminals preferentially accumulated pTau, which might indicate the subcortical origin of pTau in the ADn; these may be the conditions required for misfolded forms of Tau to be able to spread between postsynaptic and presynaptic structures (Figure 4.5). The above results suggest that vGLUT2+ boutons might be involved in the transsynaptic spread of pTau between postsynaptic ADn neurons and presynaptic mammillary body neurons within the Papez circuit (Figure 6.1).

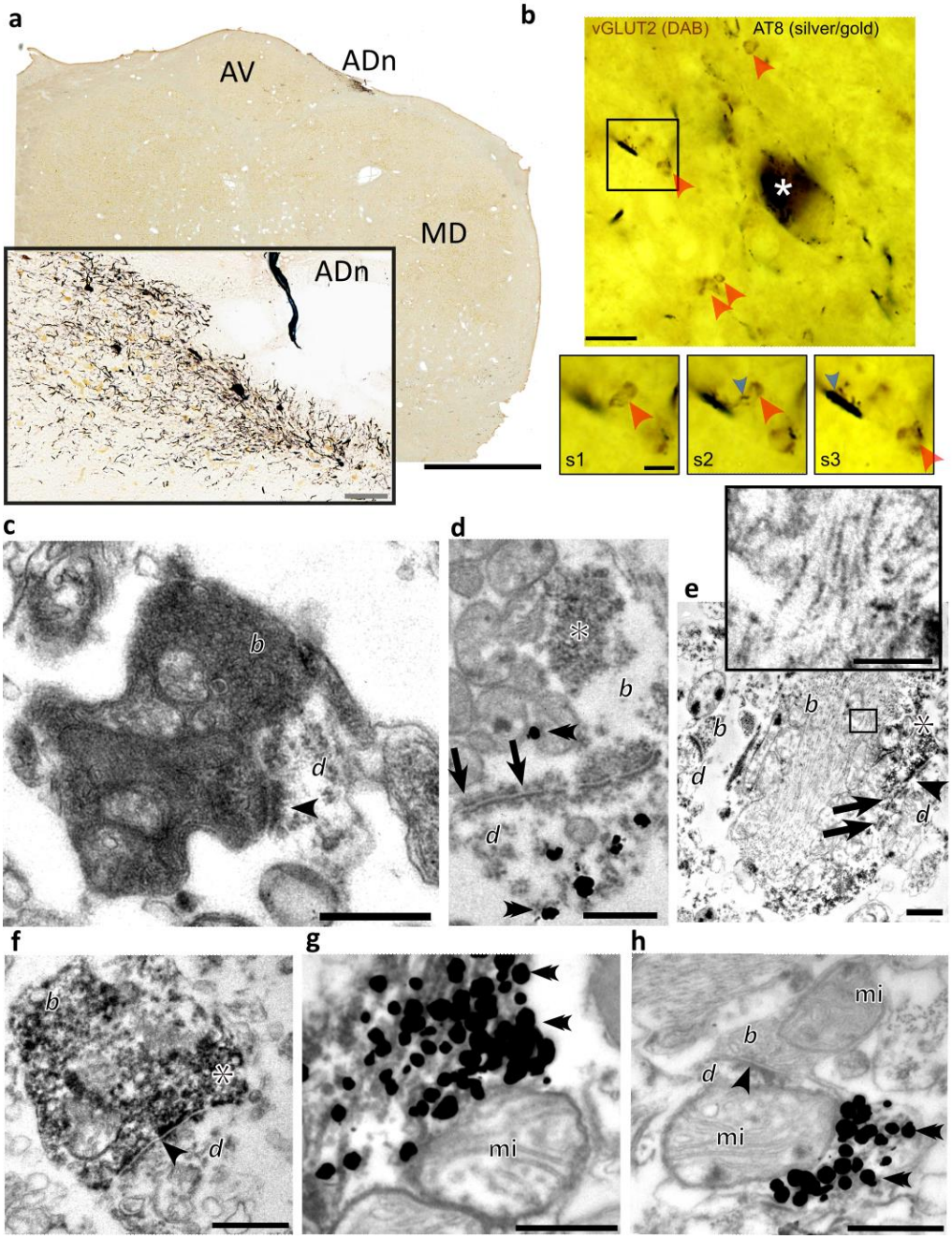


Figure 4.4 Light and electron microscopic localization of pTau to vGLUT2+ presynaptic terminals and postsynaptic dendrites in the ADn

Light and electron microscopic localization of pTau to vGLUT2+ presynaptic terminals and postsynaptic dendrites in the ADn. (a) Brightfield image of ptau (AT8 immunoreactivity; HRP-based DAB end-product) in a 50-µm-thick section of the rostral thalamus, showing pTau restricted to the ADn. Inset, pTau is localised primarily to neuronal processes in the ADn. Braak Stage II, Case 23. (b) Identification of pTau (AT8, black, gold- silver particles) and vGLUT2+ terminals (HRP-based DAB end-product, brown, e.g. red arrows). Asterisk, a cell body containing pTau. Insets, consecutive optical sections (s1-s3) showing two vGLUT2+ boutons associated with pTau; 1 bouton innervates a pTau+ dendritic appendage (blue arrowhead). Braak stage IV, Case 14. (c) An electron opaque ('dark') bouton making a synapse (arrowhead) with a dendrite. Braak stage VI (Case 17). (d) Puncta adherentia (e.g. arrows) between a bouton and a dendrite. Asterisk, vGLUT2 (HRP-based DAB). Gold-silver particles (double arrowheads) recognizing pTau (AT8) were detected in both the vGLUT2+ bouton and

in the dendrite. Braak stage III (Case 12). (e) A vGLUT2-immunopositive bouton (asterisks: dark DAB end-product around vGLUT2+ vesicles) containing filaments forming a synapse with a dendrite. Inset, detail of filaments. Braak stage II (Case 25). (f) A vGLUT2+ bouton forms a synapse with a dendrite. Braak stage II (Case 25). (g-h) Dendrites containing bundles of pTau+ filaments. Braak stage VI (Case 17). Dendrite, d; bouton, b; mitochondrion, mi. Scale bars: (a) 4 mm, 80 µm (inset); (b) 10 µm, 4 µm (insets); (c-h) 0.5 µm, 0.2 µm (e inset).

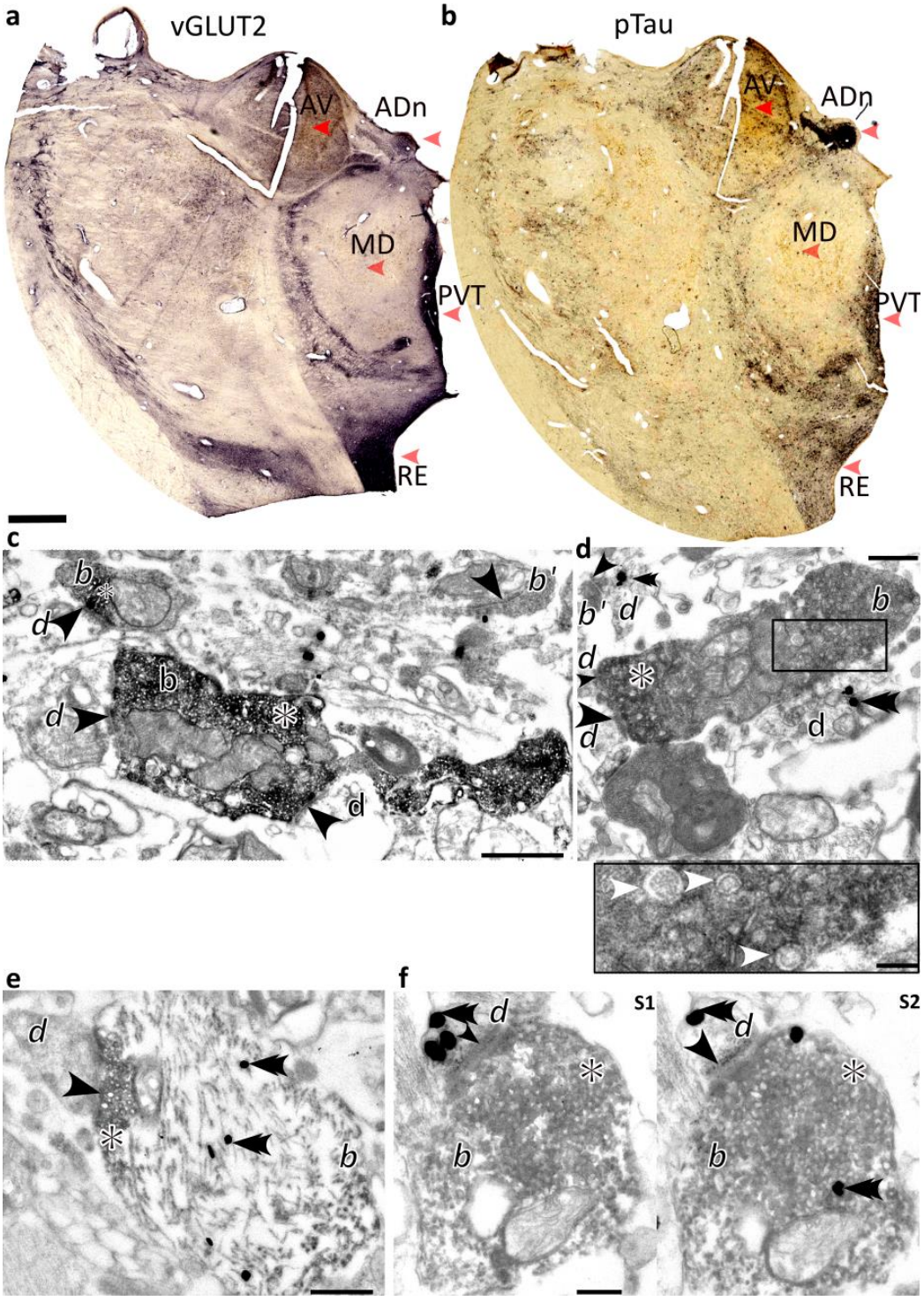


Figure 4.5 Localization of pTau to vGLUT2-expressing presynaptic terminals

(a) Brightfield microscope images of rostral thalamus (serial sections, late stage, Case 17) reacted for vGLUT2 (left) and pTau (AT8, right); HRP-based diaminobenzidine end products (DAB). Note similar distributions for vGLUT2 and pTau (red arrowheads). (b–f) Electron micrographs showing pTau filaments (AT8 immunolabelling, e.g., double arrowheads mark gold–silver particles) and vGLUT2- immunolabelled boutons (DAB) from the ADn of Case 17. Abbreviations: *b*, bouton; *d*, dendrite. Black arrowheads mark synaptic junctions. (b) A vGLUT2-immunopositive (vGLUT2+) bouton containing pTau filaments in the middle. Inset, higher magnification of helical pTau filaments from boxed region. c Two vGLUT2+ boutons (DAB) and a vGLUT2- bouton (*b′*, top right) lacking pTau, a silver particle is adjacent to the

bouton. (d) A large vGLUT2+ terminal (b) containing double-walled vesicles and clumped mitochondria. Inset, detail of boxed region showing vesicles (e.g., marked by white arrowheads). A small bouton (*b′*, top left) forms a synapse with a pTau immunopositive dendrite. e A large vGLUT2+ bouton (note DAB end product on vesicles at the synapse) containing dense ptau filaments. (f) Electron micrographs of sequential sections (S1, S2) showing pTau in both the vGLUT2+ bouton and the postsynaptic dendrite. Double arrowheads mark examples of gold–silver particles; asterisks label dark DAB product around vGLUT2+ vesicles. Scale bars: 2 μm (a), 0.5 μm (b, d, e), 1 μm (c), 0.25 μm (f), 150 nm (b,d insets).

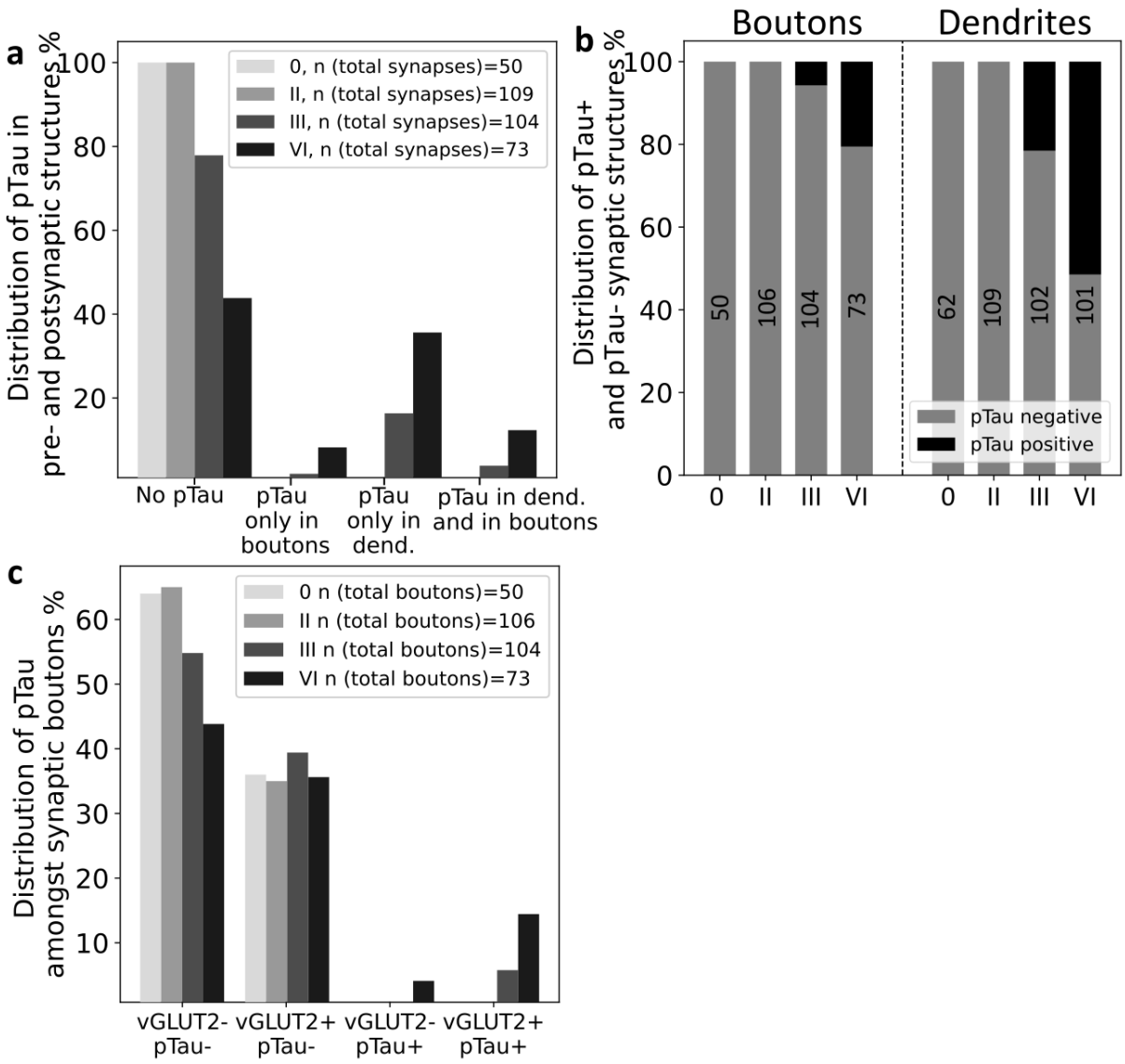


Figure 4.6 Accumulation of pTau pre-, and postsynaptically

(a) Proportion of synapses (%) in the ADn with or without pTau in the presynaptic bouton and/ or postsynaptic dendrite at Braak stages 0, II, III, VI. (b) Proportions of synaptic boutons (%, left) and dendrites (right) containing pTau at the different stages. (c) Proportion of synaptic boutons (%) with or without vGLUT2 and pTau immunoreactivities at the different stages.

4.3.6 Lack of extracellular amyloid-beta plaques in the ADn

I obtained electron microscopic samples from 4 cases (Cases 4, 12, 25, 17) that were appropriately preserved to identify different structures (Braak stages 0, II, III, and VI) (Figure 4.7 a, b, c). Surprisingly, I did not observe any amyloid-beta plaques in the ADn of the cases which could be easily recognised using electron microscopy, consistent with previous findings where only a few amyloid patches were observed in the ADn in contrast to other nuclei (Braak & Braak 1991b). I confirmed that the MD and AV nuclei adjacent to the ADn showed several plaques (n=1, Case 17) (Figure 4.7 a, b, c). This suggests that ADn is resistant to plaque formation despite being largely affected by tau pathology (although sample size should be increased to make a more reliable conclusion).

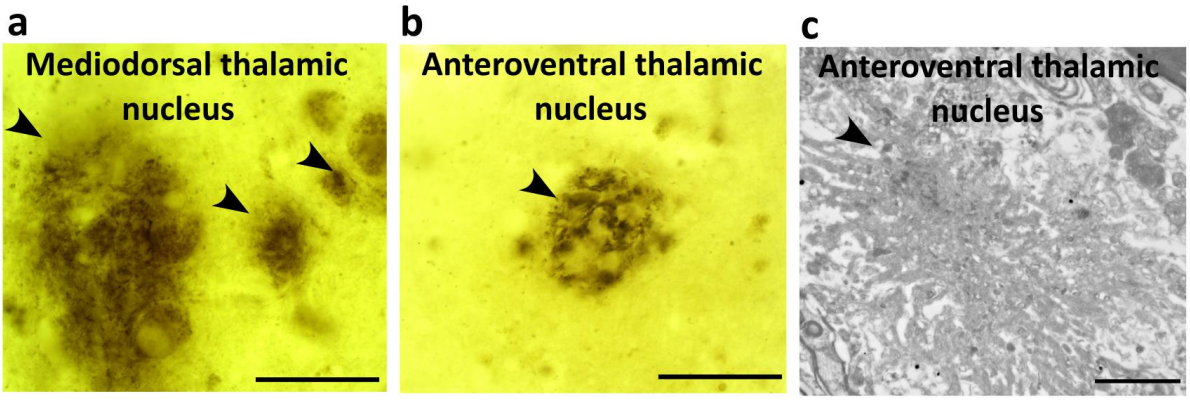


Figure 4.7 . Amyloid plaques accumulated in nuclei adjacent to the ADn
Case 17, Braak stage VI, arrowheads mark amyloid plaques visualised with HRP-based DAB end product using beta Amyloid-β 1-42 antibody. (a-b) Light microscopic images of the localization of amyloid plaques to the MD (a) and to the AV (b) visualised with HRP-based DAB. (c) Electron micrograph of an amyloid plaque in the AV. Scale bars: 40 μm (a,b), 2 μm (c).

4.4 Discussion

4.4.1 Subcellular localisation of pTau

Disentangling which subcellular structures accumulate misfolded pathogenic proteins including pTau, alpha-synuclein, TDP-43, is crucial for the understanding of its propagation in the brain. Animal models are useful to understand the consequence of pTau accumulation and a wider range of methods can be applied in animal experiments. However, animal models might not exactly recapitulate the neuroanatomical and neurochemical characteristics of its propagation, therefore, it is crucial to assess human brain tissues.

Examining perfusion-fixed human brain tissue in combination with immunogold labelling, I observed pTau in the forms of paired helical filaments in presynaptic boutons and postsynaptic dendrites, to best of my knowledge for the first time. By carrying out double labelling immunoreactions I was able to localise pTau in cell bodies, in dendrites, and in myelinated axons of CR-expressing neurons. Interestingly, pTau accumulated on both sides of dendrodendritic gap junctions (Figure 4.2 c). This might suggest that pTau is able to spread via these junctions.

4.4.2 Subcortical glutamatergic input linked to pTau accumulation

Despite the paradigm that pTau originates from cortical areas including the EC, pTau was not found in cortical terminals in the ADn, even in the late stage of the disease. However, subcortical boutons expressing vGLUT2 preferentially accumulated pTau. Moreover, in human thalamic sections at Braak stage IV I detected pTau within dendritic appendages in close apposition to vGLUT2+ terminals, which also contained pTau (Figure 4.4). This is in line with previous research that showed that glutamatergic input predisposes pTau accumulation in the thalamus (Xuereb et al 1990). Interestingly, large vGLUT2 boutons form puncta adherentia (a neuronal form of adherence junctions) with postsynaptic dendrites; corticothalamic

terminals lack such structures (Rovó et al 2012). This might indicate that puncta adherentia are required for the transfer of pTau between synaptic structures. Corticothalamic terminals that lack pTau in the ADn do not form puncta adherentia but other other sites of propagation including between mossy fibers of dentate gyrus and CA3 pyramidal cells form this type of adherentia junction (Amaral & Dent 1981, Mizoguchi et al 2002).

I propose that pTau has a distinct subcortical origin in the ADn but I cannot rule out pTau spreading from the dendrites of cortical neurons to the vGLUT2+ boutons of ADn, then from ADn dendrites to the mammillothalamic terminals. However, the early appearance of pTau immunopositive neurons in the ADn prior to cortical neurons makes this route unlikely. An alternative explanation is that pTau emerges independently in different brain regions. Although, several studies have shown that pTau is able to spread via anatomical connectivity (Clavaguera et al 2009, Cornblath et al 2021, Franzmeier et al 2020).

I also observed pTau+ terminals in the RSc in early cases which might indicate that pTau spread from ADn to the RSc (See Chapter 3).

It has also been shown that tau protein is associated with the cytosolic surface of synaptic vesicles (Tracy et al 2022), which suggests that misfolded tau proteins might disrupt neurotransmission. Synaptic dysfunction can be an early event of Alzheimer's disease; pTau can induce synaptic dysfunction in several ways. By binding to synaptic vesicles, it reduces their mobility and release rate in fly and rat neurons (Zhou et al 2017).

4.4.3 Transsynaptic spread of pTau

A growing body of evidence indicates that pTau can spread between cells and anatomically connected brain regions. A popular hypothesis posits that pTau has a prion-like transmission. It has been shown that injection of brain extracts from mice that express human P301S tau induce the formation of tau filaments in ALZ17 mice. This mouse line which express

the longest human brain tau isoform (441 amino acids) do not exhibit filamentous tau aggregates express the longest human brain tau isoform (441 amino acids) which normally do not exhibit filamentous tau (Clavaguera et al 2009).

This study was followed-up; brains extract from donors with different tauopathies was injected into the cortex or hippocampus of the same mouse line. After the injection the tau aggregated in the brains of the mice both in neurons and in oligodendrocytes (Clavaguera et al 2013). It has been reported that pTau oligomers extracted from donors who suffered from Alzheimer's disease propagated the misfolded tau confirmation of endogenous murine tau in wild type mice (Lasagna-Reeves et al 2012). Furthermore, I show in Chapter 5 that pTau is able to propagate to oligodendrocytes from neurons in Thy-Tau22 tauopathy model mice (Viney et al 2022). The observation that pTau localised to both the bouton and dendrite in the same synaptic structure (Figure 4.5 f) provides supporting evidence that pTau can spread via synapses. An important question associated with pTau spread is whether it spreads in an anterograde or retrograde manner, or a combination. My observation that pTau preferentially accumulates in dendrites (Figure 4.6 a,b) might support the theory of retrograde spread. Additionally, anterograde spread was supported by PET studies carried out with Alzheimer patients (Seemiller et al 2021).

Moreover, it has been shown that pTau extracted from Alzheimer brains injected intracranial in mice spreads preferentially in a retrograde direction (Cornblath et al 2021).

4.4.4 Double-walled vesicles

I observed large (80-100 nm) double-walled vesicles in degenerating boutons (Figure 4.5 d). Similar structures were described in the cortex of Alzheimer cases (Kidd 1964). These vesicles are likely to be autophagosomes. Indeed, the clearance of autophagic vacuoles is impaired in Alzheimer's disease (Boland et al 2008). The mammalian target of rapamycin

(mTOR) inhibits autophagy; an allosteric inhibitor is rapamycin. It has been shown that the activation of autophagy by rapamycin relieves cognitive deficits in PDAPP mice which exhibit extracellular amyloid plaques (Spilman et al 2010). Moreover, it has been shown that pTau enclosed within extracellular vesicles are enriched in endo-lysosomal proteins (Fowler et al 2023).

Alternatively, or in addition, these structures could also be vesicles that might be able to transfer pTau between neurons. It has been shown that extracellular vesicles isolated form brains of donors with Alzheimer's disease were enriched in tau oligomers (Ruan et al 2021).

4.4.5 Plaques do not emerge in ADn

It has been a popular view in terms of Alzheimer's disease progression that amyloid beta plaques represent the starting point of the pathological changes in the brain, leading to the accumulation of pTau, vascular damage and cell loss (Hardy & Higgins 1992). The fact that ADn lacked plaques but accumulated a high number of pTau immunopositive cells may indicate that there is no direct link between the amyloid beta and pTau. However, it is possible that the amyloid plaques affect axon terminals that are arising from other brains regions and trigger pTau accumulation in the origin of these terminals (Edwards 2019). According to this hypothesis, amyloid plaques in the RSg would trigger tau pathology in the ADn via axon terminals that originate from projection neurons of the ADn. Interestingly, the MD and AV that were relatively resistant to pTau, showed a high density of plaques. It is important to note that the pathology of Alzheimer's disease is more complex than the accumulation of pTau and amyloid beta. It has been shown that glial cells and impairments of vascular structures might be involved development of the disease (Barisano et al 2022, Overmyer et al 1999, Swanson et al 2020).

However, it is still the subject of a debate whether these are a prelude to the pathological changes or a consequence of it.

4.5 Limitations of the study

The main limitation of study is the low number of cases with adequate tissue quality. I assessed 17 cases and only 4 of them were suitable for quantification. Only the AT8 antibody was used to identify pTau; in future studies it would be interesting to test antibodies that label dimeric or oligomeric forms of pTau. Some of the terminals were dark (Figure 4.7 c), which might have been caused by *post-mortem* delay/inadequate fixation or this can be sign of neurodegeneration (Colonnier 1964, Szentágothai et al 1966). These terminals were not included in the quantification as they likely lost their immunogenicity.

5 Results: Propagation of pTau, and glial and vascular contribution to neurodegenerative diseases

5.1 Introduction

A dynamic and highly regulated homeostasis is established between neurons, glial cells and blood vessels sustaining the intricate function of the brain. Impairment in any of these components triggers pathological changes and potentially causes cognitive decline and motor dysfunction.

Several factors can affect neurons, glia and the vasculature in the brain including ageing, genetics, infections, injuries, and diabetes (Hou et al 2019, Mielke et al 2022, Nguyen et al 2020, Smeland et al 2023). Ageing has been described as the primary risk factor for most neurodegenerative diseases, and is associated with several disruptive molecular and cellular processes including genomic instability, cellular senescence, and telomere attrition (Hou et al 2019). It has been shown that chaperone mediated autophagy declines with ageing and contributes to disrupted neuronal proteostasis (Bourdenx et al 2021). I also observed structures in large degenerating vGLUT2+ boutons that resembled autophagosomes (Chapter 4, Figure 4.8 d). Furthermore, the natural decline of blood brain barrier (BBB) function with ageing has been described (Verheggen et al 2020). In different neurodegenerative diseases, the involvement of neurons, glial cells and blood vessels varies, although all of them are affected to some extent. Alzheimer's disease is mainly considered as a 'neuronal disease' although oligodendrocytes (Nishimura et al 1995), astrocytes (Verkhratsky et al 2010), microglia cells (Hansen et al 2018) and blood vessels (Klohs 2019) are also affected.

There are 6 tau isoforms in the brain; they differ by the absence or presence of 1 or 2 N-terminal inserts and either three (3R) or four (4R) 31- or 32-amino acid repeats in the microtubule-binding domain.

These isoforms accumulate in different kinds of neurons and glia in different tauopathies, and they can have different spatiotemporal distributions. Alzheimer's disease, amyotrophic lateral sclerosis, Niemann-Pick disease type C, and chronic traumatic encephalopathy have a mixture of 3R and 4R tau. Those with only 3R tau include Pick's disease and some types of FTDP. The 4R tauopathies include CBD, PSP and Huntington's disease (Goedert et al 2017, Komori 1999). In oligodendrocytes, pTau surrounds the nucleus and fill a few processes these are often referred in the literature as 'coiled bodies' (Arima 2006, Yoshida 2006). Interestingly, some studies claim that astrocytes are causative of neurodegenerative diseases, it has been shown that GABA from reactive astrocytes impairs memory in APP/PS1 mice (di Domenico et al 2019, Escartin et al 2021). Moreover, a study suggested excessive hydrogen peroxide arising from monoamine oxidase B in severe reactive astrocytes causes glial activation, tauopathy, neuronal death (Chun et al 2020).

Although, astrocytes accumulate pTau as part of normal ageing, termed aging-related tau astrogliopathy (ARTAG). Astrocytes containing pTau were shown in several cortical and subcortical areas including the thalamus (Kovacs et al 2017, McCann et al 2021). The presence of pTau+ glial cells are a common characteristic of progressive supranuclear palsy (PSP), corticobasal degeneration (CBD) and Pick's disease (PiD) (Komori 1999); however, there are still many unknown factors including the causes and progression. I also detected pTau+ astrocytes in 6 cases (Chapter 3 Figure 3.7c, Table 3.2).

It has been shown that the blood flow decrease is an early sign of Alzheimer's disease and that the vascular transcriptomics significantly changes in the disease (İş et al 2024, Korte et al 2020). Blood vessels are intricately linked to the glymphatic system, a macroscopic waste clearance system formed by astroglial cells; it has been shown that its disruption supresses the clearance of soluble amyloid-β (Iliff et al 2012).

To understand some specific aspects of the pathology the most informative to assess human *post-mortem* brain tissues such as vulnerable cell types, distribution of pTau or vascular changes but for other aspects animal models have several benefits. Animal models might be able to mimic the propagation of pTau including the involvement of glial cells. THY-Tau22 mice express the human 4-repeat mutated tau. This genetic modification causes the phosphorylation of tau on several Alzheimer's disease-related epitopes and induces tau accumulation. It has been described that these mice show spatial memory deficits (Schindowski et al 2006). I aimed to assess the age-related propagation of pTau in transgenic and examine whether the thalamus become affected. Moreover, I assessed vascular changes in the human anterodorsal thalamic nucleus to gain a comprehensive view of the tau pathology.

5.2 Methods

5.2.1 Animals

All procedures involving experimental animals were under approved personal and project licences according to UK Animals (Scientific Procedure) Act 1986 and associated regulations. I assessed the distribution of pTau and its localization to neurons and glia in different age groups of THY-Tau22 mice (Viney et al 2022): very young animals, <4.5 months (n=14 mice); young animals, 8-16 months old (n=5 mice); ageing mice, 8-16 months old (n=3 animals); aged mice, >16 months old (n=7 mice).

THY-Tau22 mice express the human 4-repeat tau mutated at sites G272V and P301S under Thy1.2-promoter. In these mice the level of tau increases with age (Schindowski et al 2006). In addition, to model tau pathology in the mouse ADn, I used wild type (C57BL6/j) male and female mice (n=15; Table 5.1) for targeted viral expression of human tau (see below). Some of the virus injections were carried out by Dr Tim Viney and I assessed the brains.

ID	sex	genotype	virus	target	age at injection (w)	expression time
CBCB1975.3i	f	wt	AAV-CBh-GFP	left ADn	44	2m
M01805079	f	wt	AAV-CBh-GFP	bilateral ADn+LD	33	5m
TTPS14.1d	f	wt	AAV-CBh-GFP	bilateral ADn+LD	20	11m
TTPS15.2c	f	wt	AAV-CBh-GFP	bilateral ADn+LD	17	5m
M01922431	m	wt	AAV-CBh-GFP	bilateral ADn+LD	11	5m
M01922432	m	wt	AAV-CBh-GFP	bilateral ADn+LD	11	7.5m
CBCB1990.2e	f	wt	AAV-CBh-hTau-2A-GFP	left ADn	43	4m
CBCB1990.2f	f	wt	AAV-CBh-hTau-2A-GFP	left ADn	43	4m
CBCB1975.3j	f	wt	AAV-CBh-hTau-P301L-2A-GFP	left ADn	44	1m
CBCB1990.2d	f	wt	AAV-CBh-hTau-P301L-2A-GFP	left ADn	42	2m
M01805080	f	wt	AAV-CBh-hTau-P301L-2A-GFP	bilateral ADn+LD	33	5m
TTPS15.1h	f	wt	AAV-CBh-hTau-P301L-2A-GFP	bilateral ADn+LD	19	11m
TTPS15.2d	f	wt	AAV-CBh-hTau-P301L-2A-GFP	bilateral ADn+LD	17	5m
TTPS13.1i	f	wt	AAV-CBh-hTau-P301L-2A-GFP	bilateral ADn+LD	68	5m
M01922433	m	wt	AAV-CBh-hTau-P301L-2A-GFP	bilateral ADn+LD	11	7m

Table 5.1 List of mice injected with virus
Abbreviations: m, month; wt, wild type; AAV, Adeno-associated virus, ADn, anterodorsal thalamic nucleus; LD, laterodorsal thalamic nucleus; CBh promoter, ubiquitous chicken β-actin hybrid

5.2.2 Mouse tissue processing

Mice were deeply anaesthetized with 0.1 mL Pentobarbitone (20 % w/v, intraperitoneal injection) and transcardially perfused with 0.1 M PB followed by fixative (4% paraformaldehyde, 15% v/v saturated picric acid, 0.05% glutaraldehyde in 0.1 M PB at pH 7.4). Some brains were postfixed overnight in glutaraldehyde-free fixative at 4°C. After fixation, brains were washed in 0.1 M PB, coronal sections (70 μm) were cut in the coronal plane using a Vibroslicer (Leica VT 1000S, Leica Microsystems) with stainless steel razorblades and stored in 0.1M PB with 0.05% sodium azide at 4°C for further processing. Next, selected sections were permeabilized by either 3x freeze-thaw (cryoprotected in 20% sucrose in 0.1 M PB) with liquid nitrogen or by 0.1 % Triton-X100 in tris-buffered saline (TBST-X).

5.2.3 Virus injections

Animals were anesthetized by 4% isoflurane (IsoFlo, Abbott) in O_2 using an anaesthetic vaporiser, followed by a subcutaneous administration of analgesic Buprenophrine (Vetergesic, 0.1 mg/kg). After clipping the scalp, the mice were fixed into a stereotaxic frame. An incision was made posterior to anteriorly at the midline of the scalp. Sites were identified and marked relative to Bregma. The craniotomies were made above the rostral thalamus targeting ADn and LD: Antero-posterior (AP) -3.20 mm, medio-lateral (ML) -1.90 mm and DV 2.50 mm. 100 nl of virus was injected into the rostral thalamus. The injected AAV encoded GFP (Table 2.3), a short linker peptide sequence and human tau: GFP-2a-huTau (human tau protein) or the same construct with mutated tau: GFP-2a-huTau (P301L) (Table 5.1). The short 2a peptide sequence catalyses a self-cleaving. As a consequence, neurons that are transduced with the virus will express GFP and huTau as individual proteins, whereas cells that receive huTau from other cells will bear huTau without having GFP (Wegmann et al 2019). Finally, the scalp was sutured, and the animals were allowed to recover from anesthesia on a 37°C warming pad before returning them into a clean home cage.

5.2.4 Fluorescent immunohistochemistry

Permeabilized sections were first blocked in TBS/TBST-X with a 20 % (vol/vol) NHS for 1 h at room temperature to prevent non-specific antibody binding. Next, sections were washed in TBS/TBST-X and incubated with primary antibodies (Table 2.1) (in TBS/TBST-X, 1% horse serum) for 3 days. After primary antibody incubation, sections were washed again and incubated with secondary antibodies conjugated to a fluorophore (in TBS/TBST-X). Finally, sections were washed 3 times for 10 minutes each and mounted with Vectashield on glass slides.

5.2.5 Single- and double-labelling pre-embedding immunohistochemistry and electron microscopy

Next, sections from animals (22.5-month-old female and TT33G 21.5-month-old female) were blocked in 5% (vol/vol) NGS. Subsequently, sections were incubated with AT8/Olig2 primary antibodies (Table 2.1) in TBS for 6 d at 4°C. Next, sections were incubated overnight at 4°C in 1:300 biotinylated goat anti-rabbit IgG (Vector Labs, BA-1000) and 1:200 donkey anti-mouse ultrasmall immunogold (Aurion, 100.322) in CWFS solution. After repeated washes in TBS, sections were incubated overnight at 4°C in avidin-biotinylated horseradish peroxidase complex (Vectastain ABC Elite kit, Vector Laboratories) in TBS. To enlarge the gold particles further, sections were then incubated in silver enhancement solution (SE-LM, Aurion) for 20 min at 20°C and washed in ECS. Subsequently, peroxidase was visualized using 3,3-diaminobenzidine (DAB; 0.5 mg/mL, Sigma-Aldrich) as chromogen developed with 0.01% H_2O_2. After washing sections in PB, they were treated with 0.5% OsO4 (a fixative and heavy metal contrasting agent) in 0.1 M PB. Next, dehydration of sections was carried out in ascending ethanol series (50%, 70%, 90%, 95%, 100%) and in acetonitrile. To enhance contrast for electron microscopy, sections were incubated in 1% uranyl acetate diluted in 70% ethanol for 25 min between the 70% and 90% ethanol steps. Next, sections were placed in epoxy resin (Durpucan AMC, Fluka, Sigma-Aldrich), incubated overnight at RT and transferred onto slides. For polymerization, sections were incubated at 55°C for 2 d. Selected regions of ProS were re-embedded into Durcupan blocks. A series of ~50-60 nm-thick sections were cut with an ultramicrotome (Leica Ultracut UTC) and collected on pioloform-coated copper grids.

To assess blood vessels in the human ADn, 4 cases were selected: a case without cortical tau pathology (Case 3, Braak stage 0), an early stage case (Braak stage II, Case 25), a mid stage case (Case 12, stage III). These are either the same sections that were used for double-

labelling immunohistochemistry or processed as described in Chapter 4 (Initial electron microscopic assessment of brain sections).

5.2.6 Imaging

Electron microscopy

Specimens were studied on three microscopes: a Jeol 1010 transmission electron microscope equipped with a digital GATAN Orius camera, at the Department of Physiology, Anatomy and Genetics, Oxford University; a JEOL 1400 transmission electron microscope equipped with a Rio digital camera, at the Sir William Dunn School of Pathology, Oxford University; and a Hitachi 7100 electron microscope with a Veleta CCD camera (Olympus Soft Imaging Solutions, Germany), at the Institute of Experimental Medicine, Budapest, Hungary.

Confocal microscopy

An LSM 710 was used with Plan-Apochromat 40×/1.4, 63×/1.4, and 100×/1.46 objectives (ZEN 2008 5.0 or ZEN Black 14.0 software). For representative confocal images, maximum intensity projections were used for z-projections.

5.3 Result

5.3.1 Propagation of pTau in THY-Tau22 mice

I assessed different age groups of THY-Tau22 mice to map the age-dependent propagation of pTau. It has been shown that in these mice that the number of high-firing neurons is significantly decreased (Viney et al 2022). I noticed coiled bodies in several brain areas, especially in white matter, I hypothesised that these were non-neuronal as they were very small (8-10 μm). Moreover, pTau is expressed under Thy1 promoter which is active in neurons (Caroni 1997). To understand their presence, I checked whether they emerge in an age-

dependent manner. To do this first I described the pTau distribution at a higher temporal resolution by assessing different age groups.

At 2-3 months old, I observed several pTau immunopositive cells in the dorsal ProS (Table 5.1a) which is a region between hippocampal dorsal CA1 (CA1d) and dorsal subiculum (Ding et al 2020). The distal part of CA1d (hippocampal dorsal CA1, closest to ProS) and SUBd contained only a few pTau+ pyramidal cells.

The intensity of pTau in ProS was the highest after 8 months, with large numbers of pTau+ somata and processes (Table 5.1 a, b). The number of neurons that were immunoreactive for pTau increased in the CA1d, in the CA2 and in the SUBd. The density of pTau cells decreased in aged mice (>16 months); this can be explained by the cell loss.

In young mice (<16 months) pTau immunopositive dentate granule cells were rare at the septal pole (sparse pTau: n = 4/5 mice (this was observed in 4 out of 5 mice); moderate pTau: n = 1/5 mice) but more common at the temporal pole (moderate or extensive: n = 3/6 mice; absent or sparse: n = 3/6 mice; Figure 5.1 a; 5.2 a-c). Mossy fibres showed variable levels of pTau, likely originating from granule cells of the temporal pole (Figure 5.2 a, c).

In aging mice (2-24 months old), the septal pole contained mostly moderate pTau (n = 2/3 mice; sparse: n = 1/3 mice) and the temporal pole more extensive pTau (n = 2/3 mice; moderate: n = 1/3 mice). I found that in aged mice, the septal pole was varying (moderate or extensive: n = 5/10 mice; sparse: n = 5/10 mice), whereas the temporal pole contained extensive pTau (n = 6/7 mice; sparse: n = 1/7 mice; Figure 5.1 a and Figure 5.2 a, Figure 5.2 c). The basolateral amygdala showed a prominent pathology even in very young animals <4.5 months (n=14 mice) (Viney et al 2022). I observed that the entorhinal cortex had modest levels of pTau at all ages (Table 5.2 d). In isocortex, pTau was localised to layer 5, remaining sparse until much later in life (sparse in n = 10/10 young and aging mice; moderate or extensive in n = 7/9

aged mice; Figure 5.1 c, Figure 5.2 a, Figure 5.2 c). In wild type littermates, pTau was not observed (n = 16/16 mice, 2–24 months old).

In conclusion, in this mouse model the hippocampal formation, the basolateral amygdala, and the isocortex were mainly affected by pTau. Subcortical areas that are affected in Alzheimer's disease such as the thalamus and mammillary body lacked pTau+ neurons. Other areas of the hypothalamus and basal ganglia were also largely unaffected (Figure 5.2 a).

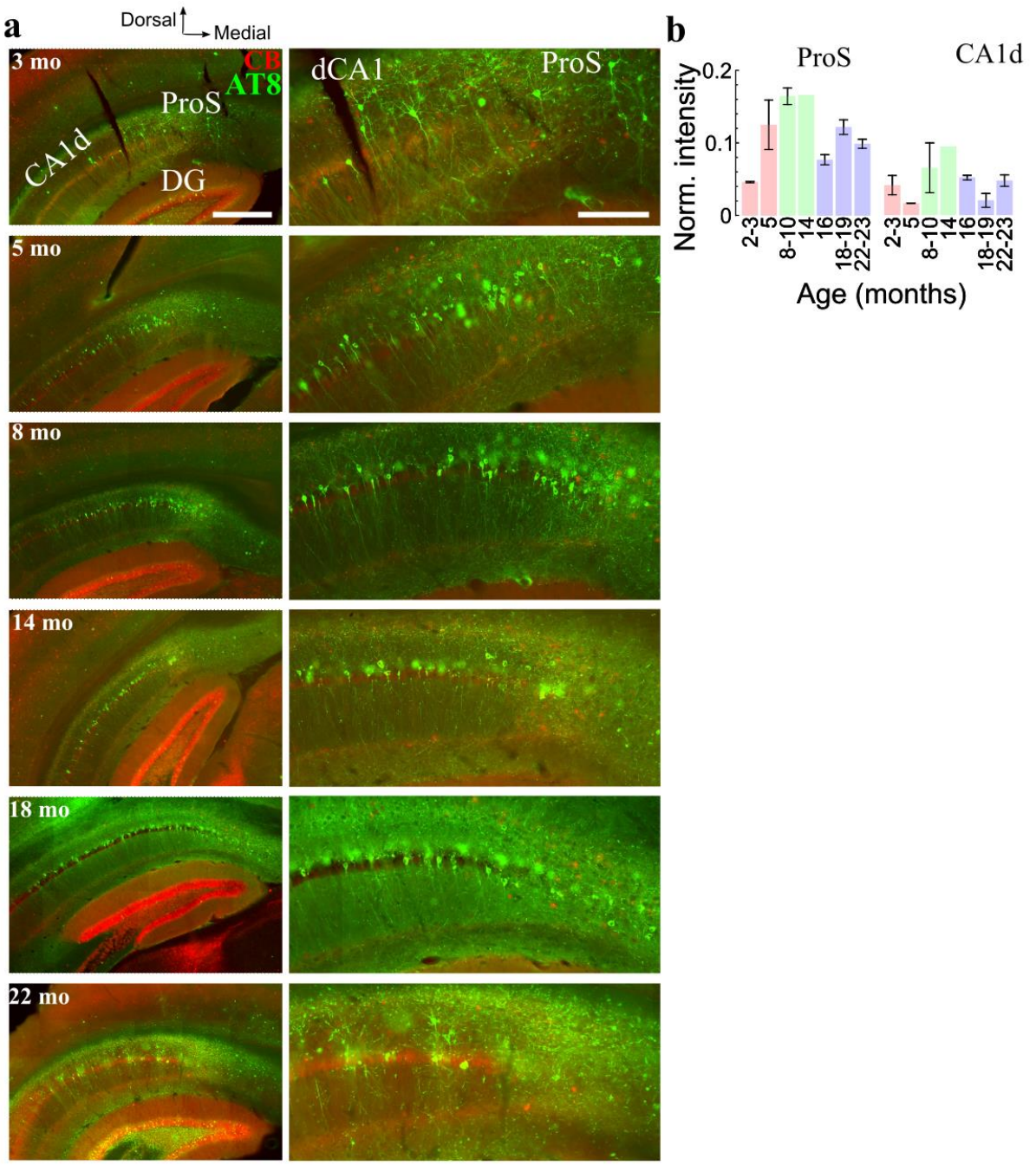


Figure 5.1 Age-related increase of pTau in THY-Tau22 mice

(a) Immunoreactivity for AT8 (pTau+, green) in coronal sections containing the hippocampal formation at different ages (months old, mo). Calbindin (CB, red). Right, enlarged views of distal CA1 (dCA1) and dorsal prosubiculum (ProS). Widefield epifluorescence. (b) Normalized intensity measurements of AT8 immunoreactivity (mean, standard error) at six different age ranges in ProS and dorsal CA1 (CA1d). Age ranges (left to right): young (pink), 2– 3 months (n = 2) and 5 months (n = 2); aging (green), 8–10 months (n = 2) and 14 months (n = 1); aged (purple), 16 months (n = 2), 18–19 months (n = 2), and 22–23 months (n = 2). Scale bars: 500 mm (a, left); 200 mm (a, right). Cases in (a) (top to bottom; mouse, sex): TT114A, male (m); TV132, m; TV143, m; TV136, female (f); TV139, m; TT33G, f. Intensity measurements from b were provided by Dr Tim Viney (Viney et al 2022).

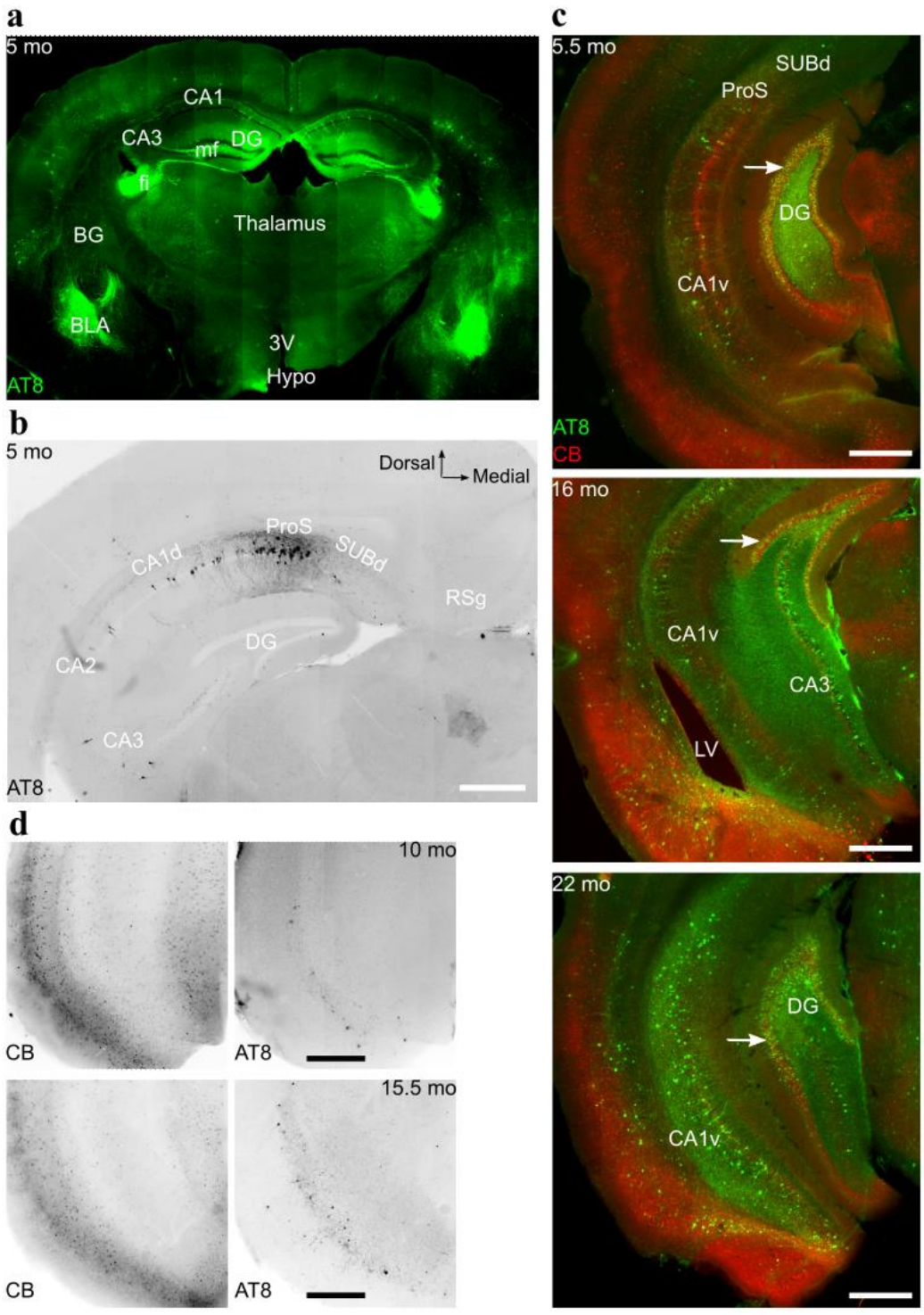


Figure 5.2 Selective distribution of pTau in THY-Tau22 mice

(a) 70 µm thick coronal section of a tg mouse (case TT71G, female, 5 months) immunoreacted for AT8 (epifluorescence tile). Note similar distribution in both hemispheres. The lack of detectable AT8-immunoreactive granule cell somata of the dentate gyrus (DG) but immunolabelled mossy fibers (mf) suggests that the affected granule cells are from more temporal regions of the DG. (b) Dense pTau localized to the ProS of a different 5-month-old transgenic mouse (case TT71F, female, littermate of case shown in (a)). Note lack of pTau in the DG, SUBd, RSg, CA2 and most of cortex. Section more caudal than that shown in (a). Inverted contrast epifluorescence. Dorsal and medial directions also apply to (c) and (d). (c)

Caudal sections from 3 different cases (top to bottom: TV133, male, 6 months; TT11F, male, 16 months; TV145, male, 22 months) immunoreacted for pTau (AT8, green) and CB (red). Note pTau+ granule cells of the DG (arrows). (d) Sections of entorhinal cortex (CB and AT8, inverted contrast epifluorescence) for cases TV134 (female, 10 months, top row) and TT21E (female, 16 months, bottom row). All scale bars 500 µm. Abbreviations: BG, basal ganglia (putamen and pallidum); Hypo, hypothalamus; 3V, third ventricle; RSg, granular retrosplenial cortex; CA1v, ventral CA1; LV, lateral ventricle. This panel was made by Dr Tim Viney and the Figure 5.2 a was imaged by Dr Katja Hartwich.

5.3.2 Spread of pathological tau to oligodendrocytes from neurons in THY-Tau22 mice

I observed the pTau+ coiled bodies only in the aged (n = 11/11, 18–27 months) and aging (n = 5/6, 8–16 months) THY-Tau22 mice, but not in young animals (n = 7/7, 2–6 months). Coiled bodies were found in several brain regions, especially in white matter tracts (Figure 5.3 and Figure 5.5), such as the fimbria, fornix, dorsal hippocampal commissure, corpus callosum, and stria terminalis (Viney et al 2022). Coiled bodies were also in hippocampal stratum oriens, subicular complex, RSg, dorsal striatum, and lateral septum. Similar structures have been described in Alzheimer's disease (Nishimura et al 1995). The rostral thalamus and mammillary bodies had scattered coiled bodies. In the brainstem, the substantia nigra pars reticulata, ventral tegmental area, pontine nuclei, and interpeduncular nucleus contained coiled bodies, a pathology found in 4R tauopathies such as CBD and PSP (Arima 2006, Komori 1999).

To test whether coiled bodies were in non-neuronal cells, I tested Olig2, an oligodendrocyte transcription factor, and found that 100% of pTau+ coiled bodies colocalized with Olig2 (Figure 5.3, Figure 5.5 e, and Figure 5.5 f). Smaller coils (<2-μm diameter) associated with Olig2-immunoreactive nuclei (Figure 5.3 c) may represent densely packed pTau. As it was expected, Olig2 was not found in $pTau^{+}$ neurons (Figure 5.5 e) I used electron microscopy to confirm the accumulation of filamentous tau in oligodendrocytes (Figure 5.3 e) (Lin et al 2003, Peters & Sethares 2004). To my knowledge, the Thy1 promoter is not active in oligodendrocytes (Caroni 1997). Because coiled bodies were not observed in younger mice, despite accumulation of pTau in neurons at all ages investigated and because the control animal that expressed GFP under the Thy1 promoter lacked GFP in oligodendrocytes, I suggest that pTau spreads from neurons to oligodendrocytes during ageing (Figure 5.3).

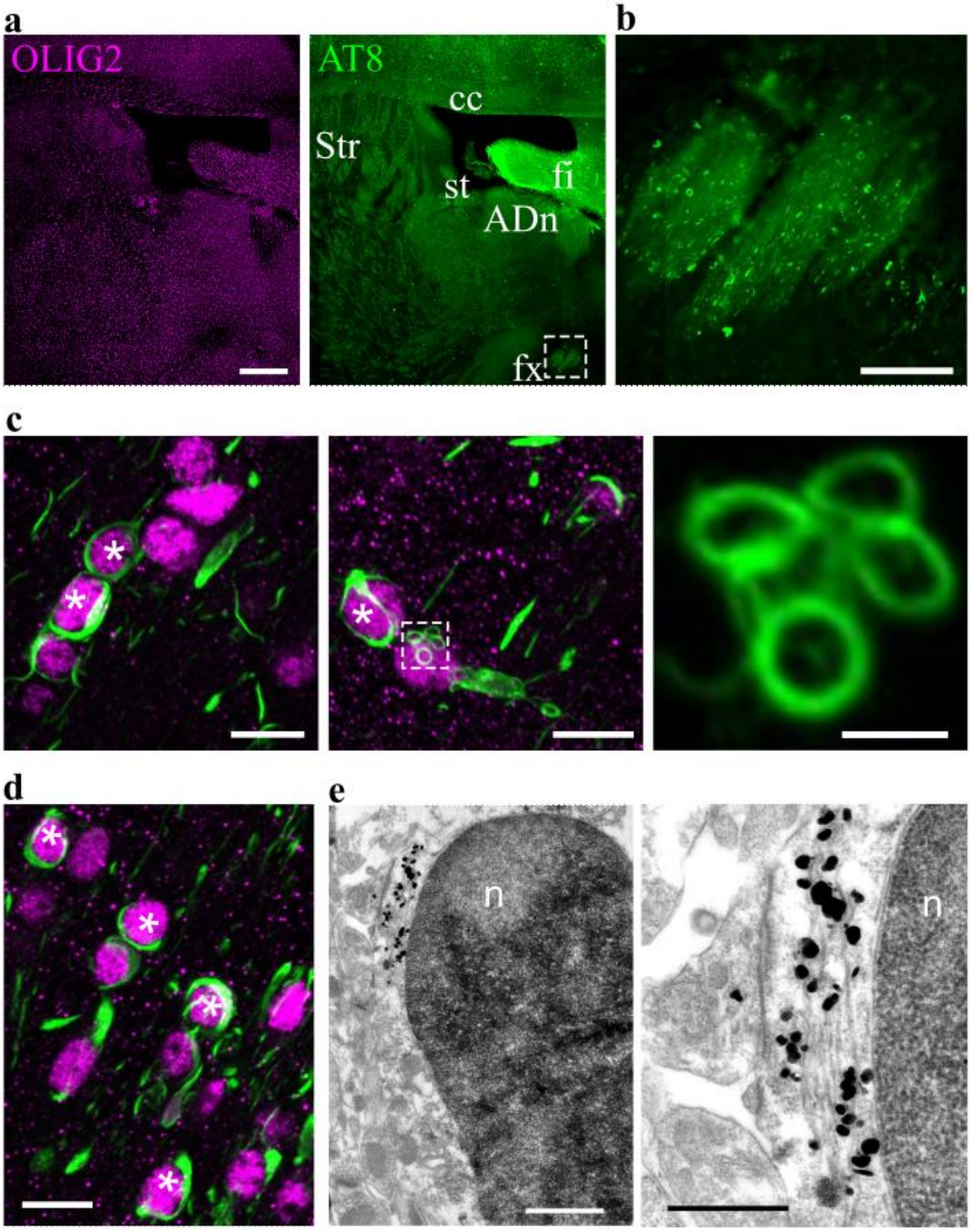


Figure 5.3 Accumulation of pTau in oligodendrocytes
(a) Olig2 (magenta) and pTau (AT8, green) from an aged (20-month-old) transgenic mouse (widefield epifluorescence). Note high density of pTau in fimbria (fi). (b) Enlarged view of boxed region from (A) of the fornix (fx), showing neuropil threads (axons) and coiled bodies. (c) Nuclear immunoreactivity for Olig2 (magenta, asterisks) surrounded by coiled bodies (green, AT8). Right, enlarged view of "microcoils" near an Olig2+ nucleus (boxed region, middle panel). (d) Coiled bodies colocalizing with Olig2+ nuclei in the fimbria. (e) AT8+ filaments (gold-silver particles) in the cytoplasm of an oligodendrocyte in the ProS next to an

Olig2-immunolabeled nucleus (n) (peroxidase labelling) from an aged mouse (23 months). Right, higher magnification. Scale bars: 500 μm (a); 100 μm (b); 10 μm (c, left and middle; d); 2 μm (c, right); 1 μm (e, left); 0.5 μm (e, right). Confocal maximum intensity z-projection thickness: 4, 9.6, and 2.4 μm (c); 4 μm (d). ADn, anterodorsal thalamic nucleus; cc, corpus callosum; st, stria terminalis; Str, dorsal striatum. See also Figure 5.5.

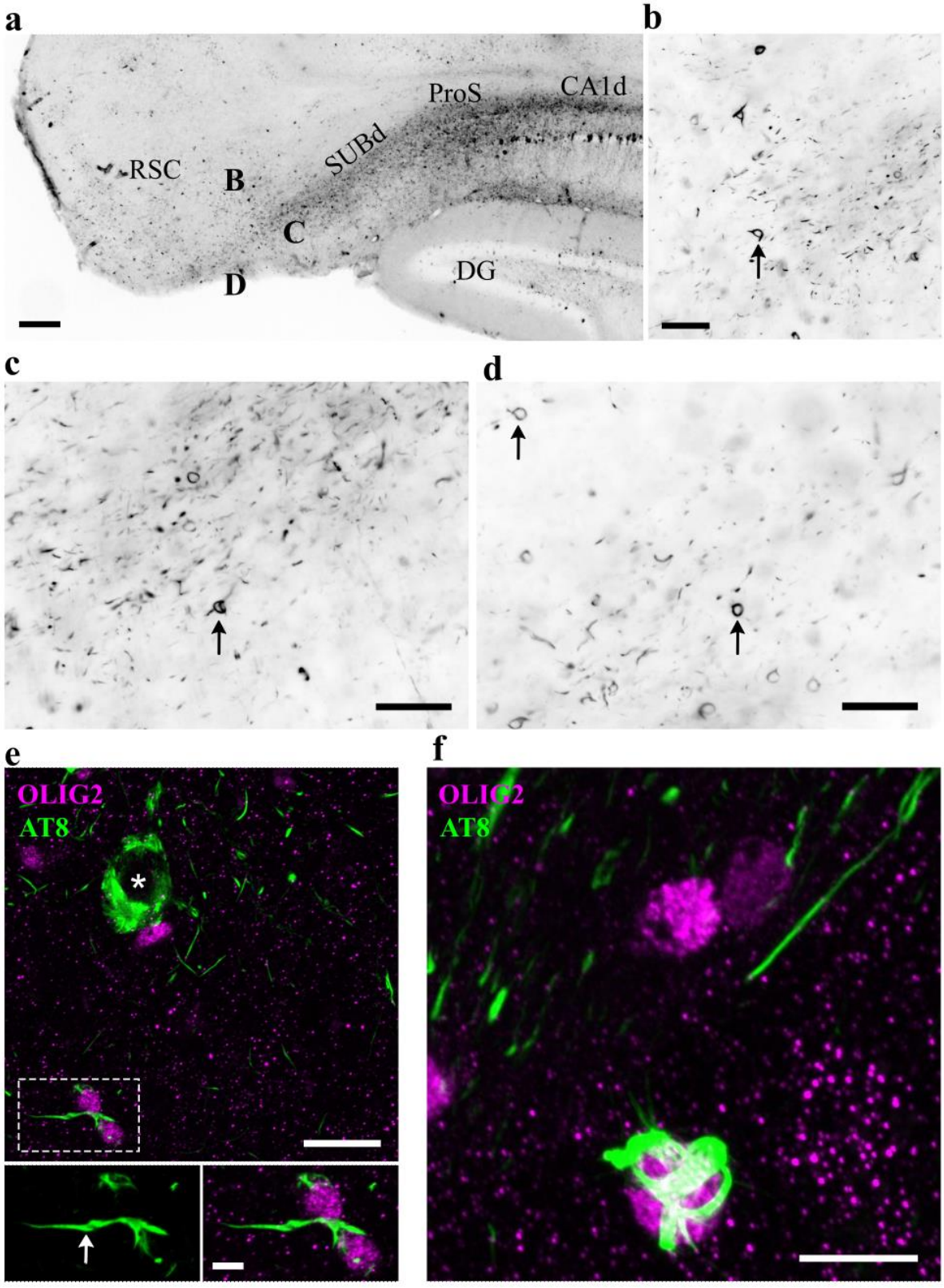


Figure 5.4 . Cortical pTau+ neurons and oligodendrocytes
(a) Part of the hippocampal formation (SUBd, DG, CA1d) and retrosplenial cortex (RSC) in an aged transgenic mouse (23 months). Note lack of pTau+ neurons in ProS, SUBd and RSC in contrast to CA1d. Widefield epifluorescence (inverted contrast). (b-d) Enlargement of the areas marked in (a). Arrows highlight typical coiled bodies. (e) Neurofibrillary tangles (asterisk, AT8, green) in a deep layer cortical neuron, which lacked immunoreactivity for Olig2

(magenta). Bottom, enlarged view of two oligodendrocytes from boxed region, indicating a long process marked by pTau (arrow). (f) An unusually dense coiled body surrounding an Olig2+ nucleus in the fornix. Scale bars: 200 µm (a); 50 µm (b-d); 20 µm (e, top); 5 µm (E, bottom); 10 µm (f). Confocal maximum intensity projection thickness: 2.8 µm (e); 4.8 µm (f).

5.3.3 Modelling of rostral thalamic tau pathology in wild type mice

In THY-Tau22 mice I did not observe pTau+ neurons in the thalamus (Figuree 5.2 a) and to my knowledge there is no mouse model that would show tau pathology in this region. Moreover, THY-Tau22 mice cannot be used to assess the effect of the pathology in the ADn as the cortex was severely affected, therefore, it would not be possible to tell which brain area causes the impairment of memory.

I aimed to develop a mouse model that mimics the rostral thalamic pathology (see Chapters 3 and 4) to understand the role/effects of pTau *in vivo* and to assess its effects on neuronal activity on memory. It has been shown that the lesion of anterior thalamic nuclei with the lesion of LD causes severe memory deficit (Warburton et al 1997). The ADn which is part of the anterior thalamic nuclei and the LD were early affected in Alzheimer's disease (Chapter 3 and 4). Also, I aimed to assess whether pTau spread in an age-dependent manner similarly to THY-Tau22 mice. An AAV encoding a mutant form (P301L) of the human tau protein huTau and GFP (Wegmann et al 2019) was injected into the rostral thalamus of wild type mice (C57BL/6J) (Figure 5.6). During the translation the GFP and huTau are separated which allows to map the spread of huTau. Control mice were injected with an AAV-GFP construct to test the hypothesis that pTau is able to spread but GFP is not able to propagate. The infected neurons were not immunopositive for AT8 antibody or AT100 but they showed immunoreactivity for the T231-tau which detects human tau phosphorylated at T231 (Table 2.1). This indicates that the pTau was phosphorylated at a different epitope compared to what was observed in the THY-Tau22 mice.

In the assessed neurons, GFP and T231-tau always colocalized, I did not observe neurons that were immunopositive for only T231-tau which indicates that huTau did not spread between the neurons. This can be explained by the observation that the spread of pTau depends on the mouse lines; some strains showed more tau spreading than others (Dujardin et al 2022).

Alternatively, the GFP and pTau were not cleaved after translation. In conclusion, this mouse model can be used to assess the effect of thalamic tau pathology but the pTau does not propagate at an age-dependent manner as it was observed in humans (Chapter 3 and 4) and in THY-Tau22 mice.

Moreover, I did not observe glial cells that expressed pTau. The experiments will reveal which cell types are affected, what is the effect of pTau accumulation on neuronal activity and behaviour. At the time of writing, experiments are being performed in the laboratory to test whether pTau accumulation in injected mice affects neuronal activity, with hypothesis that it decreases the firing rates of head direction (HD) cells, just like in Thy-tau22 mice the distribution of ProS complex spike cells is shifted to the left (i.e. lower firing rates) (Viney et al 2022).

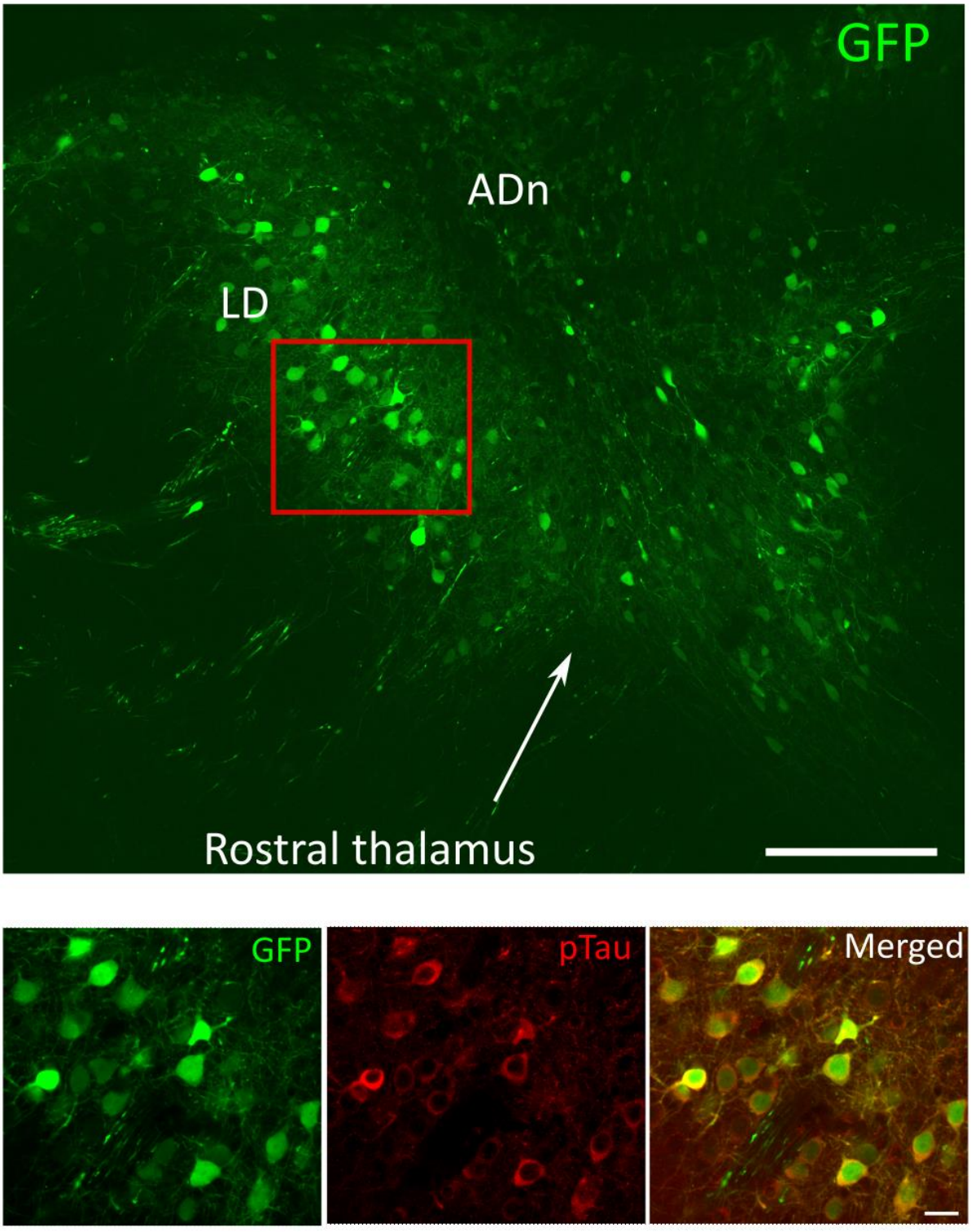


Figure 5.5 PTau expressed in the rostral thalamus after AAV-GFP-Tau (P301L) injection
Epifluorescence image of the GFP immunopositive neurons in the rostral thalamus (ADn-anterodorsal thalamic nucleus, LD-laterodorsal thalamic nucleus) of a wild type mouse. Insets represent the co-expression of GFP and pTau in the rostral thalamus. Scale bars: top-200 µm, bottom-20 µm.

5.3.4 Disrupted vascular structure in the human ADn

While assessing tau pathology in the ADn I observed striking structural changes of the blood vessels in cases with tauopathy. I assessed the vascular structures of cases with tau pathology (n=3 cases) and without tau pathology (n=2 cases). In cases without tau pathology (Braak stage 0, Case 3, Case 4) there were no observed pathological changes (Figure 5.7 a). In the early case (Braak stage II, Case 25) a striking railway track-like structure emerged around the basal lamina (Figure 5.7 b). Similar structure surrounded the blood vessel in the middle stage of pathology (Braak stage III, Case 12) (Figure 5.7 c), moreover, the basal lamina was thickened and enlarged. In the late stage (Braak stage VI, Case 17) (Figure 5.7 d) the basal lamina protruded and it was surrounded by the same remarkable structure. The adjacent MD and AV (Figure 5.7 e), which did not exhibit tau pathology, lacked the pathological characteristics around the vessels.

In conclusion, the blood vessels in the ADn show pathological changes from early stages and further investigation is needed to determine whether these changes driver or result of the tau pathology.

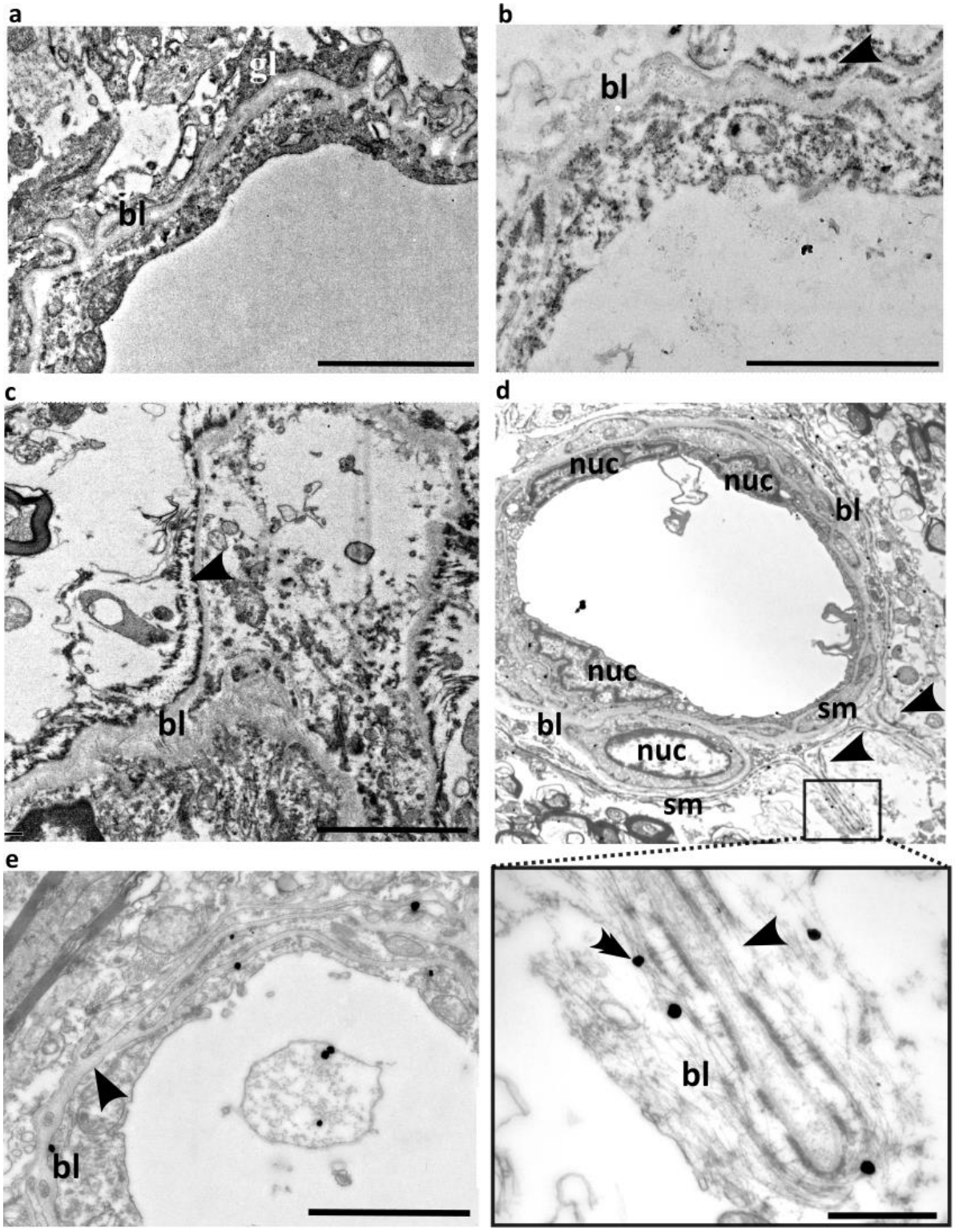


Figure 5.6 Electron micrographs of disrupted blood vessels in the ADn of cases with tau pathology

(a) Blood vessel of case without tau pathology with no obvious pathological changes (Case 3, Braak stage 0). (b) In the early stage (Braak stage II, Case 25), basal lamina is surrounded by a railway track-like structure. (c) In the mid stage, basal lamina is thickened, enlarged and surrounded by a railway track-like structure (Case 12, stage III). (d) In the late stage, basal lamina is protruding and surrounded by a railway track-like structure (arrow head) (Case 17, stage VI). (e) In the late stage, the basal lamina (arrowhead) is intact in the AV (Case 17, stage

VI). Inset, detail of the boxed region showing a railway track-like structure containing thin filaments (double arrowheads mark gold–silver particles arising from unspecific labelling). Basal lamina, bl; Endothelial cell, end; Glial cell, gl; Pericyte, pc; Nucleus, nuc; Smooth muscle cell, sm. Scale bar: 2 μm.

5.4 Discussion

5.4.1 Modelling of neurological diseases

Neurological diseases caused by several factors including neuronal, glial and vascular pathology. For most diseases the cause is not well-understood, therefore, it has been challenging to model them. Although, animal models can be advantageous to understand a distinct aspect of the pathology such as the spread of a pathological protein. Different genetic tools allowed researchers to develop mouse models that express the mutant form of tau protein which induces its spread and accumulation (Clavaguera et al 2009, Lin et al 2003, Schindowski et al 2006). It has been described that THY-Tau22 mice shows impaired hippocampal synaptic transmission and reduced spatial memory (Schindowski et al 2006). I aimed to assess the propagation of pTau in these mice and whether the thalamus is involved in the pathology.

I observed the age-dependent propagation of pTau. Similarly to Alzheimer's disease (Braak & Braak 1991b), in these transgenic mice the hippocampal formation, the basolateral amygdala and the layer 5 of isocortex were affected by pTau, however, the entorhinal cortex showed only a modest level of tau pathology. Subcortical areas such as the thalamus and the MB lacked pTau. Our research group showed that there were fewer high-firing prosubicular pyramidal cells in THY-Tau22 mice, but the firing population retains its coupling to theta oscillations. Spatial memory tests showed that the transgenic mice had reduced short-term familiarity. Their spatial working and reference memory were apparently intact but the they had a delay initiating behavioural tasks (Viney et al 2022). This might indicate that subcortical regions are involved in the development of memory deficit. Alternatively, tau pathology without any other pathological changes is not able to induce memory impairment.

To investigate whether subcortical pathology affects memory I aimed to develop a mouse model that displays tau pathology in thalamus. I injected a virus the encodes pTau into the LD and into the adjacent ADn as it has been shown that inactivation of these nuclei impairs

spatial memory likely due the disruption of head direction system (Wilton et al 2001). After the injection with AAV that encodes huTau (will be named as pTau) and GFP I found the expression of pTau in the targeted area (Figure 5.5). It contrast to a previous finding (Wegmann et al 2019), I did not observe the spread of pTau, after this finding a paper was published showing that C57BL/6 mice are resilient to pTau propagation (Dujardin et al 2022). The effect of the pTau accumulation on neuronal activity and on behaviour in the rostral thalamus is currently being investigated by our team (Shan Jiang, Dr Sara Hijazi, Sarkany, Verena Gautsch, Dr Michael Hasselmo, Dr David Bannerman, and Dr Tim Viney, *unpublished*). It is hypothesized that pTau disrupts neuronal activity in the ADn which contains HD cells (Taube 1995). This can lead to impairment in spatial navigation, which is one the first signs of Alzheimer's disease (Tangen et al 2022).

5.4.2 Oligodendrocytes might facilitate the spread of pTau

It has been shown that the three different glial cells; astrocytes, oligodendrocytes, microglia cells are involved in neurodegenerative diseases (Hansen et al 2018, Nishimura et al 1995, Verkhratsky et al 2010). Oligodendrocytes form myelin sheaths around axons but these cells have more complex role than passive insulation. They also support the energy metabolism of axons by releasing lactate through the monocarboxylate transporter 1; lactate is metabolized by axons to generate ATP (Saab et al 2013). The term oligodendrogliopathy indicates that oligodendrocytes have predominant role in neurodegenerative diseases.

Oligodendrocytes are affected in several diseases with abnormal protein aggregates such multiple system atrophy, Lewy body disease, Alzheimer's disease, Creutzfeldt-Jakob's disease. Oligodendrocytes are overlooked in Alzheimer's disease and they are mainly associated with PSP (Jäkel et al 2019, Komori 1999). Interestingly, these cells are able to produce amyloid-β and contribute to plaque formation (Sasmita et al 2024); moreover, aberrant

Erk1/2 signalling of oligodendrocytes was observed in transgenic mice (Park et al 2023). I observed that oligodendrocytes in aged THY-Tau22 mice accumulated pTau. These animals express human tau mutated at sites G272V and P301S under Thy1.2-promoter. It was unexpected to observe pTau in oligodendrocytes as the Thy1 promoter is not active in oligodendrocytes (Caroni 1997) because the control animal that expressed GFP under the Thy1 promoter lacked GFP in oligodendrocytes (Table 5.3). This is line with a study that showed that after pTau inoculation into the corpus callosum from brain extracts with Alzheimer's disease, PART, globular gial tauopathy, PSP, Pick's disease, and frontotemporal lobar degeneration linked to P301L mutation; pTau seeding occured in oligodendrocytes (Ferrer et al 2019). The next question was to investigate how pTau spread from neurons to oligodendrocytes. One possibility that pTau enters the oligodendrocytes via node of Ranvier. Nodes of Ranvier occur along the axon where the axolemma is not insulated with myelin sheath (Rasband & Peles 2015). This can be assessed by electron microscopy using gold-silver particles to label pTau (as in Chapter 4). Alternatively, oligodendrocytes may uptake exosomes filled with pTau. There is a study indicating that pTau propagation is dependent on EV transmission between astroglia and neurons (Dinkins et al 2016); oligodendrocytes might play a similar role in pTau propagation.

5.4.3 Vascular pathology in Alzheimer's disease and in other neurodegenerative diseases

It is important to mention that vascular changes frequently occur in neurodegenerative diseases (Kalaria 2003). It is still not well-understood whether vascular dysfunction in Alzheimer's disease is a prelude to pathological changes or consequence of it. Various studies revealed that there is a correlation between cardiovascular diseases and risk of developing Alzheimer's disease, leading to the so-called vascular hypothesis. Vascular risk factors including hypertension and hyperhomocysteinemia are linked to a significantly increased

chance to develop Alzheimer's disease (Scheffer et al 2021, Smith et al 2018). It has been shown that vascular changes emerge early in Alzheimer's disease; insoluble pathogenic proteins such as amyloid-beta and pTau accumulate along the blood vessels (Apátiga-Pérez et al 2022, Hoglund et al 2024). Cerebral amyloid angiopathy is a type of angiopathy in which amyloid-β deposits in the wall of blood vessels, the disease is associated with haemorrhages and cognitive decline (Wang et al 2024). The presence of cerebral amyloid angiopathy in Alzheimer's disease is associated with a more progressive and severe cognitive decline (Greenberg et al 2020). I observed that in brains of donors with tau pathology the vascular structure altered and showed the sign of pathological changes (Figure 5.7). Basal lamina separates the endothelial cells from neurons and glial cells and contributes to vessel development and maintenance of BBB (Morris et al 2016). Even in the early case the basal lamina was surrounded by a railway-track like structure (Figure 5.7 b). This structure is likely to be part of the astrocytic endfeet which are involved in the maintenance of the BBB (Kubotera et al 2019). It has been shown that in Alzheimer's disease the expression of astrocytic endfoot genes including aquaporin-4 are altered (Yang et al 2016); disruption of astrocytic endfoot might affect the main function of the glymphatic system, the clearance (Simon et al 2018). In cases with tau pathology the basal lamina was remarkably thickened, similar pathological changes have been described in cortical blood vessels of Alzheimer cases (Mancardi et al 1980). In conclusion blood vessels are disrupted early in Alzheimer's disease.

5.5 Limitations of the study

Animal models have several advantages including opportunity for genetic modification, low genetic diversity. However, due to the complexity of neurological diseases they do not model diseases accurately. Moreover, most animal models in Alzheimer research overexpress pTau including THY-Tau22 mice (Schindowski et al 2006) and AAV-injected animals. The

observed pathological changes can be contributed to the increased quantity of the proteins. In Alzheimer's disease the level of tau protein in the brain is not increased, instead the tau proteins undergo pathological structural changes (Goedert et al 2010). Moreover, in these animal models the tau protein is mutated to induce propagation and aggregation but in Alzheimer's disease there is no mutation in the tau protein. Interestingly, the tau protein is mutated in frontotemporal dementia and parkinsonism linked to chromosome 17 (Hutton et al 1998). The AAV injection allow us to develop pTau in the thalamus similarly to the the human brain. However, it is challenging to target the ADn due its small size which might result differences between affected brain areas. The adjacent LD was also affected by tau pathology (Chapter 3). To mimic the pathology observed in the human brain and to see a significant spatial memory impairment the LD was also target (Warburton et al 1997). Moreover, another important limitation of the study that mice have shorter life expectancy, ~2 years compare to human which might too short for pTau propagation. It has been important to investigate the brain of younger donors to understand whether pTau accumulation in the ADn is pathological or part of ageing.

The younger life expectancy of the mice might explain why I did not observe AT8/AT100 immunoreactivity. Different tau epitopes become phosphorylated at different time, however, AT8 has been described as an early indicator of tau pathology (Su et al 1994). I assessed ageing (from 8 to 20-month-old) GFP-2a-huTau (P301L) and GFP-2a-huTau mice, and in these animals pTau propagation was not detected. Similarly, coiled bodies were not observed.

6 General discussion

6.1 Main findings

- The human ADn, in contrast to other rostral thalamic nuclei, exhibits very early tau pathology and is severely affected in Alzheimer's disease
- Neurons expressing CR in the ADn are vulnerable to pTau accumulation as early as Braak stage 0
- Paired pre- and postsynaptic structures contain pTau, suggesting transsynaptic spread
- Large vGLUT2+ boutons, likely originating from the LMB, preferentially accumulate pTau, in contrast to rare pTau in corticothalamic boutons
- The ADn lacks amyloid-beta plaques, in contrast to the adjacent MD and AV
- In the mouse tauopathy model, THY-Tau22, pTau spreads from neurons to oligodendrocytes (starting at 8 months of age)
- Viral expression of GFP-2a-huTau in C57BL/6J mice does not lead to tau propagation (maximum expression time 11 months)
- Blood vessels are selectively disrupted in the ADn from human cases with tau pathology

6.2 Significance and origin of tau pathology

Most neurodegenerative diseases involve misfolded proteins. Alzheimer's disease is the most common neurodegenerative disease; the two main pathological hallmarks are the accumulation pTau (Arima et al 1998, Braak & Braak 1991b) and amyloid-β (Hampel et al 2021). Less than 5% of cases are familial (Piaceri et al 2013). Well-known risk factors are ageing, diabetes, smoking, cardiovascular problems, head injuries, viral and bacterial infections, air pollution, sight problems and social isolation (Breijyeh & Karaman 2020, Livingston et al 2024). Despite Alzheimer's research being in the spotlight there is no effective therapy; however, prevention can significantly reduce the probability of the development of the disease. Prevention can focus on several factors such as depression, obesity, hyperhomocysteinaemia, hypertension (Yu et al 2020).

The latest medication which was approved by Food and Drug Administration (FDA) called Lecanemab. This drug is a monoclonal antibody that binds with a high-affinity to amyloid-β protofibrils with high affinity (Abbasi 2018). It is important to note that there are several controversies regarding the clinical trial of the drug such as not assessing controls properly. Moreover, antibody therapies that target amyloid-β are associated with cerebral atrophies (Nadeau 2024). Most of the alternative antibody therapies that target pTau aggregates do not succeed (Imbimbo et al 2023). In order to develop a more or effective tau antibody therapy, mRNA-encoded antibodies have been also developed, however, they were only tested in cell cultures (Wongsodirdjo et al 2024). Another novel approach is to reduce the level of tau by using antisense oligonucleotide, this approach was tested in phase 1b clinical trial which showed dose-dependent reduction in the cerebrospinal fluid total-tau concentration (Mummery et al 2023). A different therapeutic approach is targeting the sigma-1 receptor with an antagonist called blarcamesine. The activation of the receptor might block tau phosphorylation at epitopes linked to pathological changes (Lahmy et al 2013). Moreover, activation of sigma receptor promotes autophagy (Christ et al 2019). Furthermore, the activated receptor attenuates the disruption of the BBB by inhibiting amyloid-β accumulation in mice (An et al 2022).

This approach is promising as it targets several pathological changes instead of focusing only one component.

It is crucial to untangle which brain regions affected first to understand whether the different drugs are able to stop the propagation and for early diagnosis. Moreover, the identification of vulnerable cell types can help to identify novel drug targets, as it is the case for dopaminergic neuronal loss in Parkinson's disease (Kalia & Lang 2015). Alzheimer's disease is diagnosed with a set of diagnostic tools although the early recognition is challenging. Several imaging techniques are applied to diagnose Alzheimer's disease such as PET, MRI,

fMRI. During the application of these techniques the focus is on the cortical areas which might delay the diagnosis and the potential therapy.

I observed that the ADn was affected early on by tau pathology that in fact preceded significant cortical pathology. The consistency of tau pathology in the ADn was striking, as nearly 90% of cases had the same pattern. I found pTau+ neurons and processes (axons and dendrites) restricted to the ADn even in controls ('pre-Braak' stage 0; Chapter 3). It is important to note that this can be part of normal ageing. In future studies, young cases should be assessed to determine whether pTau accumulation emerges in the ADn. The commonly observed tau pathology in aged people called PART, it is almost universally detected among elderly (Crary et al 2014). Not only neurons but astrocytes are also affected by ageing. Ageing-related tau astroglial pathology refers to pTau immunopositive astrocytes that mainly contain 4R pTau (Kovacs et al 2016). An important question to ask is why the ADn is more vulnerable than other brain regions. There are several possible explanations. One of them is that the ADn 'ages faster' than other brain regions. I observed that in mice the ADn cells contain a much higher density of lipofuscin compared to the adjacent nuclei; lipofuscin is an indicator of ageing (Moreno-García et al 2018). Moreover, I observed putative autophagosomes in vGLUT2+ boutons in the ADn which accumulation increases with age (Nixon et al 2005). An interesting experiment would be to check the DNA methylation patterns of the ADn cells, which is another indicator of ageing (Horvath 2013). It is known that the ADn neurons have long axons which might make neurons more vulnerable; neurons with long projecting axons are dependent on efficient proteolysis and autophagy, a complex and sensitive process that requires autophagosomes to travel long distances to reach the degenerative lysosomes in the cell body (Lee et al 2011). Noradrenergic LC neurons are thought to be vulnerable due to their long-range axonal projections (Gilvesy et al 2022). Likewise, the ADn neurons have relatively long axons projecting to different cortical areas (Jiang et al 2024). Similarly, the RE cells have long

projection axons, however, they are very low activity cells which indicates that for increased vulnerability both long axons and high activity with large energy demand is required (Dolleman-Van Der Weel & Witter 1996, Hauer et al 2019). Although all the anterior thalamic nuclei (ADn, AV, AM) project to the same cortical regions such as granular RSC, PreS and EC (Shibata 1993a, Shibata 1993b, Shibata 1998) but they might target partially different cell populations. The AV and AM receive inputs from multiple cortical areas including the EC, yet the ADn only receives input from the dorsal part of the RS and not from the EC (Kaitz & Robertson 1981, Saunders et al 2005). If pTau had spread directly from the EC to the anterior nuclear group, the pTau would early emerge in the AV, but it was sparse even at the middle stage (Chapter 3). Another critical difference between the anterior thalamic nuclei is that the ADn receives glutamatergic input from the LMB, whereas the AV and AM receive input from the MMB (Guison et al 1995, Hayakawa & Zyo 1989).

Moreover, the different thalamic nuclei consist of different types of neurons which might be associated with their vulnerability. Different thalamic cells express different calcium binding proteins such as CR, PV, CB (Münkle et al 2000), PCP-4 (Murray et al 2007). These calcium binding proteins act as calcium buffers and regulate the intracellular calcium level. Interestingly, the lack of CR in granule cells alter neuronal excitability (Gall et al 2003). In Chapter 3 I reported that CR-expressing neurons were susceptible to pTau accumulation in the ADn even before cortical tau pathology emerged (Braak stage 0). There are genes that are selectively and highly expressed in the ADn neurons such as PTCHD; mutations in this gene cause cognitive impairment (Roy et al 2021). Similarly, the mammalian target of rapamycin (mTOR) is also highly expressed in the ADn, and mTOR regulates cellular metabolism including autophagy, which is impaired in Alzheimer's disease (Boland et al 2008). Two of the earliest signs of Alzheimer's disease are the impairment of spatial memory and the increased number of falls (Swaddiwudhipong et al 2022). It has been shown that lesions of the anterior

thalamic nuclei (ADn, AV, AM) impairs spatial reference and working memory in rats (Frost et al 2021, Mitchell & Dalrymple-Alford 2006) and its degeneration in humans causes memory deficits (Harding et al 2000). Therefore, anterior thalamic nuclei are linked to the early signs of Alzheimer's disease (Aggleton et al 2016). Moreover, the ADn contains HD neurons; these cells increase their firing rates when the head points in a specific direction (Taube 1995). The disruption of HD cells by pTau might cause deficit in spatial navigation and falls. The high energy demand of HD cells might be associated with pTau accumulation. This is supported with the observation that other part of the head direction system such as RSC, LD, LMB are also affected early in the disease progression (Chapter 3). The adjacent AV, which comprises less energetically demanding theta rhythmic neurons, were only mildly affected, even in late Braak stages.

There are sensory modalities that are integrated by the ADn including vestibular, visual and proprioceptive (Hitier et al 2014, Perry & Mitchell 2019, Wijesinghe et al 2015). Moreover, the ADn is involved in gravity sensation. It has been shown that pTau disrupts neuronal activity (Busche 2019, Menkes-Caspi et al 2015). This indicates that the tau pathology in the ADn may be responsible for disorientation and falls.

To provide additional context for the very early subcortical tau pathology in the thalamus, in Chapter 3 I also assessed the LC, which is susceptible to pTau at 'pre-Braak' stages (Ehrenberg et al 2017, Gilvesy et al 2022). At early stages, in contrast to the sparse–moderate levels of pTau in the ADn, I detected only sparse pTau (Chapter 3).

The LMB, which projects to the ADn as a unidirectional projection (Veazey et al 1982), lacked pTau in early stage cases. This indicates that pTau might spread retrogradely from the ADn to the MB. In one Braak stage II case, the ADn exhibited moderate-dense pTau and the LMB showed mild–moderate pTau level. In middle and late stages, moderate–dense pTau was present in the LMB. The DRn also showed moderate pTau in one tested Braak stage II case but

further cases are needed to make a conclusion. Interestingly, it has been shown that pTau emerges in the DRn of cases without dementia and in mice the overexpression of P301L-tau caused depressive-like behaviours (Pierson et al 2024). The DRn also has extensive projections including to the frontal cortex, basal ganglia and ventral tegmental area (Hamada et al 2024); the last is also affected in the pre-cortical phase (Stratmann et al 2016). In conclusion, subcortical areas, especially the ADn, are affected by tau pathology before the cortex and they might be responsible for the early signs of Alzheimer's disease such as falls and impaired spatial navigation.

6.3 Propagation of pathological proteins

Several neurodegenerative diseases such as Alzheimer's disease, Parkinson's disease, PSP, amyotrophic lateral sclerosis, and Creutzfeldt-Jakob disease are characterized by the appearance of misfolded proteins in the nervous system (Sweeney et al 2017). These proteins can gain a toxic function or lose their physiological function (Winklhofer et al 2008). The most well-known infectious proteins are prions, which are misfolded proteins that induce pathological conformational changes in other proteins (Prusiner 1982). Interestingly, it has been shown that amyloid-β is transmissible by contaminated preparations; patients who were treated with contaminated cadaveric pituitary growth hormone developed amyloid-β pathology (Purro et al 2018).

There are several hypotheses about pTau propagation, one of the most popular ones is the prion-like spread. This means that the pTau would spread via neuroanatomical connectivity from donor cells to a recipient cell in which the pTau would induce the misfolding of other tau proteins (Mudher et al 2017). This theory is supported by previous research showing that injection of brain extract from mutant P301S tau-expressing mice into wild-type tau-expressing mice induced the aggregation of tau into filaments and spreading from the site of injection to

neighbouring brain regions (Clavaguera et al 2009). Furthermore, it has been shown that the intracerebral injection of synthetic full-length wild type human tau mixed with dextran-sulphate causes tau propagation in mice (Masuda-Suzukake et al 2020). Similarly, in transgenic mice that expressed tau in the EC, tau propagated to connected areas such as the SUB and dentate gyrus (Liu et al 2012). A research study also showed that pTau spreads in synaptic vesicles, which might be mediated by AMPA receptors (Pooler et al 2013). Another study showed that neurons release exosomes following depolarisation (Wang et al 2017). Synaptic dysfunction is associated with pTau accumulation and it is an early characteristic of Alzheimer's disease. A protein called synaptogyrin-3 mediates the binding of pTau to synaptic vesicles. This can cause the excessive aggregation of synaptic vesicles and restrict the presynaptic vesicle mobility (Largo-Barrientos et al 2021, McInnes et al 2018).

Interestingly, excitatory neurotransmission is particularly vulnerable to tau pathology due to the loss of glutamatergic receptors (Italia et al 2022). Nuclei adjacent to the ADn such as the AV and MD were relatively resistant to pTau, even in late stages. I suggest, at least in the rostral thalamus, that propagation of pTau is facilitated via synapses and circuits rather than geometrical proximity with regional vulnerability contributing. A still unsolved question is whether pTau spreads anterogradely, retrogradely, or in a bidirectional manner. Recent research suggested that pTau is able to spread in a bidirectional manner after injection of oligomeric and fibrillar tau int the medial EC of wild type rats (Langer Horvat et al 2023).

Retrograde spread was supported by a study in which mice expressed tau with P301S mutation and the propagation of pTau was followed by a whole brain staining method (Ramirez et al 2023). Moreover, human PET studies also confirmed that pTau is able to spread retrogradely along Braak stages (Seemiller et al 2021).

To understand the propagation of pTau it is critical to describe its subcellular distribution because different forms of tau may be packaged or organised/processed in

particular ways that facilitates the release from cells and uptake to connected cells. The ADn is an ideal candidate to assess pTau distributions as the pathology emerges early in this thalamic nucleus. I observed pTau in somata, dendrites, myelinated axons, and at both sites of synaptic structures. Using perfusion-fixed human brain tissue and immunogold labelling, I localized, to my knowledge for the first time, pTau to presynaptic boutons and postsynaptic dendrites, with paired helical filaments resembling those described previously in cases of Alzheimer's disease and other tauopathies (Arima 2006, Arima et al 1998, Kidd 1963, Kidd 1964, Terry et al 1964, Terry 1963). This suggests that pTau might be able to spread via synapses in the human brain. Surprisingly, I could show that pTau accumulated on both sides of dendro-dendritic gap junctions (Chapter 4). This might suggest that pTau is also able to spread via these junctions. Further electron microscopy studies could reveal how pTau propagate via these junctions; also it would be important to assess whether they spread as monomers or as oligomers. Interestingly some of the terminals in the ADn were electron opaque, or "dark". These dark terminals can occur by *post-mortem* delay/inadequate fixation or this can be sign of neurodegeneration (Colonnier 1964, Szentágothai et al 1966).

These dark terminals might arise from the LMB which potentially undergoes early neurodegeneration.

I observed (in Chapter 4) that the terminals containing tau filaments were large both in the middle and late stages. The origin of the large terminals is subcortical, and cortical of the small ones. Large presynaptic terminals of subcortical origin predominantly contain vesicular vGLUT2 (Rovó et al 2012). I observed a striking overlap between the distributions of vGLUT2 and AT8 immunoreactivities at light microscopic level. I hypothesized that this overlap indicates a critical association between vGLUT2 and pTau which is supported by the observation that thalamic nuclei that receive dense glutamatergic input might be predisposed to pTau accumulation (Xuereb et al 1990). Moreover, the network spread of pTau shows

association with the expression of glutamatergic-related genes in the human brain (Montal et al 2022).

The TRN, which only contains GABAergic neurons, lacked pTau+ cells bodies despite containing pTau+ axons. Surprisingly, despite the classical hypothesis of pTau spreading via corticocortical pathways originating in the EC (Braak et al 2011) pTau was not localised to corticothalamic boutons in the ADn. Instead, pTau was preferentially localised to large vGLUT2-expressing subcortical terminals. This supports the transsynaptic pTau propagation theory and highlights an alternative or parallel major subcortical glutamatergic pathway necessary for driving the spread of pTau.

Based on my observations I hypothesize (Figure 6.1) that pTau first accumulates in the CR-expressing ADn neurons of the Papez circuit. Subsequently, pTau spreads to the large mammillothalamic vGLUT2+ terminals from dendrites in the ADn. Axons of the ADn cells transfer pTau to the vGLUT2+ terminals in the TRN and to cortical target regions such as the RSg. The observation that TRN lacks pTau+ cell bodies indicates that that the predominantly GABAergic cell population is resistant to the spread of pTau from vGLUT2+ boutons, whereas cortical neurons postsynaptic to ADn neurons are likely to be susceptible. Although, it cannot be ruled out that pTau spreads retrogradely from cortical neuron dendrites into ADn vGLUT2+ terminals, then from ADn dendrites to mammillothalamic terminals at the early stages. In some early stage cases there were AT8+ axon terminals in first layer of granular RS (data not shown). However, the very early present of pTau+ neurons in the ADn prior to cortical neurons makes this route unlikely.

Anterograde spread of pTau from the cortex to the ADn is also not supported by my data, as small cortical terminals lacked pTau in the middle and late stages. Furthermore, I did not observe pTau in the LMB at Braak stage 0 (when pTau was present in the ADn) which rules out anterograde propagation from the LMB, at least in the cases I examined. The

vGLUT2+ mammillothalamic terminals are especially vulnerable due to a nearly threefold increase of pTau in these boutons from the middle stage to late stage. These large boutons form structures called puncta adherentia that may even be required for the transfer of pTau (Figure 6.1).

Surprisingly, the ADn lacked amyloid plaques despite that the surrounding AV and MD contained several plaques. If the amyloid-β hypothesis is true it would mean that the RSg contains amyloid plaques that trigger tau pathology in the ADn via axon terminals that originate from projection neurons of the ADn. It has been shown that RS dysfunction emerges during early stages of amyloid production in Tg2576 mice (Poirier et al 2011).

In future studies it would be important to test whether amyloid-β accumulation in the RSg precedes the pTau accumulation in the ADn in humans. In conclusion, my data suggest that the ADn might be a hub for tau pathology and from this region pTau propagates transsynaptically to other cortical and subcortical areas.

6.4 Propagation of pTau in transgenic mice

Several studies have showed that most neurodegenerative diseases, including Alzheimer's disease, involve glial and vascular pathology (Hansen et al 2018, Klohs 2019, Verkhratsky et al 2010). To prevent the different neurodegenerative diseases and to develop effective therapies, the neuron-centric approach should be changed to a more inclusive one. There are 6 tau isoforms in the brain; they are different by the absence or presence of 1 or 2 N-terminal inserts and 3R or 4R 31- or 32-amino acid repeats in the microtubule-binding domain (Goedert et al 2017). All six tau isoforms are present in disease filaments in Alzheimer's disease, chronic traumatic encephalopathy, familial British dementia, Down's syndrome, PART, and in several other diseases, whereas Pick bodies are only made of 3R tau. 4R tau makes up the filaments in e.g. CBD, argyrophilic grain disease, PSP (Goedert et al 2017). Tau

filament structures vary in different diseases, even when comprised of the same isoforms (Fitzpatrick et al 2017) which can be explained by that different posttranslational modifications (PTMs) alter the structure of tau protein (Ferrer et al 2014).

Tau undergoes of a broad variety PTMs including phosphorylation, acetylation, ubiquitination, glycation, glycosylation, SUMOylation, methylation, oxidation, and nitration. The role of these modification in different diseases is not well known but the phosphorylation of distinct epitopes is linked to different tauopathies (Alquezar et al 2020, Ferrer et al 2014). The accumulation of pTau in glial cells frequently causes disease specific glial phenotypes such as tufted astrocytes in PSP, astrocytic plaques in CBD (Ferrer et al 2014).

Animal models can mimic some aspects of tauopathies including the accumulation of pTau in distinct brain regions. These animals express the mutant tau which emerges in familial form of dementia (Joel et al 2018). Most animal models overexpress pTau, and whilst some drugs show therapeutic effect in these mice, they are not effective in clinical trials, highlighting the limitations or translational potential of these models (Wenger et al 2023). However, assessing these transgenic animals can facilitate an understanding on the propagation of pTau and its effects at different levels such as disrupting neuronal network activity or behaviour.

In Chapter 5 I mapped the propagation of pTau in THY-Tau22 mice, which showed age-dependent spread in agreement with the original study (Schindowski et al 2006). I found that pTau preferentially accumulated in deep-layer pyramidal neurons. Moreover, using silicone probe recording our research group observed the loss of high-firing pyramidal neurons in ageing and aged mice (16-24 months old). Despite this, we did not detect spatial working and reference memory deficit; however, transgenic mice had a delay before initiating the tasks (Viney et al 2022). This can be explained by subcortical areas that are affected early by pTau in Alzheimer's disease and part of the circuit of Papez such as the ADn and LMB lacked pTau+ neurons in this mouse model (Chapter 3).

I observed that the pTau spread from neurons to oligodendrocytes in aged (18–27 months) and aging (8–16 months) THY-TAU22 mice, but not in young animals. Coiled bodies were found in several brain regions, especially in white matter tracts (Chapter 5) (Viney et al 2022). This is line with a previous study that showed that after injection of pTau into the corpus callosum, oligodendrocytes accumulated pTau in wild type mice (Ferrer et al 2019). Thus, THY-Tau22 mice can reveal how pTau spread in different tauopathies. It has been shown that in PSP which is a 4R-tauopathy, oligodendrocytes accumulate pTau in several brain regions such as thalamus and globus pallidus (Kovacs 2020). The role of oligodendrocytes in Alzheimer's disease is overlooked despite that they were observed in patients almost 3 decades ago (Nishimura et al 1995). Oligodendrocytes are responsible for myelin formation, the degradation of myelin is a common characteristics of Alzheimer's disease which might lead to disrupted neuronal communication (Huang et al 2024). To develop a mouse model that mimics the thalamic tau pathology I injected an AAV encoding a mutant form (P301L) of the human tau protein and GFP (Wegmann et al 2019) into the rostral thalamus of wild type mice (C57BL/6J). With this approach I also aimed to assesses whether pTau propagates similarly to THY-Tau22 animals and humans. I observed pTau expression in the targeted LD and ADn but pTau did not propagate from these neurons. This can be explained by the finding that the spread of pTau depends on the mouse lines; C57BL/6J mice might be resistant to the tau confirmation that is generated by the P301L mutation (Dujardin et al 2022). At the time of thesis writing, experiments are being performed in the laboratory to assesses whether pTau accumulation in injected mice affects neuronal activity, with the hypothesis that it decreases the firing rates of HD cells (Jiang et al 2024), just like in THY-Tau22 mice the distribution of ProS complex spiking cells is shifted to the left (i.e. lower firing rates) (Viney et al 2022). Moreover, the accumulation of pTau in the rostral thalamus might cause spatial navigation deficit in these

mice as it has been shown that the lesion of anterior thalamic nuclei including lesion of LD causes severe memory deficits (Warburton et al 1997).

In conclusion, this mouse model can be used to examine the effect of thalamic tau pathology but the pTau does not propagate at an age-dependent manner as it was observed in humans (Chapter 3 and 4) and in THY-Tau22 mice.

6.5 Vascular pathology of ADn

Although the diverse triggers of neurodegenerative disease including Alzheimer's disease are still the topic of extensive debate, the possible contribution of cerebrovascular deficiencies has been promoted in recent years.

To get a detailed picture of the neurodegenerative disease I assessed vascular changes in the human rostral thalamus. The BBB operates within the neurovascular unit, which includes clusters of glial cells, neurons and pericytes; it is a highly selective semipermeable border of endothelial cells the controls the transfer of different molecules between the circulatory system and the central nervous system (Daneman & Prat 2015). The breakdown of BBB has been shown in Alzheimer's disease (Zlokovic 2011) and there is a considerable overlap between cerebrovascular disease and Alzheimer's disease in patients. The most frequent vascular pathologies are the small vessel disease and cerebral amyloid angiopathy and Alzheimer's disease (Attems & Jellinger 2014). Due to the disruption of blood vessels the cerebral metabolism including glucose supply become impaired (Farkas & Luiten 2001). It has been shown that the isoform ε4 of Apolipoprotein E is the strongest genetic risk factor for Alzheimer's disease and a known promoter of BBB dysfunction (Salloway et al 2002).

While assessing tau pathology in the human ADn I observed disrupted blood vessels in cases with tauopathy (Figure 6.1) even in early case (Braak stage II). The basal lamina splits up and a railway track-like structure emerged around it moreover, the basal lamina was

thickened and enlarged (Figure 5.7). Similar pathological features were observed in the cortex of patients with Alzheimer's disease (Farkas & Luiten 2001). The surrounding thalamic nuclei the AV and the MD lacked obvious pathological changes in blood vessels.

This suggests that the disruption of blood vessel in the ADn emerges early in tauopathies. Further experiments required to investigate whether the vascular changes are the cause or consequence of the tauopathies. Alternatively, both pathological features are cause by a third factor such an ageing or inflammation.

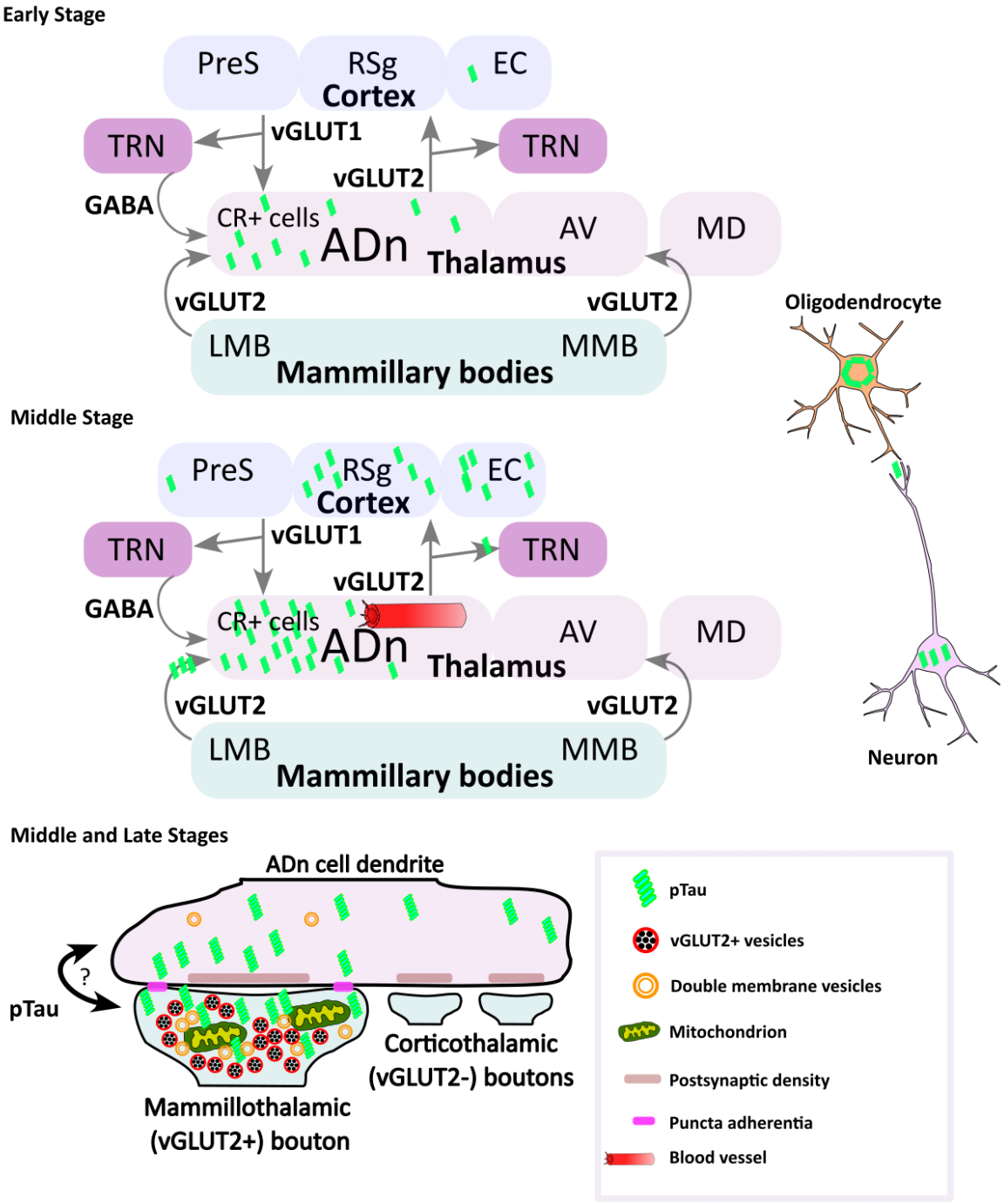


Figure 6.1 Hypothesis of pTau propagation in Alzheimer's disease
Schematic of pTau propagation and disrupted blood vessels. Scheme summarizing the data. According to my hypothesis, in the early stage (top), pTau (green) initially accumulates in CR+ cells of the ADn. By the middle stage, ptau has accumulated in cortical areas postsynaptic to the ADn, mainly the granular RS and EC. In the thalamus, pTau is present in ADn axons innervating the TRN and in mammillothalamic (vGLUT2+) terminals innervating the ADn. The GABAergic cells in the TRN are not invaded by pTau, nor are the corticothalamic terminals in the ADn. Bottom, details of pTau within the ADn at the middle stage (also applies to the late stage). Transsynaptic spread between the large vGLUT2+ mammillothalamic boutons and ADn dendrites may be retrograde or anterograde, potentially mediated through puncta adherentia.

Puncta adherentia are not found between small corticothalamic boutons and postsynaptic dendrites, and pTau was not observed in these presynaptic terminals at either middle or late stages, despite pTau in presynaptic cortical areas. The pathology might have been induced by the disrupted blood vessels in the ADn. Another possible way of pTau propagation is mediated via oligodendrocytes.

6.6 Limitations of the study

One of the main limitations of the study is the low sample size due to the difficulty to maintain well preserved human brain tissues. This arising from the fact that the human *post-mortem* perfusion is a complicated and rare procedure. Generally, before human tissue fixation the *post-mortem* delay is long which significantly impair the tissue quality. Moreover, there is a high diversity in donors including comorbidities, age, sex, education.

In this study I mainly used the AT8 antibody which recognises tau phosphorylated at both serine 202 and threonine 205 (Goedert et al 1995). The AT8 antibody is the most commonly used antibody but it does not reveal all forms of pathological tau protein e.g oligomeric ones.

Many scientific papers use the term of "Alzheimer model" which can be misleading. Animals do not model Alzheimer's disease as the pathology is not well-understood. Most of these animals overexpress amyloid-β or tau proteins and express mutated genes despite that less than 5% of Alzheimer cases are familial (Piaceri et al 2013) and these proteins are not overexpressed. However, the propagation and effect of the pathological proteins can be described with these animal models. The THY-Tau22 mice lacked the thalamic pathology which is an early characteristic of Alzheimer's disease and at 12 months the level of tau is approximately six-fold higher (Schindowski et al 2006). To model the thalamic pathology, I injected an AAV encoding a mutant form (P301L) of the human tau protein and GFP (Wegmann et al 2019) into the rostral thalamus of wild type mice (C57BL/6J). Due the small size of these nuclei there was variability in the injected area.

The combination of human and mouse studies can help to partially overcome these challenges as with the human tissue work I was able to see the exact pathology and mice allow me to assess the pTau propagation at a larger scale in a homogenous population.

6.7 Conclusion and outlook

Major questions regarding tauopathies are how the pTau spread between cells and which cell types are vulnerable. With the combination of assessing human *post-mortem* brain tissues and animal models I gained insight into pTau propagation.

I observed that thalamic nuclei differ in their vulnerability and the propagation of pTau correlates with the Braak stages. The first and most severely affected nucleus was the ADn which contains head direction cells and involved in spatial navigation and orientation. This suggests that specific thalamic nuclei may be driving the progression of early functional deficits in the progression of Alzheimer's disease, such as spatial disorientation.

I determined that tau pathology preferentially affected the CR-expressing subpopulation of glutamatergic neurons in agreement with the theory of cell-type-specific vulnerability. Future studies exploiting transcriptomics might identify other affected cell types and biochemical pathways which will be able to serve as potential target of novel drugs to cure Alzheimer's disease.

At the subcellular level, I detected pTau immunoreactivity in ADn cell bodies, dendrites, and in a specialized type of presynaptic terminal that expresses vesicular glutamate transporter 2 (vGLUT2) and likely originates from the LMB. In contrast, cortical terminals lacked pTau. This indicates that the subcortical pathology precedes the cortical involvement. Shifting the focus more on the thalamus might facilitate early diagnosis and drug development.

By assessing THY-Tau22 mice I observed that pTau spreads from neurons to oligodendrocytes. This indicates that pTau is able to spread in different ways such as extracellular vesicles and nanotubes not only via synapses. I hypothesize that pTau spreads from neurons to oligodendrocytes via nodes of Ranvier, and this can be tested using electron microscopy and immunogold labelling. The identification of entry point of pTau can facilitate of the development of therapy in tauopathies with significant oligodendropathy.

I developed a new mouse model by injecting an AAV encoding GFP-2a-huTau in the rostral thalamus of wild type mice. This mouse model allows the assessment of the effects of pTau on the function of rostral thalamus neurons including the ADn *in vivo* using electrophysiology and behavioural tests which might facilitate to detect the earliest signs of the thalamic pathology.

In conclusion, the ADn is affected by tau pathology very early on in disease progression and might serve as a 'hub' for pTau, which probably spreads via synapses involving vGLUT2-expressing terminals. Moreover, in THY-Tau22 mice, pTau spreads from neurons to oligodendrocytes.

7 References

Abbasi J. 2018. Promising Results in 18-Month Analysis of Alzheimer Drug Candidate. *Jama* 320: 965

Aggleton JP, Brown MW. 1999. Episodic memory, amnesia, and the hippocampal-anterior thalamic axis. *Behav Brain Sci* 22: 425-44; discussion 44-89

Aggleton JP, Nelson AJD, O'Mara SM. 2022. Time to retire the serial Papez circuit: Implications for space, memory, and attention. *Neurosci Biobehav Rev* 140: 104813

Aggleton JP, O'Mara SM. 2022. The anterior thalamic nuclei: core components of a tripartite episodic memory system. *Nat Rev Neurosci* 23: 505-16

Aggleton JP, Pralus A, Nelson AJ, Hornberger M. 2016. Thalamic pathology and memory loss in early Alzheimer's disease: moving the focus from the medial temporal lobe to Papez circuit. *Brain* 139: 1877-90

Allison SL, Fagan AM, Morris JC, Head D. 2016. Spatial Navigation in Preclinical Alzheimer's Disease. *J Alzheimers Dis* 52: 77-90

Alquezar C, Arya S, Kao AW. 2020. Tau Post-translational Modifications: Dynamic Transformers of Tau Function, Degradation, and Aggregation. *Front Neurol* 11: 595532

Alzheimer A, Stelzmann RA, Schnitzlein HN, Murtagh FR. 1995. An English translation of Alzheimer's 1907 paper, "Uber eine eigenartige Erkankung der Hirnrinde". *Clin Anat* 8: 429-31

Amaral DG, Dent JA. 1981. Development of the mossy fibers of the dentate gyrus: I. A light and electron microscopic study of the mossy fibers and their expansions. *J Comp Neurol* 195: 51-86

An Y, Qi Y, Li Y, Li Z, Yang C, Jia D. 2022. Activation of the sigma-1 receptor attenuates blood-brain barrier disruption by inhibiting amyloid deposition in Alzheimer's disease mice. *Neurosci Lett* 774: 136528

Andrade DM, Zumsteg D, Hamani C, Hodaie M, Sarkissian S, et al. 2006. Long-term follow-up of patients with thalamic deep brain stimulation for epilepsy. *Neurology* 66: 1571-3

Andrés-Benito P, Fernández-Dueñas V, Carmona M, Escobar LA, Torrejón-Escribano B, et al. 2017. Locus coeruleus at asymptomatic early and middle Braak stages of neurofibrillary tangle pathology. *Neuropathol Appl Neurobiol* 43: 373-92

Apátiga-Pérez R, Soto-Rojas LO, Campa-Córdoba BB, Luna-Viramontes NI, Cuevas E, et al. 2022. Neurovascular dysfunction and vascular amyloid accumulation as early events in Alzheimer's disease. *Metab Brain Dis* 37: 39-50

Arendt T, Stieler J, Strijkstra AM, Hut RA, Rüdiger J, et al. 2003. Reversible paired helical filament-like phosphorylation of tau is an adaptive process associated with neuronal plasticity in hibernating animals. *J Neurosci* 23: 6972-81

Arima K. 2006. Ultrastructural characteristics of tau filaments in tauopathies: immuno-electron microscopic demonstration of tau filaments in tauopathies. *Neuropathology* 26: 475-83

Arima K, Izumiyama Y, Nakamura M, Nakayama H, Kimura M, et al. 1998. Argyrophilic tau-positive twisted and non-twisted tubules in astrocytic processes in brains of Alzheimer-type dementia: an electron microscopical study. *Acta Neuropathologica* 95: 28-39

Ashton NJ, Brum WS, Di Molfetta G, Benedet AL, Arslan B, et al. 2023. Diagnostic accuracy of the plasma ALZpath pTau217 immunoassay to identify Alzheimer’s disease pathology. *medRxiv*: 2023.07.11.23292493

Attems J, Jellinger KA. 2014. The overlap between vascular disease and Alzheimer's disease - lessons from pathology. *BMC Medicine* 12: 206
Bankhead P, Loughrey MB, Fernández JA, Dombrowski Y, McArt DG, et al. 2017. QuPath: Open source software for digital pathology image analysis. *Sci Rep* 7: 16878
Barisano G, Montagne A, Kisler K, Schneider JA, Wardlaw JM, Zlokovic BV. 2022. Blood-brain barrier link to human cognitive impairment and Alzheimer's Disease. *Nat Cardiovasc Res* 1: 108-15
Bejanin A, Schonhaut DR, La Joie R, Kramer JH, Baker SL, et al. 2017. Tau pathology and neurodegeneration contribute to cognitive impairment in Alzheimer's disease. *Brain* 140: 3286-300
Biel D, Brendel M, Rubinski A, Buerger K, Janowitz D, et al. 2021. Tau-PET and in vivo Braak-staging as prognostic markers of future cognitive decline in cognitively normal to demented individuals. *Alzheimers Res Ther* 13: 137
Boland B, Kumar A, Lee S, Platt FM, Wegiel J, et al. 2008. Autophagy induction and autophagosome clearance in neurons: relationship to autophagic pathology in Alzheimer's disease. *J Neurosci* 28: 6926-37
Bourdenx M, Martín-Segura A, Scrivo A, Rodriguez-Navarro JA, Kaushik S, et al. 2021. Chaperone-mediated autophagy prevents collapse of the neuronal metastable proteome. *Cell* 184: 2696-714.e25
Braak H, Alafuzoff I, Arzberger T, Kretzschmar H, Del Tredici K. 2006. Staging of Alzheimer disease-associated neurofibrillary pathology using paraffin sections and immunocytochemistry. *Acta Neuropathol* 112: 389-404
Braak H, Braak E. 1988. Neuropil threads occur in dendrites of tangle-bearing nerve cells. *Neuropathol Appl Neurobiol* 14: 39-44
Braak H, Braak E. 1991a. Alzheimer's disease affects limbic nuclei of the thalamus. *Acta Neuropathologica* 81: 261-68
Braak H, Braak E. 1991b. Alzheimer's disease affects limbic nuclei of the thalamus. *Acta Neuropathol* 81: 261-8
Braak H, Braak E. 1991c. Neuropathological stageing of Alzheimer-related changes. *Acta Neuropathol* 82: 239-59
Braak H, Del Tredici K. 2016. Potential Pathways of Abnormal Tau and α-Synuclein Dissemination in Sporadic Alzheimer's and Parkinson's Diseases. *Cold Spring Harb Perspect Biol* 8
Braak H, Thal DR, Ghebremedhin E, Del Tredici K. 2011. Stages of the pathologic process in Alzheimer disease: age categories from 1 to 100 years. *J Neuropathol Exp Neurol* 70: 960-9
Breijyeh Z, Karaman R. 2020. Comprehensive Review on Alzheimer's Disease: Causes and Treatment. *Molecules* 25
Brion JP, Passareiro, H., Nunez, J., Flament-Durand, J. 1985. Mise en évidence immunologique de la protéine tau au niveau des lésions de dégénérescence neurofibrillaire de la maladie d'Alzheimer. *Arch Biol (Bruxelles)*
Busche MA. 2019. Tau suppresses neuronal activity in vivo, even before tangles form. *Brain* 142: 843-46
Byne W, Hazlett EA, Buchsbaum MS, Kemether E. 2009. The thalamus and schizophrenia: current status of research. *Acta Neuropathol* 117: 347-68
Calderon-Garcidueñas AL, Duyckaerts C. 2017. Alzheimer disease. *Handb Clin Neurol* 145: 325-37
Caroni P. 1997. Overexpression of growth-associated proteins in the neurons of adult transgenic mice. *J Neurosci Methods* 71: 3-9

Christ MG, Huesmann H, Nagel H, Kern A, Behl C. 2019. Sigma-1 Receptor Activation Induces Autophagy and Increases Proteostasis Capacity In Vitro and In Vivo. *Cells* 8
Christensen KR, Beach TG, Serrano GE, Kanaan NM. 2019. Pathogenic tau modifications occur in axons before the somatodendritic compartment in mossy fiber and Schaffer collateral pathways. *Acta Neuropathol Commun* 7: 29
Chun H, Im H, Kang YJ, Kim Y, Shin JH, et al. 2020. Severe reactive astrocytes precipitate pathological hallmarks of Alzheimer's disease via H(2)O(2)(-) production. *Nat Neurosci* 23: 1555-66
Clavaguera F, Akatsu H, Fraser G, Crowther RA, Frank S, et al. 2013. Brain homogenates from human tauopathies induce tau inclusions in mouse brain. *Proc Natl Acad Sci U S A* 110: 9535-40
Clavaguera F, Bolmont T, Crowther RA, Abramowski D, Frank S, et al. 2009. Transmission and spreading of tauopathy in transgenic mouse brain. *Nat Cell Biol* 11: 909-13
Cleveland DW, Hwo SY, Kirschner MW. 1977. Purification of tau, a microtubule-associated protein that induces assembly of microtubules from purified tubulin. *J Mol Biol* 116: 207-25
Colonnier M. 1964. EXPERIMENTAL DEGENERATION IN THE CEREBRAL CORTEX. *J Anat* 98: 47-53
Cornblath EJ, Li HL, Changolkar L, Zhang B, Brown HJ, et al. 2021. Computational modeling of tau pathology spread reveals patterns of regional vulnerability and the impact of a genetic risk factor. *Sci Adv* 7
Crary JF, Trojanowski JQ, Schneider JA, Abisambra JF, Abner EL, et al. 2014. Primary age-related tauopathy (PART): a common pathology associated with human aging. *Acta Neuropathol* 128: 755-66
Daneman R, Prat A. 2015. The blood-brain barrier. *Cold Spring Harb Perspect Biol* 7: a020412
Delpech JC, Pathak D, Varghese M, Kalavai SV, Hays EC, et al. 2021. Wolframin-1-expressing neurons in the entorhinal cortex propagate tau to CA1 neurons and impair hippocampal memory in mice. *Sci Transl Med* 13: eabe8455
Descarries L, Saucier G. 1972. Disappearance of the locus coeruleus in the rat after intraventricular 6-hydroxdopamine. *Brain Res* 37: 310-6
di Domenico A, Carola G, Calatayud C, Pons-Espinal M, Muñoz JP, et al. 2019. Patient-Specific iPSC-Derived Astrocytes Contribute to Non-Cell-Autonomous Neurodegeneration in Parkinson's Disease. *Stem Cell Reports* 12: 213-29
Ding SL, Yao Z, Hirokawa KE, Nguyen TN, Graybuck LT, et al. 2020. Distinct Transcriptomic Cell Types and Neural Circuits of the Subiculum and Prosubiculum along the Dorsal-Ventral Axis. *Cell Rep* 31: 107648
Dinkins MB, Enasko J, Hernandez C, Wang G, Kong J, et al. 2016. Neutral Sphingomyelinase-2 Deficiency Ameliorates Alzheimer's Disease Pathology and Improves Cognition in the 5XFAD Mouse. *J Neurosci* 36: 8653-67
Dolleman-Van Der Weel MJ, Witter MP. 1996. Projections from the nucleus reuniens thalami to the entorhinal cortex, hippocampal field CA1, and the subiculum in the rat arise from different populations of neurons. *J Comp Neurol* 364: 637-50
Dorph-Petersen KA, Lewis DA. 2017. Postmortem structural studies of the thalamus in schizophrenia. *Schizophr Res* 180: 28-35
Dujardin S, Fernandes A, Bannon R, Commins C, De Los Santos M, et al. 2022. Tau propagation is dependent on the genetic background of mouse strains. *Brain Commun* 4: fcac048
Dydyk AM, Munakomi S. 2024. Thalamic Pain Syndrome In *StatPearls*. Treasure Island (FL): StatPearls Publishing

Copyright © 2024, StatPearls Publishing LLC.
Dyson HJ. 2011. Expanding the proteome: disordered and alternatively folded proteins. *Q Rev Biophys* 44: 467-518
Edwards FA. 2019. A Unifying Hypothesis for Alzheimer's Disease: From Plaques to Neurodegeneration. *Trends Neurosci* 42: 310-22
Ehrenberg AJ, Nguy AK, Theofilas P, Dunlop S, Suemoto CK, et al. 2017. Quantifying the accretion of hyperphosphorylated tau in the locus coeruleus and dorsal raphe nucleus: the pathological building blocks of early Alzheimer's disease. *Neuropathol Appl Neurobiol* 43: 393-408
Escartin C, Galea E, Lakatos A, O'Callaghan JP, Petzold GC, et al. 2021. Reactive astrocyte nomenclature, definitions, and future directions. *Nat Neurosci* 24: 312-25
Farkas E, Luiten PG. 2001. Cerebral microvascular pathology in aging and Alzheimer's disease. *Prog Neurobiol* 64: 575-611
Ferrer I, Aguiló García M, Carmona M, Andrés-Benito P, Torrejón-Escribano B, et al. 2019. Involvement of Oligodendrocytes in Tau Seeding and Spreading in Tauopathies. *Front Aging Neurosci* 11: 112
Ferrer I, López-González I, Carmona M, Arregui L, Dalfó E, et al. 2014. Glial and neuronal tau pathology in tauopathies: characterization of disease-specific phenotypes and tau pathology progression. *J Neuropathol Exp Neurol* 73: 81-97
Fisher R, Salanova V, Witt T, Worth R, Henry T, et al. 2010. Electrical stimulation of the anterior nucleus of thalamus for treatment of refractory epilepsy. *Epilepsia* 51: 899-908
Fitzpatrick AWP, Falcon B, He S, Murzin AG, Murshudov G, et al. 2017. Cryo-EM structures of tau filaments from Alzheimer's disease. *Nature* 547: 185-90
Forno G, Lladó A, Hornberger M. 2021. Going round in circles-The Papez circuit in Alzheimer's disease. *Eur J Neurosci* 54: 7668-87
Fortin M, Asselin MC, Gould PV, Parent A. 1998. Calretinin-immunoreactive neurons in the human thalamus. *Neuroscience* 84: 537-48
Fowler SL, Behr TS, Turkes E, Cauhy PM, Foiani MS, et al. 2023. Tau filaments are tethered within brain extracellular vesicles in Alzheimer's disease. *bioRxiv*
Franzmeier N, Neitzel J, Rubinski A, Smith R, Strandberg O, et al. 2020. Functional brain architecture is associated with the rate of tau accumulation in Alzheimer's disease. *Nat Commun* 11: 347
Frost BE, Martin SK, Cafalchio M, Islam MN, Aggleton JP, O'Mara SM. 2021. Anterior Thalamic Inputs Are Required for Subiculum Spatial Coding, with Associated Consequences for Hippocampal Spatial Memory. *J Neurosci* 41: 6511-25
Gall D, Roussel C, Susa I, D'Angelo E, Rossi P, et al. 2003. Altered neuronal excitability in cerebellar granule cells of mice lacking calretinin. *J Neurosci* 23: 9320-7
Ge M, Zhang J, Chen S, Huang Y, Chen W, et al. 2022. Role of Calcium Homeostasis in Alzheimer's Disease. *Neuropsychiatr Dis Treat* 18: 487-98
Gent TC, Bassetti C, Adamantidis AR. 2018. Sleep-wake control and the thalamus. *Curr Opin Neurobiol* 52: 188-97
Gilvesy A, Husen E, Magloczky Z, Mihaly O, Hortobágyi T, et al. 2022. Spatiotemporal characterization of cellular tau pathology in the human locus coeruleus-pericoerulear complex by three-dimensional imaging. *Acta Neuropathol* 144: 651-76
Goedert M, Clavaguera F, Tolnay M. 2010. The propagation of prion-like protein inclusions in neurodegenerative diseases. *Trends Neurosci* 33: 317-25
Goedert M, Eisenberg DS, Crowther RA. 2017. Propagation of Tau Aggregates and Neurodegeneration. *Annu Rev Neurosci* 40: 189-210

Goedert M, Jakes R, Vanmechelen E. 1995. Monoclonal antibody AT8 recognises tau protein phosphorylated at both serine 202 and threonine 205. *Neurosci Lett* 189: 167-9
Goedert M, Spillantini MG, Cairns NJ, Crowther RA. 1992. Tau proteins of Alzheimer paired helical filaments: abnormal phosphorylation of all six brain isoforms. *Neuron* 8: 159-68
Goedert M, Wischik CM, Crowther RA, Walker JE, Klug A. 1988. Cloning and sequencing of the cDNA encoding a core protein of the paired helical filament of Alzheimer disease: identification as the microtubule-associated protein tau. *Proc Natl Acad Sci U S A* 85: 4051-5
Greenberg SM, Bacskai BJ, Hernandez-Guillamon M, Pruzin J, Sperling R, van Veluw SJ. 2020. Cerebral amyloid angiopathy and Alzheimer disease - one peptide, two pathways. *Nat Rev Neurol* 16: 30-42
Grinberg LT, Rüb U, Ferretti RE, Nitrini R, Farfel JM, et al. 2009. The dorsal raphe nucleus shows phospho-tau neurofibrillary changes before the transentorhinal region in Alzheimer's disease. A precocious onset? *Neuropathol Appl Neurobiol* 35: 406-16
Guison NG, Ahmed AK, Dong K, Yamadori T. 1995. Projections from the lateral mammillary nucleus to the anterodorsal thalamic nucleus in the rat. *Kobe J Med Sci* 41: 213-20
Hamada HT, Abe Y, Takata N, Taira M, Tanaka KF, Doya K. 2024. Optogenetic activation of dorsal raphe serotonin neurons induces brain-wide activation. *Nat Commun* 15: 4152
Hampel H, Hardy J, Blennow K, Chen C, Perry G, et al. 2021. The Amyloid-β Pathway in Alzheimer's Disease. *Mol Psychiatry* 26: 5481-503
Hansen DV, Hanson JE, Sheng M. 2018. Microglia in Alzheimer's disease. *J Cell Biol* 217: 459-72
Harding A, Halliday G, Caine D, Kril J. 2000. Degeneration of anterior thalamic nuclei differentiates alcoholics with amnesia. *Brain* 123 (Pt 1): 141-54
Hardy JA, Higgins GA. 1992. Alzheimer's disease: the amyloid cascade hypothesis. *Science* 256: 184-5
Harold D, Abraham R, Hollingworth P, Sims R, Gerrish A, et al. 2009. Genome-wide association study identifies variants at CLU and PICALM associated with Alzheimer's disease. *Nat Genet* 41: 1088-93
Hauer BE, Pagliardini S, Dickson CT. 2019. The Reuniens Nucleus of the Thalamus Has an Essential Role in Coordinating Slow-Wave Activity between Neocortex and Hippocampus. *eNeuro* 6
Hayakawa T, Zyo K. 1989. Retrograde double-labeling study of the mammillothalamic and the mammillotegmental projections in the rat. *J Comp Neurol* 284: 1-11
Herrero MT, Barcia C, Navarro JM. 2002. Functional anatomy of thalamus and basal ganglia. *Childs Nerv Syst* 18: 386-404
Herzog E, Bellenchi GC, Gras C, Bernard V, Ravassard P, et al. 2001. The existence of a second vesicular glutamate transporter specifies subpopulations of glutamatergic neurons. *J Neurosci* 21: Rc181
Hitier M, Besnard S, Smith PF. 2014. Vestibular pathways involved in cognition. *Front Integr Neurosci* 8: 59
Hof PR, Morrison JH. 1991. Neocortical neuronal subpopulations labeled by a monoclonal antibody to calbindin exhibit differential vulnerability in Alzheimer's disease. *Exp Neurol* 111: 293-301
Hoglund Z, Ruiz-Uribe N, Del Sastre E, Woost B, Bailey J, et al. 2024. Brain Vasculature Accumulates Tau and Is Spatially Related to Tau Tangle Pathology in Alzheimer's Disease. *bioRxiv*

Hoover BR, Reed MN, Su J, Penrod RD, Kotilinek LA, et al. 2010. Tau mislocalization to dendritic spines mediates synaptic dysfunction independently of neurodegeneration. *Neuron* 68: 1067-81
Horvath S. 2013. DNA methylation age of human tissues and cell types. *Genome Biol* 14: R115
Hou Y, Dan X, Babbar M, Wei Y, Hasselbalch SG, et al. 2019. Ageing as a risk factor for neurodegenerative disease. *Nat Rev Neurol* 15: 565-81
Huang Z, Jordan JD, Zhang Q. 2024. Myelin Pathology in Alzheimer's Disease: Potential Therapeutic Opportunities. *Aging Dis* 15: 698-713
Hur JY. 2022. γ-Secretase in Alzheimer's disease. *Exp Mol Med* 54: 433-46
Hutton M, Lendon CL, Rizzu P, Baker M, Froelich S, et al. 1998. Association of missense and 5'-splice-site mutations in tau with the inherited dementia FTDP-17. *Nature* 393: 702-5
Iliff JJ, Wang M, Liao Y, Plogg BA, Peng W, et al. 2012. A paravascular pathway facilitates CSF flow through the brain parenchyma and the clearance of interstitial solutes, including amyloid β. *Sci Transl Med* 4: 147ra11
Imbimbo BP, Balducci C, Ippati S, Watling M. 2023. Initial failures of anti-tau antibodies in Alzheimer's disease are reminiscent of the amyloid-β story. *Neural Regen Res* 18: 117-18
Iqbal K, Grundke-Iqbal I, Zaidi T, Merz PA, Wen GY, et al. 1986. Defective brain microtubule assembly in Alzheimer's disease. *Lancet* 2: 421-6
İş Ö, Wang X, Reddy JS, Min Y, Yilmaz E, et al. 2024. Gliovascular transcriptional perturbations in Alzheimer's disease reveal molecular mechanisms of blood brain barrier dysfunction. *Nature Communications* 15: 4758
Italia M, Ferrari E, Diluca M, Gardoni F. 2022. NMDA and AMPA Receptors at Synapses: Novel Targets for Tau and α-Synuclein Proteinopathies. *Biomedicines* 10
Itaya SK, Van Hoesen GW, Jenq CB. 1981. Direct retinal input to the limbic system of the rat. *Brain Res* 226: 33-42
Ittner LM, Ke YD, Delerue F, Bi M, Gladbach A, et al. 2010. Dendritic function of tau mediates amyloid-beta toxicity in Alzheimer's disease mouse models. *Cell* 142: 387-97
Iwata M, Watanabe S, Yamane A, Miyasaka T, Misonou H. 2019. Regulatory mechanisms for the axonal localization of tau protein in neurons. *Mol Biol Cell* 30: 2441-57
Jäkel S, Agirre E, Mendanha Falcão A, van Bruggen D, Lee KW, et al. 2019. Altered human oligodendrocyte heterogeneity in multiple sclerosis. *Nature* 566: 543-47
Jankowski MM, Passecker J, Islam MN, Vann S, Erichsen JT, et al. 2015. Evidence for spatially-responsive neurons in the rostral thalamus. *Front Behav Neurosci* 9: 256
Jiang S, Hijazi S, Sarkany B, Gautsch V, LaChance PA, et al. 2024. Pathological tau alters head direction signaling and induces spatial disorientation (unpublished).
Joel Z, Izquierdo P, Salih DA, Richardson JC, Cummings DM, Edwards FA. 2018. Improving Mouse Models for Dementia. Are All the Effects in Tau Mouse Models Due to Overexpression? *Cold Spring Harb Symp Quant Biol* 83: 151-61
Jones EG. 1998. Viewpoint: the core and matrix of thalamic organization. *Neuroscience* 85: 331-45
Kagan BL, Jang H, Capone R, Teran Arce F, Ramachandran S, et al. 2012. Antimicrobial properties of amyloid peptides. *Mol Pharm* 9: 708-17
Kahlson MA, Colodner KJ. 2015. Glial Tau Pathology in Tauopathies: Functional Consequences. *J Exp Neurosci* 9: 43-50
Kaitz SS, Robertson RT. 1981. Thalamic connections with limbic cortex. II. Corticothalamic projections. *J Comp Neurol* 195: 527-45

Kalaria RN. 2003. Vascular factors in Alzheimer's disease. *Int Psychogeriatr* 15 Suppl 1: 47-52
Kalia LV, Lang AE. 2015. Parkinson's disease. *Lancet* 386: 896-912
Kidd M. 1963. Paired helical filaments in electron microscopy of Alzheimer's disease. *Nature* 197: 192-3
Kidd M. 1964. ALZHEIMER'S DISEASE--AN ELECTRON MICROSCOPICAL STUDY. *Brain* 87: 307-20
Kivisäkk P, Fatima HA, Cahoon DS, Otieno B, Chacko L, et al. 2024. Clinical evaluation of a novel plasma pTau217 electrochemiluminescence immunoassay in Alzheimer's disease. *Sci Rep* 14: 629
Kleinberger G, Yamanishi Y, Suárez-Calvet M, Czirr E, Lohmann E, et al. 2014. TREM2 mutations implicated in neurodegeneration impair cell surface transport and phagocytosis. *Sci Transl Med* 6: 243ra86
Klohs J. 2019. An Integrated View on Vascular Dysfunction in Alzheimer's Disease. *Neurodegener Dis* 19: 109-27
Komori T. 1999. Tau-positive glial inclusions in progressive supranuclear palsy, corticobasal degeneration and Pick's disease. *Brain Pathol* 9: 663-79
Kopeikina KJ, Polydoro M, Tai HC, Yaeger E, Carlson GA, et al. 2013. Synaptic alterations in the rTg4510 mouse model of tauopathy. *J Comp Neurol* 521: 1334-53
Kopelman MD. 2015. What does a comparison of the alcoholic Korsakoff syndrome and thalamic infarction tell us about thalamic amnesia? *Neurosci Biobehav Rev* 54: 46-56
Korte N, Nortley R, Attwell D. 2020. Cerebral blood flow decrease as an early pathological mechanism in Alzheimer's disease. *Acta Neuropathol* 140: 793-810
Kovacs GG. 2020. Astroglia and Tau: New Perspectives. *Front Aging Neurosci* 12: 96
Kovacs GG, Ferrer I, Grinberg LT, Alafuzoff I, Attems J, et al. 2016. Aging-related tau astrogliopathy (ARTAG): harmonized evaluation strategy. *Acta Neuropathologica* 131: 87-102
Kovacs GG, Robinson JL, Xie SX, Lee EB, Grossman M, et al. 2017. Evaluating the Patterns of Aging-Related Tau Astrogliopathy Unravels Novel Insights Into Brain Aging and Neurodegenerative Diseases. *J Neuropathol Exp Neurol* 76: 270-88
Kubotera H, Ikeshima-Kataoka H, Hatashita Y, Allegra Mascaro AL, Pavone FS, Inoue T. 2019. Astrocytic endfeet re-cover blood vessels after removal by laser ablation. *Sci Rep* 9: 1263
Kumar A, Sidhu J, Lui F, Tsao JW. 2024. Alzheimer Disease In *StatPearls*. Treasure Island (FL): StatPearls Publishing

Copyright © 2024, StatPearls Publishing LLC.

Lahmy V, Meunier J, Malmström S, Naert G, Givalois L, et al. 2013. Blockade of Tau hyperphosphorylation and $A\beta_{1-42}$ generation by the aminotetrahydrofuran derivative ANAVEX2-73, a mixed muscarinic and σ_1 receptor agonist, in a nontransgenic mouse model of Alzheimer's disease. *Neuropsychopharmacology* 38: 1706-23
Langer Horvat L, Španić Popovački E, Babić Leko M, Zubčić K, Horvat L, et al. 2023. Anterograde and Retrograde Propagation of Inoculated Human Tau Fibrils and Tau Oligomers in a Non-Transgenic Rat Tauopathy Model. *Biomedicines* 11
Largo-Barrientos P, Apóstolo N, Creemers E, Callaerts-Vegh Z, Swerts J, et al. 2021. Lowering Synaptogyrin-3 expression rescues Tau-induced memory defects and synaptic loss in the presence of microglial activation. *Neuron* 109: 767-77.e5
Lasagna-Reeves CA, Castillo-Carranza DL, Sengupta U, Guerrero-Munoz MJ, Kiritoshi T, et al. 2012. Alzheimer brain-derived tau oligomers propagate pathology from endogenous tau. *Sci Rep* 2: 700

Lee S, Sato Y, Nixon RA. 2011. Lysosomal proteolysis inhibition selectively disrupts axonal transport of degradative organelles and causes an Alzheimer's-like axonal dystrophy. *J Neurosci* 31: 7817-30
Li F, Iseki E, Odawara T, Kosaka K, Yagishita S, Amano N. 1998. Regional quantitative analysis of tau-positive neurons in progressive supranuclear palsy: comparison with Alzheimer's disease. *J Neurol Sci* 159: 73-81
Lin WL, Lewis J, Yen SH, Hutton M, Dickson DW. 2003. Filamentous tau in oligodendrocytes and astrocytes of transgenic mice expressing the human tau isoform with the P301L mutation. *Am J Pathol* 162: 213-8
Liu L, Drouet V, Wu JW, Witter MP, Small SA, et al. 2012. Trans-synaptic spread of tau pathology in vivo. *PLoS One* 7: e31302
Livingston G, Huntley J, Liu KY, Costafreda SG, Selbæk G, et al. 2024. Dementia prevention, intervention, and care: 2024 report of the Lancet standing Commission. *Lancet* 404: 572-628
Lomi E, Jeffery KJ, Mitchell AS. 2023. Convergence of location, direction, and theta in the rat anteroventral thalamic nucleus. *iScience* 26: 106993
Mancardi GL, Perdelli F, Rivano C, Leonardi A, Bugiani O. 1980. Thickening of the basement membrane of cortical capillaries in Alzheimer's disease. *Acta Neuropathol* 49: 79-83
Martin Usrey W, Murray Sherman S, Sherman SM, Usrey WM. 2021. 67First and Higher Order Thalamic Relays In *Exploring Thalamocortical Interactions: Circuitry for Sensation, Action, and Cognition*, pp. 0: Oxford University Press
Masuda-Suzukake M, Suzuki G, Hosokawa M, Nonaka T, Goedert M, Hasegawa M. 2020. Dextran sulphate-induced tau assemblies cause endogenous tau aggregation and propagation in wild-type mice. *Brain Commun* 2: fcaa091
Mathiasen ML, O'Mara SM, Aggleton JP. 2020. The anterior thalamic nuclei and nucleus reuniens: So similar but so different. *Neurosci Biobehav Rev* 119: 268-80
Matthews KL, Chen CP, Esiri MM, Keene J, Minger SL, Francis PT. 2002. Noradrenergic changes, aggressive behavior, and cognition in patients with dementia. *Biol Psychiatry* 51: 407-16
Mátyás F, Komlósi G, Babiczky Á, Kocsis K, Barthó P, et al. 2018. A highly collateralized thalamic cell type with arousal-predicting activity serves as a key hub for graded state transitions in the forebrain. *Nat Neurosci* 21: 1551-62
McCann H, Durand B, Shepherd CE. 2021. Aging-Related Tau Astrogliopathy in Aging and Neurodegeneration. *Brain Sci* 11
McGrath ER, Beiser AS, O'Donnell A, Himali JJ, Pase MP, et al. 2022. Determining Vascular Risk Factors for Dementia and Dementia Risk Prediction Across Mid- to Later Life: The Framingham Heart Study. *Neurology* 99: e142-e53
McInnes J, Wierda K, Snellinx A, Bounti L, Wang YC, et al. 2018. Synaptogyrin-3 Mediates Presynaptic Dysfunction Induced by Tau. *Neuron* 97: 823-35.e8
Menkes-Caspi N, Yamin HG, Kellner V, Spires-Jones TL, Cohen D, Stern EA. 2015. Pathological tau disrupts ongoing network activity. *Neuron* 85: 959-66
Mielke MM, Ransom JE, Mandrekar J, Turcano P, Savica R, Brown AW. 2022. Traumatic Brain Injury and Risk of Alzheimer's Disease and Related Dementias in the Population. *J Alzheimers Dis* 88: 1049-59
Mirski MA, Ferrendelli JA. 1987. Interruption of the connections of the mammillary bodies protects against generalized pentylenetetrazol seizures in guinea pigs. *J Neurosci* 7: 662-70
Mitchell AS, Dalrymple-Alford JC. 2006. Lateral and anterior thalamic lesions impair independent memory systems. *Learn Mem* 13: 388-96

Mitchell AS, Sherman SM, Sommer MA, Mair RG, Vertes RP, Chudasama Y. 2014. Advances in understanding mechanisms of thalamic relays in cognition and behavior. *J Neurosci* 34: 15340-6
Mizoguchi A, Nakanishi H, Kimura K, Matsubara K, Ozaki-Kuroda K, et al. 2002. Nectin: an adhesion molecule involved in formation of synapses. *J Cell Biol* 156: 555-65
Molnár Z, Blakemore C. 1995. How do thalamic axons find their way to the cortex? *Trends Neurosci* 18: 389-97
Montal V, Diez I, Kim CM, Orwig W, Bueichekú E, et al. 2022. Network Tau spreading is vulnerable to the expression gradients of APOE and glutamatergic-related genes. *Sci Transl Med* 14: eabn7273
Moreno-García A, Kun A, Calero O, Medina M, Calero M. 2018. An Overview of the Role of Lipofuscin in Age-Related Neurodegeneration. *Front Neurosci* 12: 464
Morris AW, Sharp MM, Albargothy NJ, Fernandes R, Hawkes CA, et al. 2016. Vascular basement membranes as pathways for the passage of fluid into and out of the brain. *Acta Neuropathol* 131: 725-36
Morrison BM, Hof PR, Morrison JH. 1998. Determinants of neuronal vulnerability in neurodegenerative diseases. *Ann Neurol* 44: S32-44
Morsch R, Simon W, Coleman PD. 1999. Neurons may live for decades with neurofibrillary tangles. *J Neuropathol Exp Neurol* 58: 188-97
Mudher A, Colin M, Dujardin S, Medina M, Dewachter I, et al. 2017. What is the evidence that tau pathology spreads through prion-like propagation? *Acta Neuropathologica Communications* 5: 99
Mummery CJ, Börjesson-Hanson A, Blackburn DJ, Vijverberg EGB, De Deyn PP, et al. 2023. Tau-targeting antisense oligonucleotide MAPT(Rx) in mild Alzheimer's disease: a phase 1b, randomized, placebo-controlled trial. *Nat Med* 29: 1437-47
Münkle MC, Waldvogel HJ, Faull RL. 2000. The distribution of calbindin, calretinin and parvalbumin immunoreactivity in the human thalamus. *J Chem Neuroanat* 19: 155-73
Murphy MP, LeVine H, 3rd. 2010. Alzheimer's disease and the amyloid-beta peptide. *J Alzheimers Dis* 19: 311-23
Murray KD, Choudary PV, Jones EG. 2007. Nucleus- and cell-specific gene expression in monkey thalamus. *Proc Natl Acad Sci U S A* 104: 1989-94
Nadeau SE. 2024. Lecanemab Questions. *Neurology* 102: e209320
Nakano I, Iwatsubo T, Otsuka N, Kamei M, Matsumura K, Mannen T. 1992. Paired helical filaments in astrocytes: electron microscopy and immunohistochemistry in a case of atypical Alzheimer's disease. *Acta Neuropathol* 83: 228-32
Nguyen TT, Ta QTH, Nguyen TKO, Nguyen TTD, Giau VV. 2020. Type 3 Diabetes and Its Role Implications in Alzheimer's Disease. *Int J Mol Sci* 21
Nishimura M, Tomimoto H, Suenaga T, Namba Y, Ikeda K, et al. 1995. Immunocytochemical characterization of glial fibrillary tangles in Alzheimer's disease brain. *Am J Pathol* 146: 1052-8
Nixon RA, Wegiel J, Kumar A, Yu WH, Peterhoff C, et al. 2005. Extensive involvement of autophagy in Alzheimer disease: an immuno-electron microscopy study. *J Neuropathol Exp Neurol* 64: 113-22
O'Brien JT, Markus HS. 2014. Vascular risk factors and Alzheimer's disease. *BMC Med* 12: 218
O'Keefe J. 1976. Place units in the hippocampus of the freely moving rat. *Exp Neurol* 51: 78-109
Overmyer M, Helisalmi S, Soininen H, Laakso M, Riekkinen P, Sr., Alafuzoff I. 1999. Reactive microglia in aging and dementia: an immunohistochemical study of postmortem human brain tissue. *Acta Neuropathol* 97: 383-92

Papez JW. 1995. A proposed mechanism of emotion. 1937. *J Neuropsychiatry Clin Neurosci* 7: 103-12
Park H, Cho B, Kim H, Saito T, Saido TC, et al. 2023. Single-cell RNA-sequencing identifies disease-associated oligodendrocytes in male APP NL-G-F and 5XFAD mice. *Nat Commun* 14: 802
Partlow GD, Colonnier M, Szabo J. 1977. Thalamic projections of the superior colliculus in the rhesus monkey, Macaca mulatta. A light and electron microscopic study. *J Comp Neurol* 72: 285-318
Perry BAL, Mercer SA, Barnett SC, Lee J, Dalrymple-Alford JC. 2018. Anterior thalamic nuclei lesions have a greater impact than mammillothalamic tract lesions on the extended hippocampal system. *Hippocampus* 28: 121-35
Perry BAL, Mitchell AS. 2019. Considering the Evidence for Anterior and Laterodorsal Thalamic Nuclei as Higher Order Relays to Cortex. *Front Mol Neurosci* 12: 167
Peters A, Sethares C. 2004. Oligodendrocytes, their progenitors and other neuroglial cells in the aging primate cerebral cortex. *Cereb Cortex* 14: 995-1007
Piaceri I, Nacmias B, Sorbi S. 2013. Genetics of familial and sporadic Alzheimer's disease. *Front Biosci (Elite Ed)* 5: 167-77
Pierson SR, Fiock KL, Wang R, Balasubramanian N, Reinhardt J, et al. 2024. Tau pathology in the dorsal raphe may be a prodromal indicator of Alzheimer's disease. *Mol Psychiatry*
Plavén-Sigray P, Ikonen Victorsson P, Santillo A, Matheson GJ, Lee M, et al. 2022. Thalamic dopamine D2-receptor availability in schizophrenia: a study on antipsychotic-naive patients with first-episode psychosis and a meta-analysis. *Mol Psychiatry* 27: 1233-40
Poirier GL, Amin E, Good MA, Aggleton JP. 2011. Early-onset dysfunction of retrosplenial cortex precedes overt amyloid plaque formation in Tg2576 mice. *Neuroscience* 174: 71-83
Pooler AM, Phillips EC, Lau DH, Noble W, Hanger DP. 2013. Physiological release of endogenous tau is stimulated by neuronal activity. *EMBO Rep* 14: 389-94
Porsteinsson AP, Isaacson RS, Knox S, Sabbagh MN, Rubino I. 2021. Diagnosis of Early Alzheimer's Disease: Clinical Practice in 2021. *J Prev Alzheimers Dis* 8: 371-86
Prusiner SB. 1982. Novel proteinaceous infectious particles cause scrapie. *Science* 216: 136-44
Purro SA, Farrow MA, Linehan J, Nazari T, Thomas DX, et al. 2018. Transmission of amyloid-β protein pathology from cadaveric pituitary growth hormone. *Nature* 564: 415-19
Ramirez DMO, Whitesell JD, Bhagwat N, Thomas TL, Ajay AD, et al. 2023. Endogenous pathology in tauopathy mice progresses via brain networks. *bioRxiv*
Rao YL, Ganaraja B, Murlimanju BV, Joy T, Krishnamurthy A, Agrawal A. 2022. Hippocampus and its involvement in Alzheimer's disease: a review. *3 Biotech* 12: 55
Rasband MN, Peles E. 2015. The Nodes of Ranvier: Molecular Assembly and Maintenance. *Cold Spring Harb Perspect Biol* 8: a020495
Ri S. 2022. The Management of Poststroke Thalamic Pain: Update in Clinical Practice. *Diagnostics (Basel)* 12
Roth S, Burnie N, Suridjan I, Yan JT, Carboni M. 2023. Current Diagnostic Pathways for Alzheimer's Disease: A Cross-Sectional Real-World Study Across Six Countries. *J Alzheimers Dis Rep* 7: 659-74
Rovó Z, Ulbert I, Acsády L. 2012. Drivers of the primate thalamus. *J Neurosci* 32: 17894-908

Roy DS, Zhang Y, Aida T, Choi S, Chen Q, et al. 2021. Anterior thalamic dysfunction underlies cognitive deficits in a subset of neuropsychiatric disease models. *Neuron* 109: 2590-603.e13
Ruan Z, Pathak D, Venkatesan Kalavai S, Yoshii-Kitahara A, Muraoka S, et al. 2021. Alzheimer's disease brain-derived extracellular vesicles spread tau pathology in interneurons. *Brain* 144: 288-309
Rüb U, Stratmann K, Heinsen H, Del Turco D, Ghebremedhin E, et al. 2016. Hierarchical Distribution of the Tau Cytoskeletal Pathology in the Thalamus of Alzheimer's Disease Patients. *J Alzheimers Dis* 49: 905-15
Saab AS, Tzvetanova ID, Nave KA. 2013. The role of myelin and oligodendrocytes in axonal energy metabolism. *Curr Opin Neurobiol* 23: 1065-72
Salloway S, Gur T, Berzin T, Tavares R, Zipser B, et al. 2002. Effect of APOE genotype on microvascular basement membrane in Alzheimer's disease. *J Neurol Sci* 203-204: 183-7
Sárkány B, Dávid C, Hortobágyi T, Gombás P, Somogyi P, et al. 2024. Early and selective localization of tau filaments to glutamatergic subcellular domains within the human anterodorsal thalamus. *Acta Neuropathol* 147: 98
Sasmita AO, Depp C, Nazarenko T, Sun T, Siems SB, et al. 2024. Oligodendrocytes produce amyloid-β and contribute to plaque formation alongside neurons in Alzheimer's disease model mice. *Nat Neurosci*
Saunders RC, Mishkin M, Aggleton JP. 2005. Projections from the entorhinal cortex, perirhinal cortex, presubiculum, and parasubiculum to the medial thalamus in macaque monkeys: identifying different pathways using disconnection techniques. *Exp Brain Res* 167: 1-16
Scheffer S, Hermkens DMA, van der Weerd L, de Vries HE, Daemen M. 2021. Vascular Hypothesis of Alzheimer Disease: Topical Review of Mouse Models. *Arterioscler Thromb Vasc Biol* 41: 1265-83
Schindowski K, Bretteville A, Leroy K, Bégard S, Brion JP, et al. 2006. Alzheimer's disease-like tau neuropathology leads to memory deficits and loss of functional synapses in a novel mutated tau transgenic mouse without any motor deficits. *Am J Pathol* 169: 599-616
Seemiller J, Bischof GN, Hoenig MC, Tahmasian M, van Eimeren T, Drzezga A. 2021. Indication of retrograde tau spreading along Braak stages and functional connectivity pathways. *Eur J Nucl Med Mol Imaging* 48: 2272-82
Sherman SM. 2007. The thalamus is more than just a relay. *Curr Opin Neurobiol* 17: 417-22
Sherman SM, Guillery RW. 1998. On the actions that one nerve cell can have on another: distinguishing "drivers" from "modulators". *Proc Natl Acad Sci U S A* 95: 7121-6
Sherman SM, Usrey WM. 2024. A Reconsideration of the Core and Matrix Classification of Thalamocortical Projections. *J Neurosci* 44
Shibata H. 1993a. Direct projections from the anterior thalamic nuclei to the retrohippocampal region in the rat. *J Comp Neurol* 337: 431-45
Shibata H. 1993b. Efferent projections from the anterior thalamic nuclei to the cingulate cortex in the rat. *J Comp Neurol* 330: 533-42
Shibata H. 1998. Organization of projections of rat retrosplenial cortex to the anterior thalamic nuclei. *Eur J Neurosci* 10: 3210-9
Shin JH. 2022. Dementia Epidemiology Fact Sheet 2022. *Ann Rehabil Med* 46: 53-59
Šimić G, Babić Leko M, Wray S, Harrington C, Delalle I, et al. 2016. Tau Protein Hyperphosphorylation and Aggregation in Alzheimer's Disease and Other Tauopathies, and Possible Neuroprotective Strategies. *Biomolecules* 6: 6

Simon MJ, Wang MX, Murchison CF, Roese NE, Boespflug EL, et al. 2018. Transcriptional network analysis of human astrocytic endfoot genes reveals region-specific associations with dementia status and tau pathology. *Sci Rep* 8: 12389
Skrabana R, Skrabanova M, Csokova N, Sevcik J, Novak M. 2006. Intrinsically disordered tau protein in Alzheimer's tangles: a coincidence or a rule? *Bratisl Lek Listy* 107: 354-8
Smeland OB, Kutrolli G, Bahrami S, Fominykh V, Parker N, et al. 2023. The shared genetic risk architecture of neurological and psychiatric disorders: a genome-wide analysis. *medRxiv*
Smith AD, Refsum H, Bottiglieri T, Fenech M, Hooshmand B, et al. 2018. Homocysteine and Dementia: An International Consensus Statement. *J Alzheimers Dis* 62: 561-70
Smith AD, Smith SM, de Jager CA, Whitbread P, Johnston C, et al. 2010. Homocysteine-lowering by B vitamins slows the rate of accelerated brain atrophy in mild cognitive impairment: a randomized controlled trial. *PLoS One* 5: e12244
Somogyi G, Hajdu F, Tömböl T. 1978. Ultrastructure of the anterior ventral and anterior medial nuclei of the cat thalamus. *Exp Brain Res* 31: 417-31
Sperfeld AD, Collatz MB, Baier H, Palmbach M, Storch A, et al. 1999. FTDP-17: an early-onset phenotype with parkinsonism and epileptic seizures caused by a novel mutation. *Ann Neurol* 46: 708-15
Spillantini MG, Crowther RA, Kamphorst W, Heutink P, van Swieten JC. 1998. Tau pathology in two Dutch families with mutations in the microtubule-binding region of tau. *Am J Pathol* 153: 1359-63
Spilman P, Podlutskaya N, Hart MJ, Debnath J, Gorostiza O, et al. 2010. Inhibition of mTOR by rapamycin abolishes cognitive deficits and reduces amyloid-beta levels in a mouse model of Alzheimer's disease. *PLoS One* 5: e9979
Stoddart P, Satchell SC, Ramnath R. 2022. Cerebral microvascular endothelial glycocalyx damage, its implications on the blood-brain barrier and a possible contributor to cognitive impairment. *Brain Res* 1780: 147804
Stratmann K, Heinsen H, Korf HW, Del Turco D, Ghebremedhin E, et al. 2016. Precortical Phase of Alzheimer's Disease (AD)-Related Tau Cytoskeletal Pathology. *Brain Pathol* 26: 371-86
Su JH, Cummings BJ, Cotman CW. 1994. Early phosphorylation of tau in Alzheimer's disease occurs at Ser-202 and is preferentially located within neurites. *Neuroreport* 5: 2358-62
Swaddiwudhipong N, Whiteside DJ, Hezemans FH, Street D, Rowe JB, Rittman T. 2022. Pre-diagnostic cognitive and functional impairment in multiple sporadic neurodegenerative diseases. *Alzheimers Dement*
Swanson MEV, Scotter EL, Smyth LCD, Murray HC, Ryan B, et al. 2020. Identification of a dysfunctional microglial population in human Alzheimer's disease cortex using novel single-cell histology image analysis. *Acta Neuropathol Commun* 8: 170
Sweeney P, Park H, Baumann M, Dunlop J, Frydman J, et al. 2017. Protein misfolding in neurodegenerative diseases: implications and strategies. *Transl Neurodegener* 6: 6
Szentágothai J, Hámori J, Tömböl T. 1966. Degeneration and electron microscope analysis of the synaptic glomeruli in the lateral geniculate body. *Exp Brain Res* 2: 283-301
Tangen GG, Nilsson MH, Stomrud E, Palmqvist S, Hansson O. 2022. Spatial Navigation and Its Association With Biomarkers and Future Dementia in Memory Clinic Patients Without Dementia. *Neurology* 99: e2081-e91
Tanzi RE. 2012. The genetics of Alzheimer disease. *Cold Spring Harb Perspect Med* 2
Taube JS. 1995. Head direction cells recorded in the anterior thalamic nuclei of freely moving rats. *J Neurosci* 15: 70-86

Terry D, Robert, Gonatas K, Nicholas, Weiss M. 1964. Ultrastructural Studies in Alzheimer's Presenile Dementia. *Am J Pathol.* v.44(2): 269–97.
Terry RD. 1963. THE FINE STRUCTURE OF NEUROFIBRILLARY TANGLES IN ALZHEIMER'S DISEASE. *J Neuropathol Exp Neurol* 22: 629-42
Theofilas P, Ehrenberg AJ, Nguy A, Thackrey JM, Dunlop S, et al. 2018. Probing the correlation of neuronal loss, neurofibrillary tangles, and cell death markers across the Alzheimer's disease Braak stages: a quantitative study in humans. *Neurobiol Aging* 61: 1-12
Thierry M, Boluda S, Delatour B, Marty S, Seilhean D, et al. 2020. Human subiculo-fornico-mamillary system in Alzheimer's disease: Tau seeding by the pillar of the fornix. *Acta Neuropathol* 139: 443-61
Torrico TJ, Munakomi S. 2024. Neuroanatomy, Thalamus In *StatPearls*. Treasure Island (FL): StatPearls Publishing

Copyright © 2024, StatPearls Publishing LLC.

Tourtellotte WG, Van Hoesen GW, Hyman BT, Tikoo RK, Damasio AR. 1990. Alz-50 immunoreactivity in the thalamic reticular nucleus in Alzheimer's disease. *Brain Res* 515: 227-34
Tracy TE, Madero-Pérez J, Swaney DL, Chang TS, Moritz M, et al. 2022. Tau interactome maps synaptic and mitochondrial processes associated with neurodegeneration. *Cell* 185: 712-28.e14
Tromp D, Dufour A, Lithfous S, Pebayle T, Després O. 2015. Episodic memory in normal aging and Alzheimer disease: Insights from imaging and behavioral studies. *Ageing Res Rev* 24: 232-62
Tsanov M, Chah E, Vann SD, Reilly RB, Erichsen JT, et al. 2011. Theta-modulated head direction cells in the rat anterior thalamus. *J Neurosci* 31: 9489-502
Varela C. 2014. Thalamic neuromodulation and its implications for executive networks. *Front Neural Circuits* 8: 69
Vaughn JE. 1989. Fine structure of synaptogenesis in the vertebrate central nervous system. *Synapse* 3: 255-85
Veazey RB, Amaral DG, Cowan WM. 1982. The morphology and connections of the posterior hypothalamus in the cynomolgus monkey (Macaca fascicularis). II. Efferent connections. *J Comp Neurol* 207: 135-56
Verheggen ICM, de Jong JJA, van Boxtel MPJ, Gronenschild E, Palm WM, et al. 2020. Increase in blood-brain barrier leakage in healthy, older adults. *Geroscience* 42: 1183-93
Verkhratsky A, Olabarria M, Noristani HN, Yeh CY, Rodriguez JJ. 2010. Astrocytes in Alzheimer's disease. *Neurotherapeutics* 7: 399-412
Vertes RP, Linley SB, Hoover WB. 2015. Limbic circuitry of the midline thalamus. *Neurosci Biobehav Rev* 54: 89-107
Viney TJ, Sarkany B, Ozdemir AT, Hartwich K, Schweimer J, et al. 2022. Spread of pathological human Tau from neurons to oligodendrocytes and loss of high-firing pyramidal neurons in aging mice. *Cell Rep* 41: 111646
Vogel JW, Iturria-Medina Y, Strandberg OT, Smith R, Levitis E, et al. 2020. Spread of pathological tau proteins through communicating neurons in human Alzheimer's disease. *Nat Commun* 11: 2612
Wang L, Liu Q, Yue D, Liu J, Fu Y. 2024. Cerebral Amyloid Angiopathy: An Undeniable Small Vessel Disease. *J Stroke* 26: 1-12
Wang Y, Balaji V, Kaniyappan S, Krüger L, Irsen S, et al. 2017. The release and trans-synaptic transmission of Tau via exosomes. *Molecular Neurodegeneration* 12: 5

Warburton EC, Baird AL, Aggleton JP. 1997. Assessing the magnitude of the allocentric spatial deficit associated with complete loss of the anterior thalamic nuclei in rats. *Behav Brain Res* 87: 223-32
Wegmann S, Bennett RE, Delorme L, Robbins AB, Hu M, et al. 2019. Experimental evidence for the age dependence of tau protein spread in the brain. *Sci Adv* 5: eaaw6404
Weininger J, Roman E, Tierney P, Barry D, Gallagher H, et al. 2019. Papez's Forgotten Tract: 80 Years of Unreconciled Findings Concerning the Thalamocingulate Tract. *Front Neuroanat* 13: 14
Wenger K, Viode A, Schlaffner CN, van Zalm P, Cheng L, et al. 2023. Common mouse models of tauopathy reflect early but not late human disease. *Mol Neurodegener* 18: 10
White KE, Cummings JL. 1996. Schizophrenia and Alzheimer's disease: clinical and pathophysiologic analogies. *Compr Psychiatry* 37: 188-95
Wijesinghe R, Protti DA, Camp AJ. 2015. Vestibular Interactions in the Thalamus. *Front Neural Circuits* 9: 79
Wilton LA, Baird AL, Muir JL, Honey RC, Aggleton JP. 2001. Loss of the thalamic nuclei for "head direction" impairs performance on spatial memory tasks in rats. *Behav Neurosci* 115: 861-9
Winklhofer KF, Tatzelt J, Haass C. 2008. The two faces of protein misfolding: gain- and loss-of-function in neurodegenerative diseases. *Embo j* 27: 336-49
Wongsodirdjo P, Caruso AC, Yong AK, Lester MA, Vella LJ, et al. 2024. Messenger RNA-encoded antibody approach for targeting extracellular and intracellular tau. *Brain Commun* 6: fcae100
Xuereb JH, Candy JM, Perry EK, Perry RH, Marshall E, Bonham JR. 1990. Distribution of neurofibrillary tangle formation and [³H]-D-aspartate receptor binding in the thalamus in the normal elderly brain, in Alzheimer's disease and in Parkinson's disease. *Neuropathology and Applied Neurobiology* 16: 477-88
Yang C, Huang X, Huang X, Mai H, Li J, et al. 2016. Aquaporin-4 and Alzheimer's Disease. *J Alzheimers Dis* 52: 391-402
Yoshida M. 2006. Cellular tau pathology and immunohistochemical study of tau isoforms in sporadic tauopathies. *Neuropathology* 26: 457-70
Young KA, Manaye KF, Liang C, Hicks PB, German DC. 2000. Reduced number of mediodorsal and anterior thalamic neurons in schizophrenia. *Biol Psychiatry* 47: 944-53
Yu JT, Xu W, Tan CC, Andrieu S, Suckling J, et al. 2020. Evidence-based prevention of Alzheimer's disease: systematic review and meta-analysis of 243 observational prospective studies and 153 randomised controlled trials. *J Neurol Neurosurg Psychiatry* 91: 1201-09
Zenaro E, Piacentino G, Constantin G. 2017. The blood-brain barrier in Alzheimer's disease. *Neurobiol Dis* 107: 41-56
Zhang C, Browne A, Divito JR, Stevenson JA, Romano D, et al. 2010. Amyloid-β production via cleavage of amyloid-β protein precursor is modulated by cell density. *J Alzheimers Dis* 22: 683-984
Zhang Y, Wu KM, Yang L, Dong Q, Yu JT. 2022. Tauopathies: new perspectives and challenges. *Mol Neurodegener* 17: 28
Zhao N, Ren Y, Yamazaki Y, Qiao W, Li F, et al. 2020. Alzheimer's Risk Factors Age, APOE Genotype, and Sex Drive Distinct Molecular Pathways. *Neuron* 106: 727-42.e6

Zhou L, McInnes J, Wierda K, Holt M, Herrmann AG, et al. 2017. Tau association with synaptic vesicles causes presynaptic dysfunction. *Nat Commun* 8: 15295
Zlokovic BV. 2011. Neurovascular pathways to neurodegeneration in Alzheimer's disease and other disorders. *Nat Rev Neurosci* 12: 723-38
Zou K, Gong JS, Yanagisawa K, Michikawa M. 2002. A novel function of monomeric amyloid beta-protein serving as an antioxidant molecule against metal-induced oxidative damage. *J Neurosci* 22: 4833-41
Zubenko GS, Moossy J. 1988. Major depression in primary dementia. Clinical and neuropathologic correlates. *Arch Neurol* 45: 1182-6